



UNIVERSITAT POLITÈCNICA  
DE CATALUNYA  
BARCELONATECH

*Experimental and numerical  
modelling of co2 behaviour in the  
soil-atmosphere interface.  
Implications for risk assessment of  
carbon capture storage projects*

**Andrea Gasparini**

**ADVERTIMENT** La consulta d'aquesta tesi queda condicionada a l'acceptació de les següents condicions d'ús: La difusió d'aquesta tesi per mitjà del repositori institucional UPCommons (<http://upcommons.upc.edu/tesis>) i el repositori cooperatiu TDX (<http://www.tdx.cat/>) ha estat autoritzada pels titulars dels drets de propietat intel·lectual **únicament per a usos privats** emmarcats en activitats d'investigació i docència. No s'autoritza la seva reproducció amb finalitats de lucre ni la seva difusió i posada a disposició des d'un lloc aliè al servei UPCommons o TDX. No s'autoritza la presentació del seu contingut en una finestra o marc aliè a UPCommons (*framing*). Aquesta reserva de drets afecta tant al resum de presentació de la tesi com als seus continguts. En la utilització o cita de parts de la tesi és obligat indicar el nom de la persona autora.

**ADVERTENCIA** La consulta de esta tesis queda condicionada a la aceptación de las siguientes condiciones de uso: La difusión de esta tesis por medio del repositorio institucional UPCommons (<http://upcommons.upc.edu/tesis>) y el repositorio cooperativo TDR (<http://www.tdx.cat/?locale-attribute=es>) ha sido autorizada por los titulares de los derechos de propiedad intelectual **únicamente para usos privados enmarcados** en actividades de investigación y docencia. No se autoriza su reproducción con finalidades de lucro ni su difusión y puesta a disposición desde un sitio ajeno al servicio UPCommons No se autoriza la presentación de su contenido en una ventana o marco ajeno a UPCommons (*framing*). Esta reserva de derechos afecta tanto al resumen de presentación de la tesis como a sus contenidos. En la utilización o cita de partes de la tesis es obligado indicar el nombre de la persona autora.

**WARNING** On having consulted this thesis you're accepting the following use conditions: Spreading this thesis by the institutional repository UPCommons (<http://upcommons.upc.edu/tesis>) and the cooperative repository TDX (<http://www.tdx.cat/?locale-attribute=en>) has been authorized by the titular of the intellectual property rights **only for private uses** placed in investigation and teaching activities. Reproduction with lucrative aims is not authorized neither its spreading nor availability from a site foreign to the UPCommons service. Introducing its content in a window or frame foreign to the UPCommons service is not authorized (*framing*). These rights affect to the presentation summary of the thesis as well as to its contents. In the using or citation of parts of the thesis it's obliged to indicate the name of the author.



UNIVERSITAT POLITÈCNICA  
DE CATALUNYA  
BARCELONATECH



**AMPHOS**<sup>21</sup>

**Programa de Doctorat en Enginyeria Ambiental**

**EXPERIMENTAL AND NUMERICAL MODELLING OF CO<sub>2</sub> BEHAVIOUR  
IN THE SOIL-ATMOSPHERE INTERFACE. IMPLICATIONS FOR RISK  
ASSESSMENT OF CARBON CAPTURE STORAGE PROJECTS**

**Andrea Gasparini**

PhD. Dissertation

**Supervisors:**

Fidel Grandia i Borràs

Amphos21 Consulting S.L.

Jordi Bruno i Salgot

Amphos21 Consulting S.L.

**Tutor:**

Joan de Pablo i Ribas

Departament d'Enginyeria Química – Universitat Politècnica de Catalunya

## INDEX

<b>1. PhD motivation</b> .....	1
<b>2. Abstract</b> .....	3
<b>3. Acknowledgements</b> .....	6
<b>4. List of Figures and Tables</b> .....	7
<b>5. Structure of the PhD dissertation</b> .....	12
<b>6. PhD. background</b> .....	14
<b>6.1. The risk of leakage in geological carbon storage</b> .....	14
<b>6.2. State of the art of CO<sub>2</sub> investigation in the unsaturated zone</b> .....	17
<b>6.3. State of the art of atmospheric dispersion modelling for risk assessment</b> .....	18
<b>7. Modelling tools and basics of formulation implemented</b> .....	19
<b>7.1. TOUGH family of numerical codes</b> .....	19
<b>7.1.1. EOS3 module (water, air) in TOUGH2</b> .....	20
<b>7.1.2. EOS7CA module (modelling of systems with water, brine, non-condensable gas, gas tracers, air heat)</b> .....	21
<b>7.2. TWODEE2 software for atmospheric dispersion modelling</b> .....	24
<b>8. Research article 1: Experimental and numerical modelling of CO<sub>2</sub> leakage in the vadose zone</b> .....	26
<b>8.1. Introduction</b> .....	26
<b>8.2. Materials, methodology and experimental conditions</b> .....	28
<b>8.2.1. Experimental PISCO2 unit</b> .....	28
<b>8.2.2. Experimental injection</b> .....	30
<b>8.2.3. Weather conditions during the injection experiment</b> .....	31
<b>8.2.4. Monitoring procedure</b> .....	31
<b>8.2.5. Modelling tools</b> .....	33
<b>8.2.5.1. TOUGH2 code and EOS7CA experimental module</b> .....	33
<b>8.2.6. Numerical model</b> .....	33
<b>8.3. Results</b> .....	38
<b>8.3.1. Experimental injection</b> .....	38
<b>8.3.2. Numerical modelling</b> .....	40
<b>8.3.2.1. Model A</b> .....	40
<b>8.3.2.2. Model B</b> .....	42
<b>8.3.2.3. Model C</b> .....	44

8.3.2.4.	Model D .....	46
8.3.2.5.	Model E.....	46
8.3.3.	Pressure and liquid saturation evolution.....	48
8.3.4.	Quantitative representation of model calibration to field data.....	49
8.4.	Discussion.....	51
8.5.	Conclusions.....	59
8.6.	Acknowledgments.....	59
9.	<b>Research article 2: Atmospheric dispersion modelling of a natural CO<sub>2</sub> degassing pool from Campo de Calatrava (central Spain) natural analogue. Implications for carbon storage risk assessment.....</b>	<b>60</b>
9.1.	Introduction.....	60
9.2.	Natural CO <sub>2</sub> emission from underground. Examples from the Campo de Calatrava Volcanic Field.....	62
9.3.	Measurement of CO <sub>2</sub> flow from underground and CO <sub>2</sub> concentration in air....	65
9.3.1.	Telaire.....	65
9.3.2.	SAP system (Sistema Alta Portata).....	66
9.4.	Atmospheric dispersion modelling.....	67
9.5.	Model set-up.....	67
9.6.	Results.....	68
9.6.1.	CO <sub>2</sub> concentration in air.....	68
9.6.2.	SAP system.....	70
9.6.3.	Numerical modelling results.....	71
9.7.	Discussion and Interpretation for risk assessment.....	74
9.8.	Conclusions.....	78
10.	<b>Research article 3: Atmospheric dispersion modelling of CO<sub>2</sub> emission in the Colli Albani volcanic district (central Italy).....</b>	<b>79</b>
10.1.	Introduction.....	79
10.2.	Geological setting.....	80
10.3.	CO <sub>2</sub> soil flux emissions.....	83
10.4.	Field data.....	84
10.4.1.	Air CO <sub>2</sub> concentration.....	84
10.5.	Meteorological data.....	87
10.6.	Atmospheric dispersion modelling.....	90
10.6.1.	Numerical code.....	90

<b>10.6.2. Numerical model set-up.....</b>	<b>90</b>
<b>10.7. Results.....</b>	<b>91</b>
<b>10.8. Discussion.....</b>	<b>99</b>
<b>10.9. Conclusions.....</b>	<b>102</b>
<b>11. General discussion.....</b>	<b>103</b>
<b>12. Conclusions and key messages from this PhD.....</b>	<b>104</b>
<b>13. Further work.....</b>	<b>105</b>
<b>14. References.....</b>	<b>106</b>

## 1. PhD. motivation

In 2010, I took part at the 34<sup>th</sup> *Course of the International School of Geophysics on densely populated settings: the challenge of siting geological facilities for deep geothermic, CO<sub>2</sub> and natural gas storage, and radioactive waste disposal*, held at Erice (Sicily, Italy). During that school, I had the opportunity to meet Professor Jordi Bruno, CEO of Amphos21, a Spanish company working on scientific and strategic environmental consulting. An interesting round table at the end of the School made me think about a PhD project to improve knowledge and to manage an advanced modelling technique. After a fast email exchange with Jordi Bruno and with the authorization of the Istituto Nazionale di Geofisica e Vulcanologia (INGV), the research institute for which I work, in 2011 I started a PhD project at the Institute of Sustainability of Universitat Politècnica de Catalunya (Barcelona, Spain), at the Càtedra Enresa-Amphos 21.

The International Energy Agency (IEA) considers Carbon Capture and Storage (CCS) a crucial part of worldwide efforts to limit global warming by reducing greenhouse-gas emissions. The IEA has estimated that the broad deployment of low-carbon energy technologies could reduce projected 2050 emissions to half 2005 levels and that CCS could contribute about one-fifth of those reductions in a least-cost emissions reduction portfolio. Reaching that goal, however, would require around 100 CCS projects to be implemented by 2020 and over 3000 by 2050 (IEA, 2010). The first article of the CCS Directive 2009/31/EC of the European Parliament and the Council states: “The purpose of environmentally safe geological storage of CO<sub>2</sub> is the permanent containment of CO<sub>2</sub> in such a way as to prevent and, where this is not possible, eliminate as far as possible negative effects and any risk to the environment and human health”. CO<sub>2</sub> geological storage is one of the options technologically viable in order to decrease the industrial emissions of this gas species that strongly contribute to the greenhouse effect in the atmosphere (IPCC, 2005).

As in nature oil and gas are stored in porous rocks that have the same key geological features required for CO<sub>2</sub> storage, CCS aims to recreate a natural process to trap carbon dioxide for millions of years into deep saline aquifers or depleted oil and gas fields. The behaviour of the storage system as a whole, from the geological layers (reservoir, caprock) to the surface, has to be studied exhaustively and numerically simulated in time frames of thousands of years. Large-scale injection of CO<sub>2</sub> (meaning millions of tons per year) into geological reservoirs would induce a complex interplay of multiphase and thermal flow, structural and capillary trapping, aqueous dissolution, convection and chemical reactions that may have significant impacts on short-term injection performance and long-term fate of CO<sub>2</sub> storage (Bachu et al., 1994; Xiao et al., 2009). The main target of a CCS site is to store carbon dioxide deep underground in a safe reservoir but gas may escape

from the reservoir during different phases of the injection and storage period. For that reason, it is important to understand CO<sub>2</sub> behaviour from deep underground to up the vadose zone and even its atmospheric dispersion once it reaches ground surface. The gas spilling is called seepage when it happens in the underground due to hydrostatic pressure through porous material, while leakage is when gas passes through cracks and fissures. CO<sub>2</sub> leakage from reservoir formations into surrounding layers could have environmental impacts on fresh groundwater and could affect surface ecosystems and human beings. Groundwater acidification due to CO<sub>2</sub> dissolution would mobilize trace metals that could be transported along of CO<sub>2</sub> lateral and vertical way of migration (Bruno et al., 2009; Grivé, 2005). This eventuality is, however, very rare and at the moment reliable early alarm systems could be used to envisage the migration of the metals in shallow aquifers. In any case, long-term monitoring of CO<sub>2</sub> storage area of influence (some square kilometres) is necessary and mandatory and many efforts have been devoted so far to detect potential leakage.

Much research has been conducted dealing with CO<sub>2</sub> interactions with aquifer and seal formation rocks. These interactions can be either physical (e.g., fingering, buoyancy, fracturing) or geochemical (host rock dissolution, brine dry-out, caprock alteration) (Dávila et al., 2016a, b; García-Ríos et al., 2014). This PhD, on the other hand, focuses on the processes occurring at near-surface (vadose zone), the soil-atmosphere interface and atmosphere close to the CO<sub>2</sub> emission points. The vadose zone is the portion of soil overlaying the water surface until the soil surface. The pores present in this area are partially filled water and mostly by air. The force acting on the liquid is purely gravitational so its moves down. CO<sub>2</sub> flow from underground can cause deep changes in the physics and chemistry of the vadose zone and the ecosystems in it as well.

Also, the release of gas from underground to the atmosphere is a topic that deserves thorough research since it can result in hazardous CO<sub>2</sub> concentration in the air and, therefore, resulting in risk for living organisms. Prediction of the conditions under which the emission of gas from a particular point source can cause severe risk to the human beings is fundamental in the CCS risk assessment and it has not been treated in detail in the scientific literature.

The main motivation behind this PhD. project is to contribute to a better knowledge of the processes occurring in the interface between the top soil and the first meters of atmosphere in order to get a more complete picture of the potential risks of CO<sub>2</sub> leakage from industrial CCS projects.

## **2. Abstract**

This PhD project presents the results obtained from experimental and numerical modelling of CO<sub>2</sub> leakage from an artificial leakage site and natural analogues to provide clues for risk assessment in CCS sites. CO<sub>2</sub> is a colourless and odourless gas denser than air, being essential for life on Earth; however, it can be lethal to living beings at high concentrations locally in the atmosphere. Episodic release of CO<sub>2</sub> from underground may lead to such high concentrations and occur from natural processes (i.e., mantle degassing, thermal decarbonation) and could occur in industrial facilities (geological storage of CO<sub>2</sub>-CCS).

The physical interaction between CO<sub>2</sub> and the vadose zone has been studied using experimental data from the PISCO2 pilot plant, located at the ES.CO2 centre in Ponferrada (north Spain). The PISCO2 facilities consist of a set of units where is possible to inject and monitor CO<sub>2</sub> behaviour in the vadose zone. The experiment carried out in this thesis lasted 46 days and injected 62.1 kg of CO<sub>2</sub> through 16 micro-injectors in a 35 m<sup>3</sup> experimental unit filled with coarse sandy material. Injection started with an injection rate of 5 L·h<sup>-1</sup> reaching the maximum possible rate of 60 L·h<sup>-1</sup>, with a pressure of 250 mbar at ambient temperature. Monitoring and mapping of surface CO<sub>2</sub> flux were performed periodically to assess the evolution of CO<sub>2</sub> migration through the soil and to the atmosphere using an accumulation chamber to survey 36 sample points. Wind speed and direction, atmospheric pressure, rain, temperature and humidity were also recorded from a meteorological station in the site. Numerical simulations to reproduce experimental observations were run using TOUGH2 code with EOS7CA research module considering two phases (gas and liquid) and three components (H<sub>2</sub>O, CO<sub>2</sub>, air). The reference case model consists of 31939 regular quadratic elements and reproduces the injection experimental unit. The main observation from the experiment was that compaction had a strong effect on gas fluxes in the vadose zone: after 4 days of injection at minimum rate, CO<sub>2</sub> leakage in the vadose zone quickly comes out through preferential migration pathways and spots with the ranges of fluxes in the ground/surface interface from 2.5 to 600 g·m<sup>-2</sup>·d<sup>-1</sup>. These results show thus that gas channelling in the vadose zone mainly relates to soil compaction, adding significant implications for design-adapted detection and monitoring strategies of early leakage in commercial CO<sub>2</sub> storage. Numerical models confirm the observations made in the PISCO2 experiments. It was also predicted in the models that the presence of water in the system can delay and/or reduce soil emission as seen respectively with rainfall and soil liquid saturation.

Once carbon dioxide is released in the atmosphere its dynamics is initially governed by buoyancy and a gas cloud can accumulate above the ground due to gravitational forces leading to the formation of the so-called “CO<sub>2</sub> lakes”. With time, CO<sub>2</sub> distribution becomes a passive dispersion



governed by wind and atmospheric turbulence. In order to assess the potential impact of the formation of CO<sub>2</sub>-lakes and constrain the atmospheric conditions that promote its persistency, natural analogues of point-source CO<sub>2</sub> emission have been studied in this work. Natural analogues provide evidences of the impact of CO<sub>2</sub> leakage on vegetal cover, wild life and human beings. One of the investigated natural degassing sites in this work is located in a vineyard in the Campo de Calatrava volcanic field in central Spain, which is known for a widespread degassing of mantle-derived CO<sub>2</sub>. This site, called Cañada Real, consists of a 78 m<sup>2</sup> pool of around 6-meter depth with a degassing rate between 1 to 3 tons of CO<sub>2</sub> per day. Gas analysis revealed that the gas emission is almost pure, more than 98% CO<sub>2</sub>. Episodically, the formation of a CO<sub>2</sub> lake has been observed reaching up to 50 cm high. Field work in this thesis consisted of (1) the estimation of the amount of CO<sub>2</sub> emitted from the pool, and (2) measurement of distribution of air CO<sub>2</sub> concentration at different heights (10, 50 100 cm) around the pool (six measurement stations). The Sistema Alta Portata (S.A.P.) has been used to measure the total flux from the pool. This method consists of a plastic, half-spherical blanket with a tube on top. Particular attention must be put on the sealing system to guarantee no leakage at the blanket/soil contact. Using an anemometer, it has been possible to measure the flow at the end of the tube. To understand the atmospheric conditions promoting the accumulation of CO<sub>2</sub> on the ground, atmospheric dispersion modelling has been developed using the TWODEE2 code. A fairly match between model results and field measurements has been attained. The implications for risk assessment from this combined field-model work indicate that the risk for humans even at large emission rates is low due to the CO<sub>2</sub> dispersion effect into the atmosphere, and lethal effects are predicted only under very particular, uncommon conditions.

From the outcome from the Cañada Real site, it can be concluded that the use of atmospheric dispersion numerical models helps predict the dispersion of the CO<sub>2</sub>-enriched gas plume once emitted from underground and allows an accurate map of risk level through time under particular meteorological conditions. Then, the methodology used has been further applied to a larger, topographically more complex emission site, located in central Italy. The site is called Solforata di Pomezia, located in the Alban Hills region near the city of Rome; it is an old native sulphur mine where topography has changed in the last decades. The area between the city of Rome and the Alban Hills underwent volcanic activity during the Quaternary and is characterised by low permeability sedimentary formations that allow the accumulation of gas at shallow depths and surface. For ages, the natural leakage has been observed and previous works estimated the total amount of emitted gas ranging from 44 to 95 t·d<sup>-1</sup>.

In this study, I have performed a number of simulations using the TWODEE2 numerical code considering a set of combined CO<sub>2</sub> soil flux emission and meteorological data from literature. Two probabilistic models with emission rate five and ten times (500 t·d<sup>-1</sup> and 1000 t·d<sup>-1</sup>, respectively) higher than the actual rate have been built to evaluate the safety of the area in case of increase of soil leakage. The results fit well in the range of measured CO<sub>2</sub> concentration in air at distinct heights in the site. The model does not predict lethal gas concentration at heights 1 and 2 m above the ground based on actual soil emission rate (95 t·d<sup>-1</sup>). Model prediction, thus, does not show hazardous levels for humans' health.

### **3. Acknowledgements**

The years spent in Barcelona have been an important stone for my career. First of all, I have to say thanks to my Institute as well as Amphos21 Consulting S.L. for giving me the opportunity to build this PhD. work. Meeting Jordi Bruno at Erice has been the spark that lights the engine, and I thank Jordi for accepting me to work in a company like Amphos21. In Barcelona, I found friendly people in my new house and at the office, special people like Isabel, Asia and Maria Rosa. Once adapted myself to the Catalan daily rhythms I discovered that is possible to live in a big city revelling it.

At Amphos 21 I found a lot of people who helped me and understood my poor Spanish, especially at the beginning, and I say thanks to everybody and sorry if I did not learn much Catalan.

Working as a team with Fidel Grandia and Anthony Credoz has been very pleasant and profitable. Both of them gave me a lot to improve my scientific knowledge. There have been discussions and different ideas but always ended in a general agreement bringing our investigation to high levels with good results. I cannot forget Álvaro Sainz-García who arrived in the second part of my PhD. but carrying a fresh and happy air to the team and two more hands to work in the field. I do not forget David Angel García, working in the PISCO2 project in Ponferrada; he has been a great help during the experiments in the PISCO2 facilities.

Un grazie particolare va ai miei genitori, sempre mi hanno supportato nella mia carriera in Italia come all'estero. Ma questa volta hanno fatto di più tenendo in cura la mia Wilma per due lunghi e pesanti anni, grazie da parte mia e da Wilma a Isabella e Calvino.

Grazie mille a Tutti!

## 4. List of Figures and Tables

**Figure 1.** View of the experimental cell filled with gravel and sand. The service well is located on the left corner.

**Figure 2.** a) Picture showing the injection grid; pinholes are indicated by the red circles; b) Scheme of PISCO2 experimental unit profile.

**Figure 3.** Air temperatures (red squares) and rainfall (blue bars) recorded at PISCO2 site during the injection period.

**Figure 4.** Collection of CO<sub>2</sub> soil-atmosphere fluxes on PISCO2 unit surface.

**Figure 5.** Scheme of the location of the 36 monitoring points (red circles), the 16 CO<sub>2</sub> injectors (blue dots) and the service well (green spot).

**Figure 6.** Scheme of the model domain, from top to bottom: atmosphere boundary, sand layer (25.6 m<sup>3</sup>), gravel layer (3.2 m<sup>3</sup>), 16 injectors (light blue dots).

**Figure 7.** 3D model with the 4 compaction layers in the sand considered in the Model B.

**Figure 8.** Contour map of surface CO<sub>2</sub> flux in PISCO2 using West System accumulation chamber after 4 (a), 21 (b), 32 (c) and 46 (d) days corresponding to injection rates of 5, 20, 40 and 60 L·h<sup>-1</sup>, respectively. The measurement points are shown as red dots.

**Figure 9.** Surface CO<sub>2</sub> flux in each measurement point through time, showing the data for the 8 injection rates. On horizontal axis are reported the 36 sampling points, on the vertical axis the CO<sub>2</sub> flux at surface, symbols are different for every emission rate.

**Figure 10.** Mass balance comparison for the five model simulations.

**Figure 11.** Contour mapping of surface CO<sub>2</sub> flux predicted in the model B after 4 (a), 21 (b), 32 (c), 46 (d) days.

**Figure 12.** Three-dimensional view for the Model B showing the predicted gas velocity with vectors and the CO<sub>2</sub> mass fraction with colours. These parameters are drawn at 4 (a), 21 (b), 32 (c), 46 (d) days after the beginning of the injection.

**Figure 13.** Contour map of surface CO<sub>2</sub> flux predicted in the Model C. The represented times are 4 (a), 21 (b), 32 (c), 46 (d) days respectively.

**Figure 14.** Contour mapping of surface CO<sub>2</sub> flux predicted in the Model E. The represented times are 4 (a), 21 (b), 32 (c), 46 (d) days, respectively.

**Figure 15.** Pressure variations in depth predicted in the numerical simulations. Note that Model C and Model B show the same trend.

**Figure 16.** Root mean square error for the field experiment (red line) and the numerical models (model A green line; model B purple line; model C sky blue; model D orange line; model E blue line).

**Figure 17.** Comparison of experimental CO<sub>2</sub> flow map (on the left) and predicted flows in Model B (on the right).

**Figure 18.** Example of channelled emission and flow through very small spots in the Campo de Calatrava natural analogue (central Spain). On the bottom of the picture two spots (red circles) of high CO<sub>2</sub> (trace gases) flux (>5000 g·m<sup>-2</sup>·d<sup>-1</sup>); background emission (<20 g·m<sup>-2</sup>·d<sup>-1</sup>) related to biological activity found in the surrounding area.

**Figure 19.** Model B liquid saturation after 46 days of simulation.

**Figure 20.** Morfostructural map of the area around Cañada Real, location of the investigation site is marked by the red square (from IGME, 1983).

**Figure 21.** Aerial view of the Cañada Real site, showing the location of the air CO<sub>2</sub> concentration measurement stations (denoted as A to F).

**Figure 22.** a) Formation of a CO<sub>2</sub> lake visible in the Cañada Real site, b) View of the Cañada Real site after lighting a smoke flare. The smoke (yellow) is not able to rise due to the denser blanketed of the CO<sub>2</sub>-enriched air.

**Figure 23.** The SAP system installed and working at Cañada Real site. Note the pipe connected to the centre of the blanket to determine gas flux.

**Figure 24.** Rose diagram of dominant hourly winds. Wind directions that were dominant for one hour are plotted by short triangles, bigger triangles show wind directions that were dominant twice.

**Figure 25.** Air CO<sub>2</sub> concentration (ppm) recorded at stations A, B, C, D, E and F (see Fig 21 around the pool at different heights (10, 50 and 100 cm). The detection limit of the Telaire is 10000 ppm.

**Figure 26.** Map of the air CO<sub>2</sub> concentration for simulation S1 and S3 with an emission rate of 3 t·d<sup>-1</sup> at 980 and 1040 hPa respectively. Outputs are at 10 cm (A, B), 50 cm (C, D), 100 cm (E, F) high.

**Figure 27.** Map of the air CO<sub>2</sub> concentration for simulation S4a with an emission rate of 3 t·d<sup>-1</sup> at 980 hPa and with a wind speed of 1 m·s<sup>-1</sup>. Outputs are at 10 cm (A), 50 cm (B), 100 cm (C) high.

**Figure 28.** Comparison between box plot diagrams of CO<sub>2</sub> concentration measured on the field (purple) and that predicted by the simulation S1 (green), for the six monitoring stations at 50 cm above the ground surface.

**Figure 29.** Comparison between air CO<sub>2</sub> concentration measured on the field and that predicted by the simulation S1 for the six monitoring stations at 100 cm from surface. Experimental data have capital letters and purple boxes, numerical data have lowercase letters and blue boxes.

**Figure 30.** Extension and maximum height of the plume with a CO<sub>2</sub> concentration above the 3% threshold for simulations S1 (a), S3 (b), and S4a (c).

**Figure 31.** Aerial view of the Solforata di Pomezia, along its main axis. Picture taken from Google Maps. The red segments outline the area mined in the past for sulphur; the green circle shows an episodic flooded area.

**Figure 32.** Tectonic map of the Tyrrhenian margin of the Central Italy Peninsula (from Acocella et al., 1999). The location of Solforata di Pomezia is highlighted by a red dot.

**Figure 33.** Views of the Solforata di Pomezia site: vegetation, lakes and dry soil.

**Figure 34.** Example of gas emission point source at the Solforata di Pomezia in the summer period.

**Figure 35.** CO<sub>2</sub> soil flux map in the Solforata di Pomezia from Carapezza et al., (2012). Black dots are the 278 sampling points and numbered segments are TDL profiles. White area denotes the lake, where no measurements were performed.

**Figure 36.** Main emission points (white ellipses) around the pool (white rectangle).

**Figure 37.** CO<sub>2</sub> air concentration measured by TDL (orange line) and wind speed (blue line), during May 11th 2007 by Carapezza et al., (2012).

**Figure 38.** CO<sub>2</sub> air concentration measured by TDL (orange line) and wind speed (blue line), during May 14<sup>th</sup> and 15<sup>th</sup> 2007 by Carapezza et al., (2012).

**Figure 39.** Wind speed recorded at the Solforata di Pomezia during the days May 14<sup>th</sup> and 15<sup>th</sup> 2007 by Carapezza et al., (2012).

**Figure 40.** Air temperature versus CO<sub>2</sub> soil emission (data from Carapezza et al., 2012).

**Figure 41.** Measured (blue line) and predicted (red line) air CO<sub>2</sub> concentration.

**Figure 42** Plume dispersion at 25 cm height for S1 after 2.5 hours of simulation, for S2 after 4.5 hours, for S3 after 1 hour and for S4 after half an hour.

**Figure 43.** Prediction of the gas plume dispersion in model S1 at 25 cm high for 6, 12 and 18 h of simulation time.

**Figure 44.** Prediction of the gas plume dispersion in model S2 at 25 cm high for 6, 12 and 18 h of simulation time.

**Figure 45.** Prediction of the gas plume dispersion in models S3 and S4 at 25 cm height after 18 h of simulation time.

**Figure 46.** Predicted CO<sub>2</sub> air concentration for model S1 outputs at 1 metre and 2 metres high.

**Figure 47.** Predicted CO<sub>2</sub> air concentration for model S3 outputs at 1 metre and 2 metres high.

**Figure 48.** Predicted CO<sub>2</sub> air concentration for model S4 outputs at 1 metre and 2 metres high.

**Figure 49.** PISCO2 1-D (on the right) and 2-D (on the left) conceptual models. In Appendix 1.

**Figure 50.** Gas saturation charts at 1 minute (a), 1 hour (b), 4 hours (c) and 1 day (d).

**Figure 51.** Gas flow charts at 1 minute (a), 1 hour (b), 4 hours (c) and 1 day (d).

**Figure 52.** Gas saturation charts at 1 minute (a), 1 hour (b), 4 hours (c) and 1 day (d).

**Figure 53.** Gas flow plots at 1 minute (a), 1 hour (b), 4 hours (c) and 1 day (d).

**Figure 54.** Gas saturation charts at 1 minute (a), 1 hour (b), 4 hours (c) and 1 day (d).

**Figure 55.** Gas flow charts at 1 minute (a), 1 hour (b), 4 hours (c) and 1 day (d).

**Figure 56.** Gas saturation charts at 1 minute (a), 1 hour (b), 4 hours (c) and 1 day (d).

**Figure 57.** Gas flow charts at 1 minute (a), 1 hour (b), 4 hours (c) and 1 day (d).

**Figure 58.** Gas saturation charts at 1 minute (a), 1 hour (b), 4 hours (c) and 1 day (d).

**Figure 59.** Gas flow charts at 1 minute (a), 1 hour (b), 4 hours (c) and 1 day (d).

**Table 1.** Limits and effects on human beings on exposed to CO<sub>2</sub> (Baxter et al., 1999; Faivre-Pierret and Le Guern, 1983 and references therein; NIOSH, 1981).

**Table 2.** EOS module updating record in TOUGH2.

**Table 3.** Timetable for experimental injection and rates in June and July 2012

**Table 4.** Soil properties and Van Genuchten parameters for filling materials in the PISCO2 unit.

**Table 5.** List of numerical simulations and their distinctive features.

**Table 6.** Characteristics of permeability and porosity for the 4 layers introduced in Model B.

**Table 7.** Final liquid saturation predicted in each simulation.

**Table 8.** Root mean square errors data for the field experiment and each simulation model.

**Table 9.** Maximum, minimum and mean value of CO<sub>2</sub> surface flux for the field experiment and the five numerical models.

**Table 10.** Comparison between the leakage rate used by Oldenburg and Unger (2004) and those obtained at the PISCO2 experimental unit and from our Model B.

**Table 11.** List of simulations with the corresponding features.

**Table 12.** Data of flow speed (maximum and average), humidity and temperature at the SAP's outlet. The uncertainty for each measurement is also shown.

**Table 13.** Predicted maximum air CO<sub>2</sub> concentration in the Cañada Real site for simulations S1 and S4a, and calculated elevation reaching hazardous 3% CO<sub>2</sub> concentration threshold.

**Table 14.** Air CO<sub>2</sub> concentration measured by TDL profiles at Solforata di Pomezia (from Carapezza et al., 2012).

**Table 15.** Simulation features of the four models performed.



**Table 16.** Mesh A: atmosphere in blue, sand in yellow, gravel in green and concrete in grey. In Appendix 1.

**Table 17.** Mesh B: atmosphere in blue, sand in yellow, gravel in green and concrete in grey. In Appendix 1.

**Table 18.** Mesh C: atmosphere in blue, sand in yellow, gravel in green and concrete in grey. In Appendix 1.

**Table 19.** Data of porosity for relevant materials in the PISCO2 project (from Sanders et al.,1998, and Oldenburg and Unger, 2004). In Appendix 1.

**Table 20.** Porosity values selected for sensibility study. In Appendix 1.

**Table 21.** Range of permeability in literature. In Appendix 1.

**Table 22.** Permeability values for sensibility study. In Appendix 1.

**Table 23.** Van Genuchten parameters selected from literature. In Appendix 1.

**Table 24.** Lambda values for sensibility study. In Appendix 1.

**Table 25.** P0 values for sensibility test. In Appendix 1.

**Table 26.** Saturation values for sensibility test. In Appendix 1.

## **5. Structure of the PhD dissertation**

The core of this PhD. manuscript consists of three chapters that correspond to scientific articles that have already been published in international peer-review journals at the time of PhD. dissertation.

The first article (Section 8 in the manuscript) deals with numerical modelling of the unsaturated zone; many studies of deep aquifers are presented in literature but very few deal with the gas and liquid migration in the vadose zone, and this chapter intends to cover part of this gap.

The other two papers (Sections 9 and 10) are studies on processes occurring in the interface between top soil and atmosphere in natural analogues of underground CO<sub>2</sub>-emission; the intention is to numerically assess the potential risk related to these emissions and to extrapolate the results to CCS industrial projects. In Section 9, the Campo de Calatrava (Central Spain) natural analogue has been studied. From the outcome of this research, this area has resulted useful to test the ability of atmospheric dispersion codes to simulate point-source emission. In addition, field measurements of CO<sub>2</sub> fluxes have been tested in this site during the PhD. project, such as the Sistema Alta Portata (S.A.P.).

The Solfiorata di Pomezia (Central Italy) study is shown in Section 10. This site was selected to quantify the gas emission and accumulation on ground by using atmospheric dispersion calculations. This site is well known from the geological point of view, and emits continuously natural gases like CO<sub>2</sub> and H<sub>2</sub>S which accumulate on the ground under some weather conditions. A number of scenarios have been numerically modelled to evaluate the risk for organisms living around the site and to better understand possible risk scenarios related to CCS operations.

In addition to these three articles, this PhD. manuscript also includes a section on the background of the leakage of CO<sub>2</sub> from underground along with the state-of-the-art of main topics dealt in this work (Section 6). Also, a short description of the numerical tools used is included (Section 7). Finally, sections on general discussion and conclusions are provided to put the findings of this work in the CCS context.

## **6. PhD. background**

### **6.1. The risk of leakage in geological carbon storage**

Geological storage has raised in last decades as an effective way to reduce anthropogenic CO<sub>2</sub> emission into the atmosphere. Once captured, carbon dioxide is stored in deep (800 m depth) hosting rocks (reservoir) where is trapped in different ways (physical, residual, solubility and mineral trapping). The potential risks of geological CO<sub>2</sub> storage must be understood and geologists are required to predict how CO<sub>2</sub> may behave once stored underground (Votattorni et al., 2009). Since processes occurring during CO<sub>2</sub> stored underground are quite difficult to observe, valuable information can be obtained from either pilot plant experiments and from natural analogues. Natural analogues are those systems found in nature that show physical/geochemical/geological/biological processes that could occur in a man-made facility, such as underground waste and energy disposal. The main advantage of natural analogues is that long-term processes (e.g., impacts of chemical reactions, genetic mutation on biota, ...) can be better observed and characterized compared to laboratory-based, short-term experiments. Concerning CCS, gas leakage from reservoir formation to shallow levels and atmosphere is one of the topics that can be studied in natural analogues since its impact on aquifers, ecosystems and atmosphere can take years and cannot be assessed from present-day industrial underground injection project, which are too “young”, 30-40 years old as much. Gas leakage of natural carbon dioxide occurs in a large number of geological environments like in volcanic regions (active and quiescent), geothermal areas and sedimentary basins. Hazardous CO<sub>2</sub> concentration in atmosphere related to underground emission has been occasionally reported although the conditions favouring the persistence of such a concentration are barely studied. It should be noted, however, that in some environments the rates of CO<sub>2</sub> accumulation of natural geologic reservoirs may not be comparable to (i.e., may be much lower) CO<sub>2</sub> injection rates at storage sites. In these cases, natural analogues may not provide information on processes related to relatively rapid injection rates, such as pressure-induced geomechanical damage (Lewicki et al., 2007). It is worth mentioning that the study of natural analogues is also valid for the test and improvement of leakage monitoring techniques.

Despite a mandatory feasibility study, the reservoir can release the stored CO<sub>2</sub> due to geomechanical disturbance (fractures, fault reactivation, quakes, well-seal integrity, etc.), technical problems (head pressure, injection pressure, wellbore integrity), and geochemical attack (cement degradation and casing corrosion). Therefore, the environmental impact assessment is very relevant for a geological storage site; this assessment is based on a risk analysis that considers the data obtained on field and from numerical modelling. The mapping of risk is an important step to forecast future

affected areas by soil degassing and atmospheric gas dispersion. Continuous monitoring of a CCS site is required during the different phases of a project (pre-, sin- and post-injection).

Underground stored gases use preferential pathways to reach surface so that gas flow maps are the main tool to know where leakage occur at surface. Carbon dioxide is a heavy gas denser than air and, therefore, particular attention must be paid when comes out to the soil/atmosphere interface. CO<sub>2</sub> tends to accumulate in topographic depressions and due to its odourless and colourless characteristics is hazardous at high concentrations. CO<sub>2</sub> atmospheric concentration is 400 ppm, so at this range of concentration is innocuous. Many plants can live even in areas with very high CO<sub>2</sub> concentrations and the right amount of CO<sub>2</sub> dissolved in water can help plants growth, but for human beings can be a dangerous lethal gas. To illustrate this impact, Table 1 reports the exposure limits and the relative health effects on humans when exposed to CO<sub>2</sub> inhalation.

**Table 1.** Limits and effects on human beings on exposed to CO<sub>2</sub> (Baxter et al., 1999; Faivre-Pierret and Le Guern, 1983 and references therein; NIOSH, 1981).

<b>Exposure limits</b> (CO <sub>2</sub> % in air)	<b>Health Effects</b>
2-3	Unnoticed at rest, but on exertion there may be marked shortness of breath.
3	Breathing becomes noticeably deeper and more frequent at rest.
3-5	Breathing rhythm accelerates. Repeated exposure provokes headaches.
5	Breathing becomes extremely laboured, headaches, sweating and bounding pulse.
7.5	Rapid breathing, increased heart rate, headaches, sweating, dizziness, shortness of breath, muscular weakness, loss of mental abilities, drowsiness, and ringing in the ears.
8-15	Headache, vertigo, vomiting, loss of consciousness and possibly death if the patient is not immediately given oxygen.
10	Respiratory distress develops rapidly with loss of consciousness in 10-15 minutes.
15	Lethal concentration, exposure to levels above this is intolerable.
25+	Convulsions occur and rapid loss of consciousness ensues after a few breaths. Death will occur if level is maintained.

Once emitted to the atmosphere from a point source, CO<sub>2</sub> can be dispersed by airflows and turbulence but also can be accumulated on the ground favoured by topography depressions. Wind dispersion is a very complex process due to the presence of different sized eddies in atmospheric flow and it is not easy to reproduce in laboratory. However, through numerical modelling is possible to draw a picture of the real system and taking into account different features (like topography, regional roughness, emission source, emission rate, meteorological data) and calculate the CO<sub>2</sub> concentration downwind of the source. Prediction of the dispersion of a CO<sub>2</sub> plume allows the calculations of probability risk maps that point out the possible affected areas at different heights. To produce risk maps for a selected site it is important to create a database with meteorological data and soil gas survey. The first one is needed to model different atmospheric conditions based on recorded data; the second one is essential to know the emission rate and to recognize the main emission area. The comparison between field data and model calculations is needed to confirm that atmospheric modelling can be included as a valuable methodology in the risk assessment of leakage in natural degassing systems and in CCS projects.

The release of CO<sub>2</sub> to the atmosphere from underground is affected by physical processes occurring in the vadose zone and in the interface with atmosphere. These processes have been studied in the past at small scale in the laboratory but some gaps are still needed to be covered. The PISCO2 (*Planta de Inyección de CO<sub>2</sub> en Suelos*) project, hosted by Fundación Ciudad de la Energía and funded by the EERP EC (OXY-CFB300, <http://compostillaproject.es/>) program intended to provide new clues on the physical and biological processes occurring in the soil-atmosphere interface at large (meter-sized) scale. The PISCO2 experimental platform was operating since October 2011, and consisted of 18 experimental units of 16 square meters (squares of 4×4 m) with a depth of 2.2 meters, equipped with a CO<sub>2</sub> injection system, drainage and irrigation system along with a series of control instrumentation/equipment. Each unit had a service pipe with an installed drainage pump and a piezometer to control the water table level of the cell; CO<sub>2</sub> injection was regulated by electro-valves. The general objective of this project was to predict how the injected CO<sub>2</sub> would move laterally and vertically and to determine the critical parameters that would affect the ecosystems.

This PhD. is intended to provide clues on processes occurring in the interface between the upper part of the geosphere, i.e., top soil and the atmosphere. Two different parts of this interface have been studied: the vadose zone and the first-meter column of atmospheric air. The work has been developed in the PISCO2 facilities and in two natural occurrences of CO<sub>2</sub> emission from point sources, considered to be natural analogues of potential leakage in carbon storage commercial projects. The

general methodology applied in this work combine field measurements with numerical model calculations following the next steps:

- Set-up of a conceptual model to identify the main parameters controlling gas dynamics.
- Selection of data needed and methodologies for field measurements.
- Selection of a numerical tool for modelling purposes.
- Treatment of field data measurements.
- Calibration of numerical models from comparison of field data.
- Interpretation of results and determination of potential implications for risk assessment of CCS projects.

## **6.2.State of the art of CO<sub>2</sub> investigation in the unsaturated zone**

As CO<sub>2</sub> geological storage has been considered one of the options technologically viable in order to decrease the industrial emissions of this gas species that strongly contribute to the greenhouse effect in the atmosphere (IPCC, 2005), a number of CCS projects at international level has been programmed. At early stage, the projects focused on the research of suitable reservoirs that can host and trap carbon dioxide. Meanwhile, a series of numerical codes were improved to model the CO<sub>2</sub> injection and long-term storage interaction with the host rocks by including the capability of simulating coupled physical, chemical and geological conditions at reservoir and the caprock level. At that stage, the first international projects of CCS were: The Sleipner Project (Norway, 1996), the Great Plains Project (Weyburn) (Canada, 2000), and the In Salah project (Algeria, 2004). On the other hand, a new challenge started with the monitoring of a CO<sub>2</sub> storage site both in depth and on surface, since there were a number of circumstances that could cause CO<sub>2</sub> seepage and leakage.

An important aspect in the study of gas leakage was the CO<sub>2</sub> migration in the vadose zone, i.e., the uppermost layer of the soil. Early models dealing with this problem were based on the assumption that the principal transport mechanism for CO<sub>2</sub> is molecular diffusion (Van Bavel, 1951; De Jong and Schappert 1972; Salomon and Cerling, 1987) and did not consider other transport mechanisms or the influence of water flow and airflow. The following numerical codes were implemented with diffusive flow, viscous flow, combined flow, and pressure flow. Papendick and Runkles (1965, 1966) and Kowalik et al., (1979) developed analytical solutions for oxygen transport based on Fick's second law of diffusion. The physical processes that are involved in gas transport in the vadose zone are complex. Both diffusion and pressure flow may contribute significantly to the transport process. Moreover, the pores that comprise many soils are of such a size that at atmospheric pressure the gas molecules collide with the soil as well as with each other (Massmann and Farrier, 1992).

Since 2003 few projects focused on the monitoring techniques applied to CO<sub>2</sub> leakage detection. The CO<sub>2</sub> Field Lab in Norway (2008) planned controlled injection of CO<sub>2</sub> into the aquifer in the Svelvik ridge, and CO<sub>2</sub> displacement in the subsurface and at the surface would be monitored through assessing monitoring technologies for detection of CO<sub>2</sub> migration and ultimately leakage; the project aimed to provide a validated monitoring system through a protocol and certification scheme. The Zero Emission Research and Technology (ZERT, 2009) is a controlled field pilot developed in Bozeman, Montana, USA, to study near surface CO<sub>2</sub> transport and detection technologies. The ASGARD project (Artificial soil gassing and response detection) started in 2006 aiming to determine the effects of elevated soil CO<sub>2</sub> on crops, soil microbiology, soil flux and soil CO<sub>2</sub> concentration. Another project, called CO<sub>2</sub>CRC, started in 2003 at their research site in south west Victoria (Australia), and CO<sub>2</sub> was injected deep underground into a depleted gas reservoir and a saline formation to study how CO<sub>2</sub> interacted with geological fractures and developing less expensive and innovative ways of monitoring the CO<sub>2</sub>. The Ressacada's Farm in Brazil is a project started in 2012 and sponsored by Petrobras. It consisted of the injection of CO<sub>2</sub> between 3 and 8 meters depth in Quaternary deposits composed primarily of coarse sandy, unconsolidated sediments. The goal of this project was to rank the best, most cost-effective measuring, monitoring and verification technology alternatives. The CO<sub>2</sub> Vadose Project started in France in 2013 to also study CO<sub>2</sub> leakage migration under controlled conditions along the carbonate-rich vadose zone and to test geochemical and geophysical detection techniques. The CO<sub>2</sub> was injected at 8-meter depth in an underground quarry.

### **6.3.State of the art of atmospheric dispersion modelling for risk assessment**

Atmospheric dispersion modelling is the analytical and numerical simulations of how gases disperse in the atmosphere considering the complexity of meteorological conditions and the gas emission characteristics. The dispersion models are used to estimate and predict the downwind concentration of a contaminant emitted in air from a source. Gas atmospheric dispersion happens when a gas or a vapour emission is released into the atmosphere. It could be a leakage from the soil, factory chimneys, surface leakage of volatile compounds or pool evaporation. When such gas enters in contact with the atmosphere it scatters by dilution in it and expands by wind, meteorological conditions and topography. Thus, dispersion depends mainly on the weather conditions, topography, gas characteristics and on the emission type (continuous or discontinuous). Early studies of atmospheric dispersion date back to 1950s and 1960s, and were developed on military applications

for chemical, biological and nuclear weapons. Late in the 1960s, environmental control regulations were provided so there was a huge growth in the use of air pollutant plume dispersion calculations.

There are two methods for modelling the atmospheric dispersion of pollutants. Firstly, the Eulerian method determines concentration values for fixed points in the space using the advection-diffusion equation. On the other hand, the Lagrangian method simulates the spatial and temporal evolution for an air bulk. Both methods are deterministic mathematical models, based on a quantitative determination of the spatial-temporal evolution of concentration of pollutants in the atmosphere. The dispersion of pollutants in the atmosphere depends on meteorological conditions as well as the properties of the emissions in question.

The atmosphere is a complex system with interactions on a wide range of scales, from microphysical processes and chemistry, to global energy fluxes and Rossby waves. Such a complexity makes hard to study the atmosphere as a whole, but in some cases the application of numerical modelling and risk forecasting of atmospheric pollutants is critical for human safety. Likely, the most illustrative example is found in the prediction of ash emission from active volcanic areas, which is crucial to ensure safe flight conditions in commercial aviation.

## **7. Modelling tools and basics of formulation implemented**

### **7.1. TOUGH family numerical codes**

For the modelling of the CO<sub>2</sub> dynamics in the vadose zone, the TOUGH2 (Pruess et al., 1999) has been selected for 1D calculations since it can handle different features and settings concerning the conceptual model of PISCO2 experiments. These features are:

- Porous medium. The atmosphere can be considered as a 99,9% porous medium;
- Multiphase flow: liquid and gaseous phases interacting with water and air;
- Complexity of hydraulic conductivity and relative permeability function and capillary pressure for each material;
- Flow simulation in 1-D, 2-D and 3-D dimensions;
- Water table variations and water and gas saturation in soil;
- Consideration of one or more injecting points and variable injection rate (kg/s);
- Atmospheric influence on liquid and gaseous phase in the first soil centimeters.



TOUGH2 can handle with simulations of non-isothermal flow of multi-components and multi-phases in a porous medium or fractured material in 1-D, 2-D and 3-D. TOUGH2 is commonly used for engineering calculations of aquifers and geothermal reservoirs, nuclear waste disposal, environmental evaluation and remediation, hydrogeology in the unsaturated and saturated zone, and CO<sub>2</sub> geological storage.

The PISCO2 conceptual model includes the injection of CO<sub>2</sub> in air-filled unsaturated zones. This means that gas phase needs to be considered as a fluid with a variable composition (basically due to mixing). However, as first step, the model calculations in this work have assumed the injection of a semi ideal gaseous fluid with low solubility like air, in order to understand better all the transport processes that can act in the PISCO2 experiments. Besides, choosing air as injecting gas allows the use of TOUGH2 instead of more complex codes.

TOUGH2 integrates a number of modules regarding fluids properties. These modules are based on theoretical and empirical equations of state (EOS). The EOS3 module has been selected to simulate gas injection (air) in the vadose zone and contains thermo-physical properties described by Pruess and Wang (1987).

Within the set of modules available within the commercial license of TOUGH2, none allows the CO<sub>2</sub> component to be taken into account in the unsaturated zone. But the experimental (non-commercial) EOS7CA module developed by Oldenburg and Unger (2004) has the capability to do so, and it has been used in this work to simulate the migration of CO<sub>2</sub> leaks from a shallow aquifer to the ground and surface.

### ***7.1.1. EOS3 module (water, air) in TOUGH2***

This module is an update of the EOS module of the TOUGH simulator, with the same thermo-physical property model (Pruess and Wang, 1987). All water properties are represented by the steam table equations as given by the International Formulation Committee (1987). Air is approximated as an ideal gas, and additivity is assumed for air and vapour partial pressures in the gas phase,  $P_g = P_a + P_v$ . The viscosity of air-vapour mixtures is computed from a formulation given by Hirschfelder et al., (1954). The solubility of air in liquid water is represented by Henry's law.

EOS3 differs from the EOS module of TOUGH in one important aspect: the choice of temperature to be the third primary variable between thermodynamic variables.

This equation of state was used for the 1-D and 2-D modelling in Section 8.

### 7.1.2. EOS7CA module (modelling of systems with water, brine, non-condensable gas, gas tracers, air heat)

EOS7CA is related to a series of modules derived from the EOS3 module. The general conservation equations solved in TOUGH2 for simulating multicomponent and multiphase flow and transport in porous media are presented in Pruess et al., (1999; 2011).

The EOS7CA module has the capability of modelling two phases (gas and aqueous), and five components (water, brine, non-condensable gas, gas tracer, and air) plus heat in shallow subsurface systems. The non-condensable gas (NCG) can be chosen by the user as either carbon dioxide (CO<sub>2</sub>), nitrogen (N<sub>2</sub>), or methane (CH<sub>4</sub>).

#### Density

Accurate data on density, viscosity, and enthalpy of the gas mixtures are included in EOS7CA through the use of a real gas properties module ZEVCA. The real gas properties module has options for Peng-Robinson, Redlich-Kwong, or Soave-Redlich-Kwong equations of state to calculate gas mixture density, enthalpy departure, and viscosity as described by Reid et al., (1987), and Poling et al., (2000). Transport of the gaseous and dissolved components is by advection and Fickian molecular diffusion.

The approach taken in EOS7CA is to use the equation of state to calculate the Z factor of the mixture, where:

$$PV = ZnRT \quad (\text{eq. 1})$$

From this value, the density of the gas mixture can be calculated using:

$$\rho = \frac{MW n}{V} = \frac{P MW}{Z RT} \quad (\text{eq. 2})$$

where the MW is the molecular weight of the real gas mixture. Enthalpy real-gas mixtures depart from ideality in a way that can be modelled with cubic equations of state. The enthalpy of the real-gas mixtures is calculated using an ideal gas value with an added enthalpy departure to account for real gas effects. In ZEVCA, enthalpy is calculated as:

$$H = (H - H^{ig}) + H^{ig} = (H - H^{ig}) + \sum_i X^i H^{i,ig} \quad (\text{eq. 3})$$

where  $(H-H^{ig})$  is the enthalpy departure. ZEVCA uses cubic equations of state (e.g., Peng-Robinson) to calculate the enthalpy departures and ideal gas enthalpy change to come up with the total enthalpy change of the real gas mixture.

Standard TOUGH2 (Pruess et al., 1999, 2011) uses real-gas properties (steam tables) for steam enthalpy, and, thus produces, more accurate steam enthalpies than the cubic equations of state can provide. The user can choose to use the steam tables to calculate the enthalpy of the steam (water vapour) fraction in the gas, and ZEVCA to calculate the enthalpy of the NCG and air mixture fraction. The total gas mixture enthalpy is then calculated as a weighted combination of the SUPST and ZEVCA contributions. The reference state for enthalpy calculations in ZEVCA is normalized to agree with standard TOUGH2 and the NIST Chemistry Web Book (NIST, 2013), i.e., internal energy is zero for saturated liquid at 273.16 K (0.01 °C).

### Viscosity

Another important transport property for gas flow and transport is the viscosity of the real gas mixture. ZEVCA uses the method by Chung et al., (1988) as described in Reid et al., (1987) and Poling et al., (2000). This method is accurate to within 5-10% for the range of conditions expected in subsurface natural gas reservoirs. Solubility of gas mixture components solubility of the gas components (i) is modelled using Henry's Law, e.g.:

$$P^i = K_h^i x_{aq}^i \quad (\text{eq. 4})$$

where  $K_h^i$  is generally dependent on temperature. For the NCG component, the partial pressure of the NCG, e.g.,  $P_{CO_2}$  for CO<sub>2</sub>, is related to the mole fraction of CO<sub>2</sub> in the aqueous phase ( $X_{aq}^{CO_2}$ ) by Henry's Law where temperature dependence of  $K_h$  is calculated by the models of Cramer (1982), and D'Amore and Truesdell (1988) similar to the approach of TOUGH2/EWASG (Battistelli et al., 1997). In EOS3,  $K_h^{air}$  was approximated as  $1.0 \times 10^{10}$  Pa, i.e., temperature dependence was ignored for the solubility of air in water. In EOS7, salinity-dependence of  $K_h^{air}$  was included by increasing  $K_h^{air}$  in aqueous solutions with higher brine mass fractions. EOS7CA retains these EOS3 and EOS7 approaches to preserve continuity with EOS3 and EOS7, and extends the methods by assuming for expediency that the same effects of brine on air solubility occur also for NCG and tracer components. For example, if the Henry's Law coefficient for air in pure water and in brine at the local brine concentration are  $K_{h,H_2O}^{air}$  and  $K_{h,brine}^{air}$ , respectively, then the Henry's Law coefficient for NCG in pure water at a given temperature would be multiplied by the ratio  $K_{h,brine}^{air} / K_{h,H_2O}^{air}$  to obtain the value for the NCG Henry's Law coefficient at the given brine mass fraction. The Henry's Law

approach in EOS7CA is accurate for low-pressure conditions ( $P < 10$  bar or 1 Mpa), but overrates solubility at larger pressures.

### ***Molecular Diffusion***

EOS7CA v. 1.0 includes binary diffusion of the chemical components dissolved in aqueous and gas phases as discussed in the TOUGH2 User Guide (Pruess et al., 1999; 2011). TOUGH2 includes pressure and temperature effects on gas-phase diffusion. Specifically, molecular diffusivity is assumed to be inversely proportional to pressure ( $P$ ) by the factor  $1.0 \times 10^5/P$  (Pruess et al., 2011). For example, if pressure is  $2 \times 10^5$  Pa, the corresponding effective molecular diffusivity for the gas is one-half the input value which is referenced to  $1.0 \times 10^5$  Pa. This approach overestimates diffusivity for CO<sub>2</sub> mixtures above approximately 20 bars (Poling et al., 2000), with a total over-prediction of a factor of two at  $P = 100$  bars. Temperature effects on diffusion are also modelled by inclusion of the factor  $((T + 273.15)/273.15)^{T_{EXP}}$  (Pruess et al., 2011). If molecular diffusivity is input as a negative number in TOUGH2, the absolute value of this number is used for the phase molecular diffusivity without modification by pressure or temperature or  $S$  and  $\tau$  (saturation and tortuosity). Further details are referred to Pruess et al., (2011).

### ***Implementation of real gas components***

As shown in Table 2, EOS7CA was developed by changing the volatile radionuclide components of EOS7R into a non-condensable gas (NCG) component (CO<sub>2</sub>, N<sub>2</sub>, or CH<sub>4</sub>, as specified by the user through input parameter), and a volatile tracer. One mole of air in EOS7CA is treated internally as a mixture of 0.79 moles N<sub>2</sub> and 0.21 moles O<sub>2</sub> for calculation of gas mixture properties in ZEVCA. The properties (density and viscosity) of the whole gas mixture containing potentially water vapour, NCG, and air are calculated using ZEVCA (e.g., with Peng-Robinson equation of state). The solubility of the gas components is modelled using Henry's Law. EOS7CA is designed for two-phase conditions (i.e., gas and aqueous phases present) in the shallow subsurface and very limited testing has been done for single-phase conditions. In two-phase conditions, vapour pressure is independent of salinity of the aqueous phase. As the brine component is non-volatile, vaporization would tend to increase brine mass fractions in the aqueous phase beyond unity. Users need to be aware of this possibility, which arises from the fact that EOS7CA, like EOS7, represents the aqueous phase as a mixture of water and brine, not as a mixture of water and salt. Therefore, EOS7CA cannot be used for processes in which solubility limits would be reached, at which point solid salt would

precipitate. The tracer component in EOS7CA does not affect gas properties and is expected to exist only in trace concentrations (e.g., mass fractions of order 10<sup>-6</sup>).

**Table 2.** EOS module updating record in TOUGH2.

TOUGH2 Module	Components	Added Capability
EOS3	Water, air, heat	
EOS7	Water, brine, air, heat	Dense brine
EOS7R	Water, brine, parent radionuclide, daughter radionuclide, air, heat	Decay, adsorption, volatilization of radionuclides in trace concentrations.
EOS7CA	Water, brine, NCG (CO <sub>2</sub> , N <sub>2</sub> , or CH <sub>4</sub> ), gas tracer, air, heat	Real gas mixture properties, solubility model limited to low-pressure systems
EOS7C	Water, brine, CO <sub>2</sub> (or N <sub>2</sub> ), gas tracer, CH <sub>4</sub> , heat	Real gas mixture properties and accurate solubility model for high-pressure systems

## 7.2. TWODEE2 software for atmospheric dispersion modelling

TWODEE-2 is a shallow layer time-dependant Eulerian model for dispersion of heavy gases, written in FORTRAN 90 code that it has been derived from the optimization and improvement of a previous FORTRAN 77 code named TWODEE (Hankin and Britter, 1999a, b, c).

Under stable atmospheric conditions and/or in presence of topographic depressions, gas concentrations (e.g., CO<sub>2</sub>) can reach high values resulting in lethal effect to humans and animals. In fact, several episodes of this phenomenon were recorded at different areas in central Italy (Rogie et al., 2000). The cloud dispersion of gases denser than air released from natural sources is governed by gravity and by the effects of lateral eddies which decrease the plume density through the incorporation of surrounding air. In the initial phase the buoyancy controls the gas dispersion and the cloud follows the ground (gravitational phase); in contrast, when the density contrast becomes less important, gas dispersion is mainly governed by wind and atmospheric turbulence (passive dispersion phase) (Costa et al., 2005; Folch et al., 2007).

TWODEE2 is based on depth-averaged equations obtained by interpreting mass, density and momentum equations over the fluid depth, from the bottom up to free surface. Such an approach is

able to describe the cloud as function of time and of the two-dimensional ground positions, in term of four variables: cloud depth, two depth-averaged horizontal velocities and depth-averaged cloud concentration (Folch et al., 2007). About wind and its effects, two options are available in this software: (1) a uniform wind and (2) a spatially variable wind. In the first option, wind is considered horizontally uniform and wind data are read from the wind data file, provided by a ground-based station. For the second option, data at height  $z=z_{ref}$  are provided by the program DIAGNO, a meteorological processor that reads data at a point of the domain and assimilating terrain information, generates a zero-divergence wind field ( $u_x, u_y, u_z$ ) in a terrain following coordinate system  $x=x', y=y', z=z'-h(x'-y')$ . The vertical wind profile is described by the Monin-Obukhov Similarity Theory (MOST) as:

$$U_a(z) = \frac{u_*}{K} \left[ \ln\left(\frac{z}{z_0}\right) - \psi_m\left(\frac{z}{L}\right) \right] \quad (\text{eq. 5})$$

where  $K$  is the von Karman constant,  $z_0$  the roughness length,  $u_*$  the friction velocity,  $L$  the Monin-Obukhov length and  $\psi_m$  denotes the classical stability function for the momentum (Jacobson, 1999).  $L$  and  $u_*$  are estimated using the non-iterative method of Louis (1979) based on the bulk Richardson number  $Ri_b$  (Jacobson, 1999).

The inputs to the model are topography, terrain roughness, wind measurements from meteorological stations and gas flow rate from the ground sources. Optionally the model can be coupled with the output of a meteorological processor that generates a zero-divergence wind field incorporating terrain effects. Model outputs are gas concentration, depth-averaged velocity, averaged cloud thickness and dose (Folch et al., 2009). The dose ( $D$ ) is a temporal integrated variable of the vertical concentration distribution with a toxicity exponent.

## **8. Research article 1: Experimental and numerical modelling of CO<sub>2</sub> leakage in the vadose zone**

This paper has been published in **Greenhouse Gases: Science and Technology**, **5**, 1-24. DOI: **10.1002/ghg.1523** with the title “**Experimental and numerical modelling of CO<sub>2</sub> leakage in the vadose zone**”.

The following manuscript describes the PISCO2 project and the 3D modelling task of the project. Previously, as part of the doctorate, a series of numerical simulations in 1-D vertical geometry have been performed to select the better intrinsic input parameters of each material and optimize the mesh discretization and the time of calculation. Moreover, a sensitivity study was performed on soil properties. Both research studies are reported in Appendix 1.

### **8.1. Introduction**

CO<sub>2</sub> geological storage is one of the viable technologies to decrease industrial emissions of CO<sub>2</sub> to the atmosphere that strongly contribute to the greenhouse effect (IEA, 2010). During the geological storage, CO<sub>2</sub> leakage from reservoir formations into surrounding layers could lead to environmental impacts on fresh groundwater quality (Kharaka et al., 2010) and could also affect surface ecosystems (Annunziatellis et al., 2008; Beaubien et al., 2008) and human beings (Costa et al., 2008). Groundwater acidification due to CO<sub>2</sub> dissolution would mobilize trace metals that could be transported through the aquifers up to the surface (Kharaka et al., 2010; Grivé, 2005; Agnelli et al., 2013). In the near-surface area, CO<sub>2</sub> could perturb ecological equilibrium and modify vegetal and bacteria growth and pollute drinking water. CO<sub>2</sub> migration in the vadose zone implies multiphase multicomponent phenomena that include CO<sub>2</sub>, air and water components with their own properties (density, viscosity, and enthalpy) in both gas and liquid phases (Oldenburg and Unger, 2004). Few studies from literature have dealt with CO<sub>2</sub> transport in the unsaturated zone of the soil in the range of concentrations and fluxes expected in a potential leakage from geological storage facility (Oldenburg and Unger, 2004; Oldenburg et al., 2010a; Zhang et al., 2004; Rohmer et al., 2010; Lewicki et al., 2007; Lewicki et al., 2010). According to Koerner and Klopatek (2002) a typical ecological CO<sub>2</sub> efflux is between 5 and 50 g·m<sup>-2</sup>·d<sup>-1</sup>.

This study presents results from an integrated experimental and modelling approach for the study of CO<sub>2</sub> injection and transport in the vadose zone. The experiments have been performed in the PISCO2 project facilities at the ES.CO2 centre in Ponferrada (North Spain).

The PISCO2 project is an experimental facility for the investigation of the impact of CO<sub>2</sub> injection on different biotopes. Its main objective is the development of cost-effective and ecological biomonitoring tools for safety control of CO<sub>2</sub> geological storage. The studies of the impact of high fluxes of CO<sub>2</sub> on the biosphere have been commonly developed in natural analogues (Rogie et al., 2000; Rogie et al., 2001; Costa et al., 2008; Chiodini et al., 2010; Voltattorni et al., 2011). In these systems, the biota is exposed to CO<sub>2</sub> for long periods of time (geological timescale), leading to the occurrence of adapted species. In contrast, in the PISCO2 project, the effects are observed and quantified on non-adapted flora and fauna, which is much more realistic scenario of impact from early leakage from geological storage.

The PISCO2 project consists of a set of 18 experimental units where injection of known fluxes of CO<sub>2</sub> (from 1.0 to 60 L·h<sup>-1</sup>) is performed to monitor biological responses and identify potential bio-indicators of CO<sub>2</sub> anomalous concentrations and surface fluxes (Fig. 1) (Credoz et al., 2011a). Changes on the chemical composition of gas and water phase are also monitored.

In the present study, results from controlled CO<sub>2</sub> injection experiments and results from dedicated 3D numerical simulations have been compared. Two numerical models were constructed: (1) a model with homogeneous distribution of physical parameterization in the near-surface area, and (2) a more realistic model with a distribution of heterogeneities in permeability along the near-surface area. This new distribution is obtained after the observation of the experimental CO<sub>2</sub> flux maps. A comparison between experimental and model data may help understand the dynamics of CO<sub>2</sub> transport in the soil-atmosphere interface and provide clues for the monitoring strategies for leakage detection.

Similar projects to PISCO2 at international level with partnerships between universities and private societies and institutes are developed in Norway, U.S.A., United Kingdom, Denmark, Brazil and France. The CO<sub>2</sub> Field Lab in Norway at Svelvik is a CCS project with the aim to increase monitoring knowledge to detect CO<sub>2</sub> migration and leakage (Dillen et al., 2009; Jones et al., 2014). The ZERT project in Montana (U.S.A.) has a number of targets such as testing near-surface monitoring and its limits on detection use the site to improve models for groundwater vadose zone and atmospheric dispersion (Oldenburg et al., 2010b). This project uses a horizontal well facility, 70-metres long with a maximum depth of 2.5 m with 7 injectors, to investigate the vadose zone. The ASGARD project in Nottingham (U.K.) is a purpose-built field facility for the study of ecosystem



resources to elevated soil gas concentration and to test monitoring system for CO<sub>2</sub> leakage (Smith et al., 2013). The CO<sub>2</sub>CRC-Geosciences Australia project is placed at Ginninberra. The target of this project is to test and optimize greenhouse gas monitoring equipment, techniques and quantitative emission models. In addition, atmospheric, soil, biological and potentially groundwater studies are also carried out (Sharma et al., 2009). In Brazil, in the State of Santa Catarina at Florianopolis Island, the Ressacada's Farm is part of the Agricultural Science Centre (UFSC) where there are various field experiments on controlled CO<sub>2</sub> release (Melo, 2012; Oliva et al., 2014). The CO<sub>2</sub>-Vadose project is a French project that aims to test geochemical and geophysical detection techniques on CO<sub>2</sub> injection and leakage in a carbonate vadose zone (Loisy et al., 2013). PISCO<sub>2</sub> experimental platform offers an exclusive design in the selection of the composition, texture, structure of the filling materials and the depth of simulated leakage (Credoz et al., 2011a).



**Figure 1.** View of the experimental cell filled with gravel and coarse sand. The service well is located on the left corner.

## **8.2. Materials. Methodology and experimental conditions**

### **8.2.1. Experimental at PISCO<sub>2</sub> unit**

Each experimental unit in the PISCO<sub>2</sub> project consists of an infilling of coarse sand and gravel, and it is outlined by concrete walls 20 cm thick with a 16 m<sup>2</sup> base and 2.2 m deep. This concrete prevents mass (water, gas, microbes...) transfer in and out of the unit. Due to its potential reactivity with acidic CO<sub>2</sub>-bearing waters, the integrity of this concrete is monitored to detect degradation and leakage.

The gravel layer (0.2 m thick) is deposited at the bottom of the unit to preserve liquid flow drainage in order to maintain an unsaturated zone in the upper layers. An average grain size of 10

mm was selected. Overlying the gravel, a coarse sand layer (1.6 m thick) is deposited accounting for the 73% of the total infill of the unit. The average grain size is 3 mm with a quite good sorting for a 4 mm sieve the 100% of sand passes through and for 1 mm sieve only 2%. In the experiments, the unsaturated zone always is found in the coarse sand layer.

The CO<sub>2</sub> is injected through a grid with 16 pinholes located at 1.6 meters deep in the coarse sand (Fig. 2) with a diameter of 0.3 mm. The injection system, represented in figure 2a, is a grid that covers a surface of 9 m<sup>2</sup> where each pinhole is the node of a 1 m<sup>2</sup> mesh. The injection grid is a closed system so neither a loss of pressure nor a gap between pinholes should occur. A thin net is present above and below the injection system in order to prevent pinhole blockages due to sand grains.

As can be seen in figure 2 there are two couple of injector pipes at 1.6 and 0.8 depth but for the entire experiment was used only the deepest injector pipe.

A drainage system is present below the gravel layer to collect water.

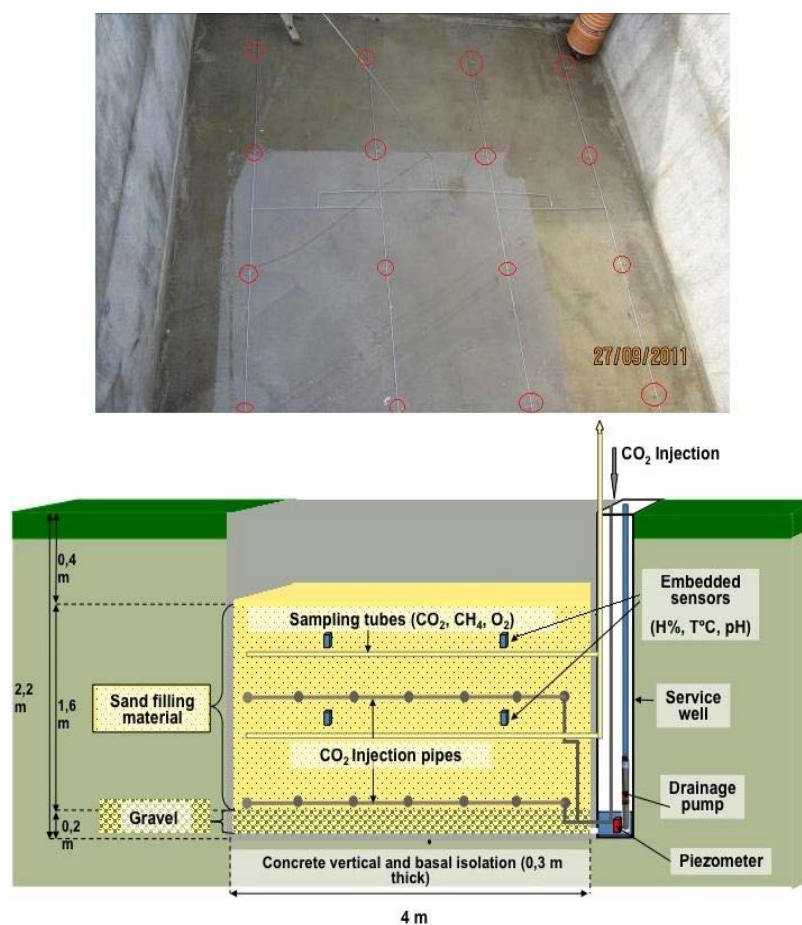


**Figure 2.** a) Picture showing the injection grid; pinholes are indicated by the red circles; b) Scheme of PISCO2 experimental unit profile.

### 8.2.2. Experimental injection

The injection of CO<sub>2</sub>, as gas phase, inside the unit started in June 2012 and lasted for 46 days, different rates were used from 5 L·h<sup>-1</sup> to 60 L·h<sup>-1</sup> (from 8.64 to 103.68 kg·h<sup>-1</sup>) with a pressure of circa 1 bar at ambient temperature (Table 3). The total amount of injected CO<sub>2</sub> during that period was 31,363 litres (62.1 kg).

Before the injection started a series of tests took place to verify the instruments, one of those was water filling and emptying in order to check the drainage pump. During that test a very fast emptying was observed, in such a manner an accidental compaction of the coarse sand could have happened due to strong pump out pressure.

**Table 3.** Timetable for experimental injection and rates in June and July 2012.

Duration of Injection (h)	Injection rate (L·h <sup>-1</sup> )	Injection rate (kg·s <sup>-1</sup> )
84	5.0	2.40x10 <sup>-06</sup>
12	0.0	0.0
72	5.0	2.40x10 <sup>-06</sup>
72	10.0	4.80x10 <sup>-06</sup>
216	15.0	7.20x10 <sup>-06</sup>
12	20.0	9.60x10 <sup>-06</sup>
12	0.0	0.0
24	20.0	9.60x10 <sup>-06</sup>
168	30.0	1.44x10 <sup>-05</sup>
96	40.0	1.92x10 <sup>-05</sup>
48	50.0	2.40x10 <sup>-05</sup>
288	60.0	2.88x10 <sup>-05</sup>

The injection experiment started with low injection rate, increasing through time up to the maximum injection rate allowed by the equipment during the final experiments. The experiment was

stopped by two electric cuts occurred along the 46 days of experiment, lasting 12 hours each one. Flux maps at surface were built with measurements performed with an accumulation chamber (see section 8.2.4. below for description) for each injection step.

### 8.2.3. Weather conditions during the injection experiment

Air temperatures and rainfall data were obtained by the meteorological equipment placed at Centro Cuenca SAIH Miño-Sil, close to the PISCO2 facilities (Fig. 3). Rainfalls during the summer period were not frequent (only 5 days with rainfall higher than 1 mm), and consequently it was decided to simulate only three rainy days for models A, B, C, and E, during the June 17<sup>th</sup> and between June 20<sup>th</sup> and 21<sup>st</sup>, and between July 25<sup>th</sup> and 26<sup>th</sup>, respectively with 3.3 mm, 4.4 mm, and 9.0 mm of rainfall. Temperature was from 14.7 °C to a maximum of 27.6 °C, with an average value of 20.2 °C. Because of model D is developed to see the effect of rainfall in a leakage site is the only model to have a constant rainfall for the entire simulation.

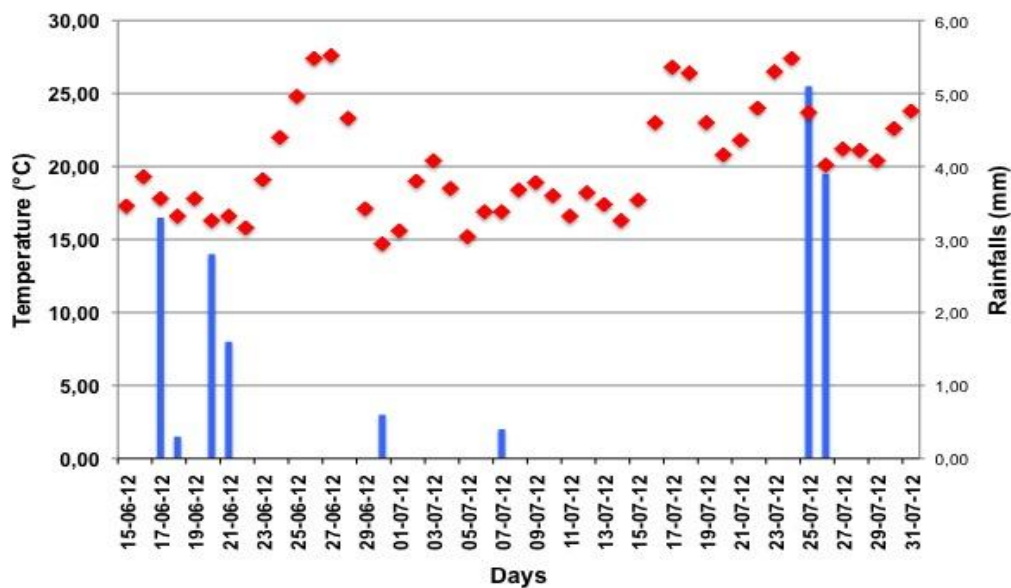


Figure 3. Air temperatures (red squares) and rainfall (blue bars) recorded at PISCO2 site during the injection period.

### 8.2.4. Monitoring procedure

As mentioned above, before, during and after an injection step, gas flux was collected in 36 spots evenly distributed in the surface using a West System accumulation chamber (Fig. 4). In

figure 5 the 36 soil flux monitoring spots are shown together with the service well and the 16 CO<sub>2</sub> injectors.



**Figure 4.** Collection of CO<sub>2</sub> soil-atmosphere fluxes on PISCO2 unit surface.

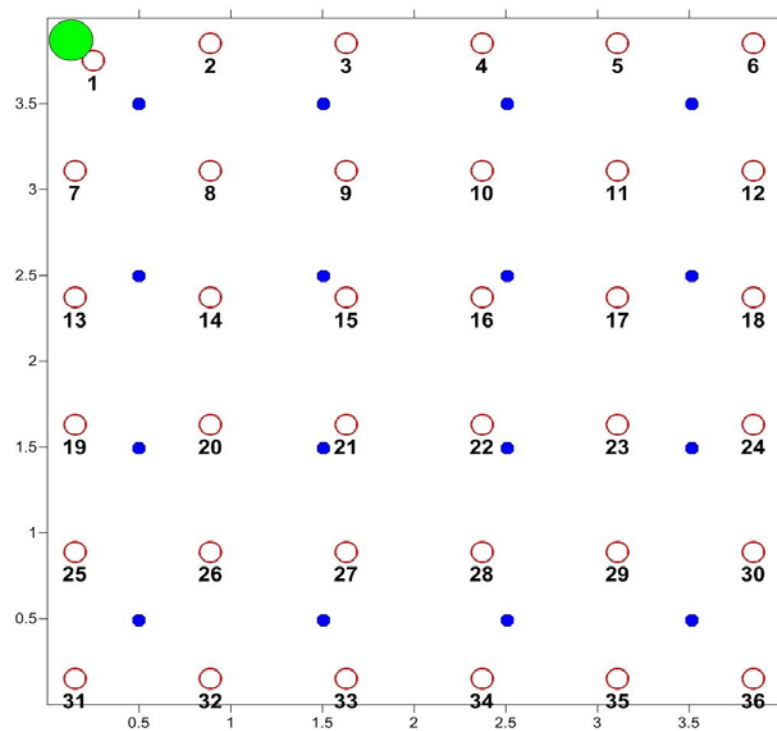


**Figure 5.** Scheme of the location of the 36 monitoring points (red circles), the 16 CO<sub>2</sub> injectors (blue dots) and the service well (green spot).

Results from Takle et al., (2003) show that under similar meteorological conditions the effects of the flux chamber on the pressure field in its near vicinity was within the range of natural pressure fluctuations. So, the presence of the accumulation chamber does not cause pressure perturbations that lead to biases in measurements of surface fluxes of CO<sub>2</sub>.

### **8.2.5. Modelling tools**

#### **8.2.5.1. TOUGH2 code and EOS7CA experimental module**

TOUGH2 is a general-purpose numerical simulation program for multi-dimensional fluid and heat flows of multiphase, multicomponent fluid mixtures in porous and fractured media (Pruess et al., 1999). The research module EOS7CA (Oldenburg and Unger, 2004; Oldenburg et al., 2010a, b) was used to simulate CO<sub>2</sub> transport in the unsaturated zone of the soil, so that temperature and pressure are close to ambient conditions. TOUGH2/EOS7CA models the Darcy flow and Fickian diffusive transport of five components (water, brine, CO<sub>2</sub>, a gas tracer and air) in gaseous and aqueous phases at near-ambient pressures and temperatures. TOUGH2 is a widely used integral finite-difference multiphase and multicomponent non-isothermal flow and transport simulator that supports a number of equation of state (EOS) modules. The governing equations and symbols used are presented in Appendix 2. TOUGH2 uses integral equation and solves them implicitly by the integral finite difference method. TOUGH2 uses Newton-Raphson iteration to handle non-linearity, a choice of conjugate gradient sparse matrix solvers to solve the Jacobian matrix at each Newton iteration, and a robust residual-based convergence criterion to ensure convergence of the coupled non-linear equations (Pruess et al., 1999). Note that the energy equation is omitted in Appendix 2 since all the simulations in this study were performed in isothermal conditions. TOUGH2/EOS7CA is designed for near-surface applications where the pseudo component air is present (Oldenburg and Unger, 2004). The use of Henry's law for modelling solubility restricts EOS7CA to shallow regions (low pressure system). Other TOUGH2 modules (e.g., ECO2N, Pruess, 2005; and EOS7C, Oldenburg et al., 2004) are available for deep subsurface (high-pressure) porous media initially saturated with brine.

### **8.2.6. Numerical model**

The 3D numerical model is based on a system consisting of 3 components (water, CO<sub>2</sub>, air) in 2 phases (liquid and gas) occupying the porosity of 3 hydraulically distinct layers: (1) atmosphere, (2) coarse sand, and (3) gravel, and with source of CO<sub>2</sub> in the injection point (Fig. 6).

The atmosphere layer represents the upper boundary of the model and extends down to the coarse sand layer. All the elements of this layer have an infinite volume (with an order of  $10^{52}$  m<sup>3</sup>) that enables the infinite vertical gas release out of the unit. No capillary properties have been defined for this layer to avoid unrealistic suction effects. No atmospheric dispersion or evaporation processes have been considered in the compartment at this stage of the study.

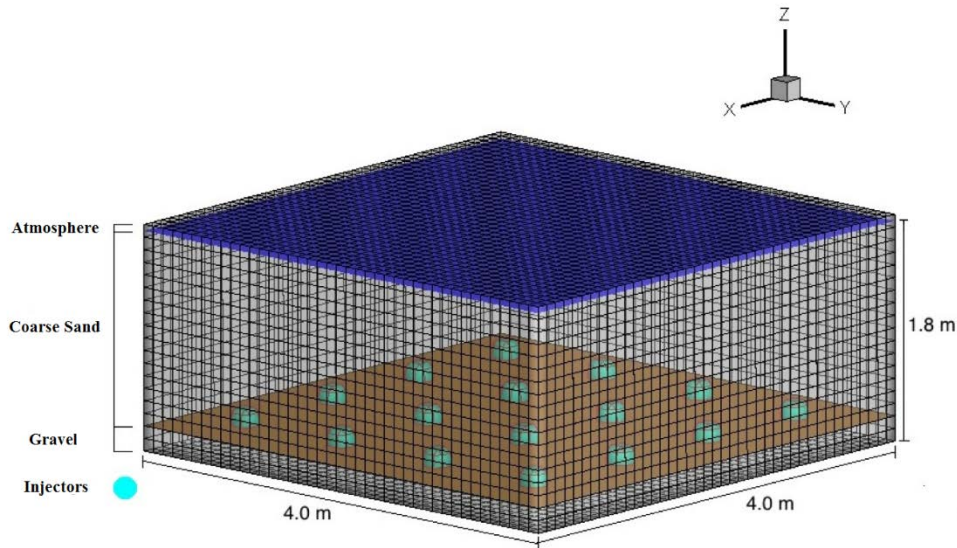


**Figure 6.** Scheme of the model domain, from top to bottom: atmosphere boundary, coarse sand layer (25.6 m<sup>3</sup>), gravel layer (3.2 m<sup>3</sup>), 16 injectors (light blue dots).

The coarse sand layer has a porosity of 0.35 and a permeability of  $3 \times 10^{-12}$  m<sup>2</sup> considering homogeneous properties. It is worth mentioning, however, that this layer underwent compaction and creation of preferential pathways for CO<sub>2</sub> migration up to the atmosphere due to experimental artefacts (intensive drainage operations and compacted zone) during the experiments. Consequently, in a second set of numerical simulations, sub-layers with porosity and permeability heterogeneity were defined to optimize the model results. In this optimized model, porosity and permeability vary from 0.25 to 0.45 and  $1 \times 10^{-13}$  to  $1 \times 10^{-11}$  m<sup>2</sup>. CO<sub>2</sub> injection has been simulated by a CO<sub>2</sub> flux of  $2.0 \times 10^{-6}$  kg·s<sup>-1</sup> in 16 elements evenly distributed in the base of the coarse sand layer.

The gravel level is defined as homogeneous along all the numerical simulations with a porosity of 0.25 and a permeability of  $1 \times 10^{-11}$  m<sup>2</sup>.

No flow has been imposed on the lateral boundary to simulate the very low permeability concrete walls of PISCO2 experimental unit.

The molecular diffusivity of the three components in the aqueous phase is  $10^{-10} \text{ m}^2 \cdot \text{s}^{-1}$  (Xu and Qi, 2001). In the gas phase, the molecular diffusivity of CO<sub>2</sub> is  $1.55 \times 10^{-5} \text{ m}^2 \cdot \text{s}^{-1}$  (Haynes, 2012) and  $1 \times 10^{-5} \text{ m}^2 \cdot \text{s}^{-1}$  for both water and air components.

The mesh is composed by 31939 regular quadratic elements with 92578 connections. The size of each element is  $0.001 \text{ m}^3$ .

A sensitivity study was performed to see how soil properties can affect the predicted CO<sub>2</sub> flow in the PISCO2 cell (Appendix 1). The selected properties for this study were porosity, permeability, lambda ( $\lambda$ ), P<sub>0</sub> and gas saturation (S<sub>g</sub>), tortuosity ( $\tau$ ) and grain size. For each test was followed a *rule of conduct* with  $a < b < c < d$ , that means that each test range was carried out from lower to higher values. A literature review was performed on papers about soil and rock intrinsic properties and papers dealing with soil classification.

The mesh dimensions for each material and the respective hydraulic parameters, thermal properties and permeability and capillary parameters for the Van Genuchten equation for hydraulic conductivity in unsaturated media are listed in Table 4.

**Table 4.** Soil properties and Van Genuchten parameters for filling materials in the PISCO2 unit.

<b>Material</b>	Atmosphere	Coarse Sand	Gravel
<b>Dimensions</b>			
X (m)	4	4	4
Y (m)	4	4	4
Z (m)	$1.0 \times 10^{-9}$	1.6	0.2
Porosity	0.35	0.35	0.25
Density (kg·m <sup>-3</sup> )	1500	1500	1700
<b>Hydraulic parameters</b>			
Isotropic permeability (m <sup>2</sup> )	$1.0 \times 10^{-12}$	$3.0 \times 10^{-12}$	$1.0 \times 10^{-11}$
<b>Thermal properties</b>			
Thermal conductivity (W·m <sup>-1</sup> ·°C <sup>-1</sup> )	1	1	1
Material specific heat (J·kg <sup>-1</sup> ·°C <sup>-1</sup> )	$1.0 \times 10^5$	835	800



<b>Van Genuchten functions</b>				
$\lambda$	-	0.2	0.2	
$1/P_0$ (Pa <sup>-1</sup> )	-	$1.0 \times 10^{-4}$	$1.0 \times 10^{-4}$	
$S_{rl}$	-	0.1	0.1	
$S_{gr}$	-	0.01	0.01	
$P_{max}$ (Pa)	-	$1.0 \times 10^7$	$1.0 \times 10^7$	

The TOUGH2/EOS7CA simulations follow step by step the injection procedure done at PISCO2. All the simulations are isothermal so that no heat exchange between the injection cell and the exterior system occurs. The three days of rain and the two electric cuts were integrated in the model.

A number of numerical models have been run (Table 5). The first one (Model A) is the base model and material properties are described in Table 4. This model simulates injection into a homogeneous soil.

Before starting the injection simulation, every model runs for 35 days to redistribute the initial liquid saturation in the cell.

**Table 5.** List of numerical simulations and their distinctive features.

<b>Model name</b>	<b>Remarks</b>
Model A	Homogenous soil
Model B	Heterogeneous soil
Model C	Heterogeneous soil and high temperature
Model D	Heterogeneous soil and rainfall
Model E	Heterogeneous soil and higher liquid saturation

Starting from the homogeneous surface model four additional layers (soil layer 1, 2, 3 and 4) with four specific permeabilities and porosities were added (Fig. 7; Table 6) in order to create a heterogeneous surface model called Model B. Such model consists of two layers (soil layer 1 and 2 in Fig. 7 and Table 6) representing preferential pathways with higher permeability and porosity compared to coarse sand and two additional layers were used to model compaction effects (soil layers

3 and 4 in Fig. 7 and Table 6) with lower permeability and porosity compared to coarse sand. The intention of the Model B was the calibration of the hydraulic parameters in the unit to reproduce the observed surface fluxes measured with an accumulation chamber in the experimental injection. Therefore, the final values of intrinsic permeability and porosity used in the Model B are actually optimized values from a sensitivity study.

Based on the Model B, an isothermal simulation called Model C has been performed to predict the effects of a higher temperature on the system since a wide temperature range has been observed in the PISCO2 experimental site. General features are the same as the homogeneous surface model except for the atmosphere temperature increased from 15° to 40° C.

**Table 6.** Characteristics of permeability and porosity for the 4 layers introduced in Model B.

	Soil layer 1	Soil layer 2	Soil layer 3	Soil layer 4
Permeability (m <sup>2</sup> )	1×10 <sup>-11</sup>	7×10 <sup>-12</sup>	1×10 <sup>-13</sup>	×10 <sup>-13</sup>
Porosity	0.45	0.40	0.25	0.30
Thickness (cm)	110	40	40	70

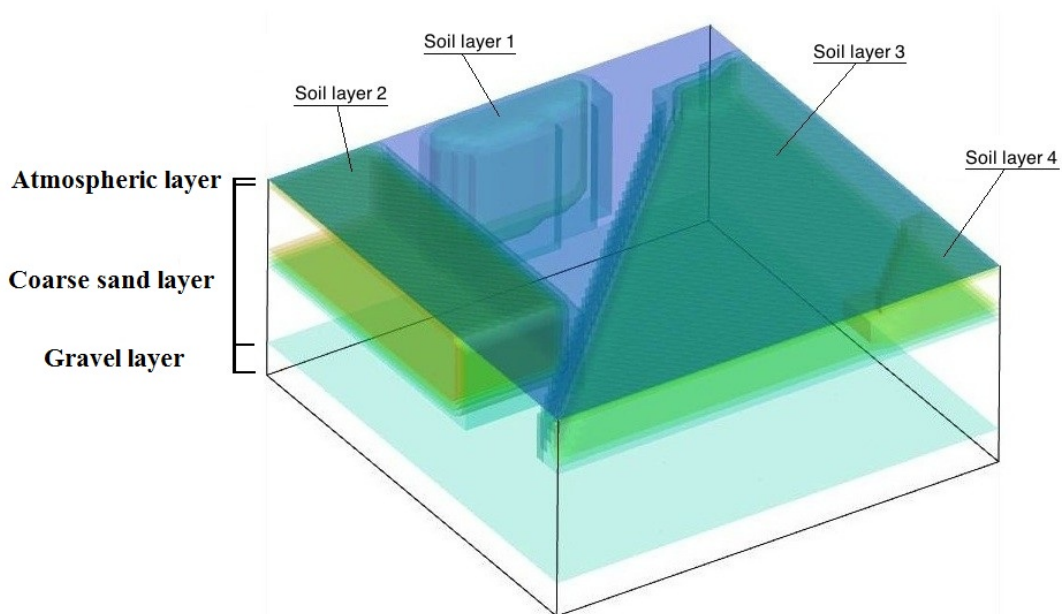


**Figure 7.** 3D model with the 4 compaction layers in the coarse sand considered in the Model B; thickness of each layer is reported in Table 6.

The assessment of the rainfall effects on CO<sub>2</sub> emission on surface was performed in a model called Model D. In this case, the numerical simulation was thought to represent a leakage in an area with an elevated rainfall. A constant rain of 6 mm·d<sup>-1</sup> for the 46 days of injection was implemented in the model for a total amount of 276 mm of rainfall. Such a test will provide a view on how rainfall can affect a surface leakage.

Finally, the impact of soil saturation (up to 0.5) on CO<sub>2</sub> transport was predicted in the Model E in order to understand how much soil water content can affect CO<sub>2</sub> leakage efflux by time and by surface dispersion.

## 8.3. Results

### 8.3.1. Experimental injection

After 4 days of injection, with the lowest injection rate (5 L·h<sup>-1</sup>), a preferential emission area at surface was observed with a maximum CO<sub>2</sub> surface flux of 27 g·m<sup>-2</sup>·d<sup>-1</sup> (Fig. 8a). CO<sub>2</sub> flux is more intense close the upper left corner, where the service well is located. This flux is in the magnitude of background CO<sub>2</sub> natural fluxes in soil due to microbiological activity and organic matter degradation according to Xu and Qi (2001) the annual average of soil-surface CO<sub>2</sub> efflux is 7.4 g·m<sup>-2</sup>·d<sup>-1</sup>. After 21 days, with an injection rate of 20 L·h<sup>-1</sup>, the preferential emission area remained in the upper left corner of PISCO2 unit. The maximum CO<sub>2</sub> flux reached 128 g·m<sup>-2</sup>·d<sup>-1</sup> (Fig. 8b). After 32 days of experiment, CO<sub>2</sub> injection rate reached 40 L·h<sup>-1</sup> (Fig. 8c), with a maximum flux of 220 g·m<sup>-2</sup>·d<sup>-1</sup> in the upper boundary. In the last day of injection, the surface flux reached 600 g·m<sup>-2</sup>·d<sup>-1</sup> in the same “hot spot” (Fig. 8d), with an injection rate of 60 L·h<sup>-1</sup>. The CO<sub>2</sub> flux is distributed into two main sectors, the first one around the hot spot in the upper left side, and a second one in the lower right side. In general, the contour line values increase from the lower right corner to the upper left corner where is placed the service well.

In conclusion, after 46 days of injection and rates from 5 to 60 L·h<sup>-1</sup>, CO<sub>2</sub> surface flux is highly heterogeneous along the 16 m<sup>2</sup> area of PISCO2 experimental unit.

The value of emitted CO<sub>2</sub> on surface for each sample point through time are shown in figure 9. Interestingly, each sample value keeps the same ranking. For example, the sample point 4 (hot spot) is always the highest emitter and the sample point 36 is the lowest one along the entire experiment. The average CO<sub>2</sub> flux in the cell after 46 days approximated 200 g·m<sup>-2</sup>·d<sup>-1</sup>.

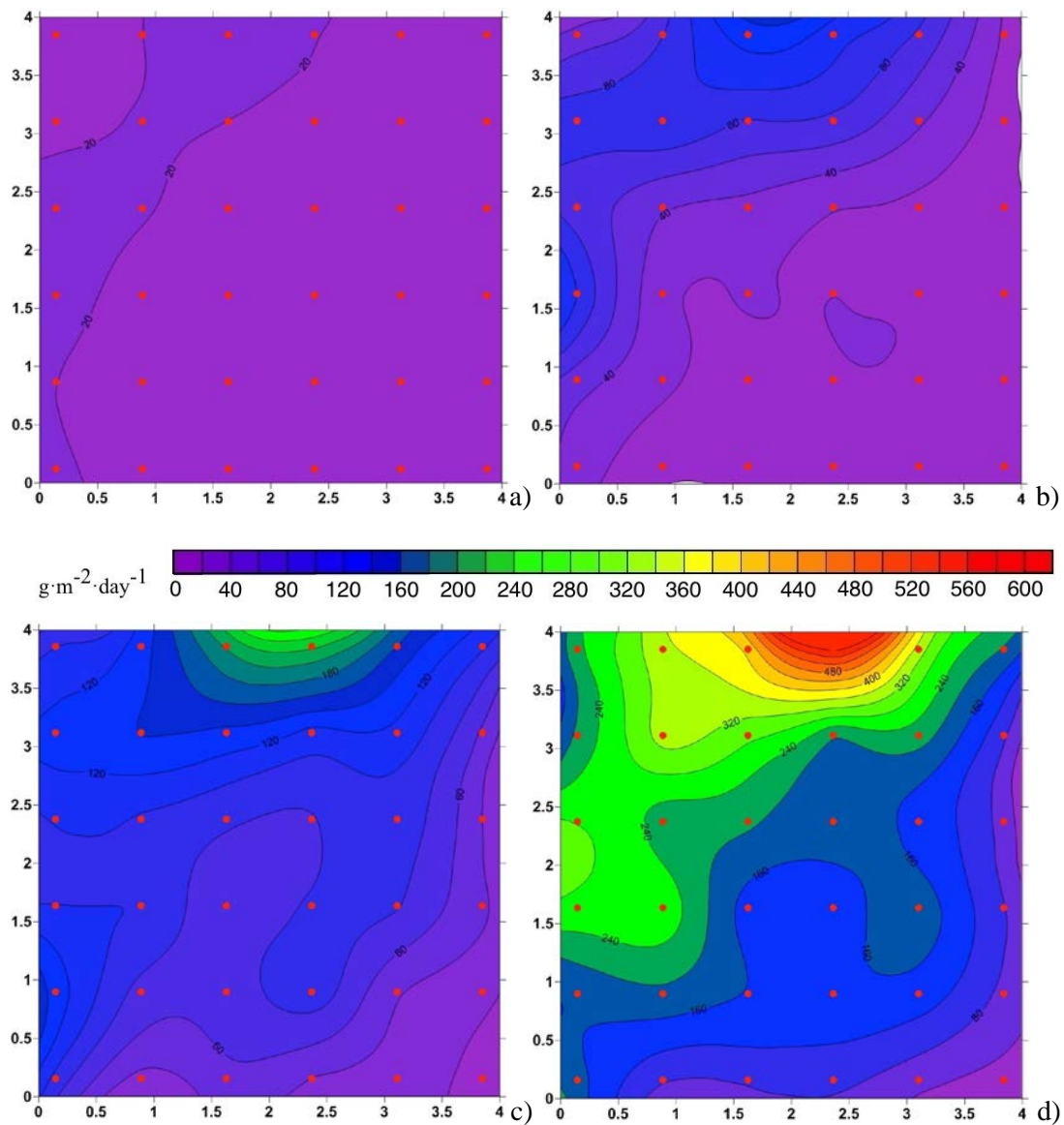


**Figure 8.** Contour map of surface CO<sub>2</sub> flux in PISCO2 using West System accumulation chamber after 4 (a), 21 (b), 32 (c) and 46 (d) days corresponding to injection rates of 5, 20, 40 and 60 L·h<sup>-1</sup>, respectively. The measurement points are shown as red dots.

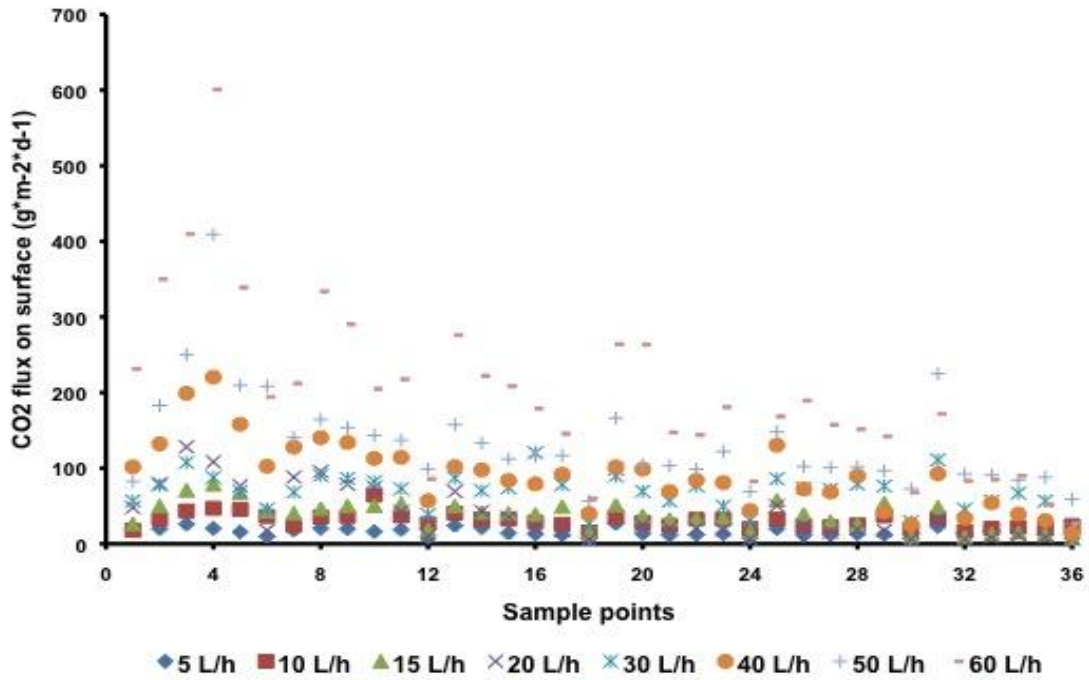


**Figure 9.** Surface CO<sub>2</sub> flux in each measurement point through time, showing the data for the 8 injection rates. On horizontal axis are reported the 36 sampling points, on the vertical axis the CO<sub>2</sub> flux at surface, symbols are different for every emission rate.

### 8.3.2. Numerical modelling

#### 8.3.2.1. Model A

In the Model A, the predicted CO<sub>2</sub> surface flux after 4 days of injection at a rate of 5 L·h<sup>-1</sup> was a homogeneous distribution with a value of 16.2 g·m<sup>-2</sup>·d<sup>-1</sup>. After 21 days, with an injection rate of 20 L·h<sup>-1</sup> the maximum flux raised to 44.1 g·m<sup>-2</sup>·d<sup>-1</sup> and the minimum to 43.2 g·m<sup>-2</sup>·d<sup>-1</sup> and after 32 days at 40 L·h<sup>-1</sup> the CO<sub>2</sub> fluxes were respectively 78.6 and 76.7 g·m<sup>-2</sup>·d<sup>-1</sup>. At the end of the experiment after 46 days with an injection rate of 60 L·h<sup>-1</sup> the maximum CO<sub>2</sub> surface flux reached 123.3 g·m<sup>-2</sup>·d<sup>-1</sup> and the minimum was 120.9 g·m<sup>-2</sup>·d<sup>-1</sup>. The maximum CO<sub>2</sub> flux is always located in the centre of the cell for all the time steps. The regime of CO<sub>2</sub> fluxes is still homogeneous during all the 46-days simulation in the whole surface of the 16 m<sup>2</sup> PISCO2 experimental unit.

No flux map regarding Model A is reported because each surface flux map was homogeneous showing a single-colour distribution.

The CO<sub>2</sub> plume is predicted to progress inside the cell uniformly from the bottom to the top and border effects were not significant. So, there is a homogenous movement of CO<sub>2</sub> from the 16 injectors disposed at 160 cm deep inside the experimental unit.

The mass balance of CO<sub>2</sub> in the simulation is presented in figure 10. It is computed from the total amount of injected CO<sub>2</sub>, the amount of CO<sub>2</sub> stored in the cell, as well as in the gas phase and in the water phase and the amount of carbon dioxide emitted on surface are reported.

For the Model A, a total amount of 62.1 kg of carbon dioxide was injected from which 51.2 kg were emitted to atmosphere and 10.9 kg were trapped in the experimental unit. The trapped CO<sub>2</sub> was split into 7.43 kg in the gas phase and 3.47 kg in the aqueous phase.

	Model A	Model B	Model C	Model D	Model E
Total CO <sub>2</sub> Injected (kg)	62.10	62.10	62.10	62.10	62.10
CO <sub>2</sub> Gas phase (kg)	7.43	7.50	6.70	4.40	7.68
CO <sub>2</sub> Liquid phase (kg)	3.47	3.50	1.70	14.90	8.52
CO <sub>2</sub> Emitted on surface (kg)	51.20	51.10	53.70	42.80	45.90

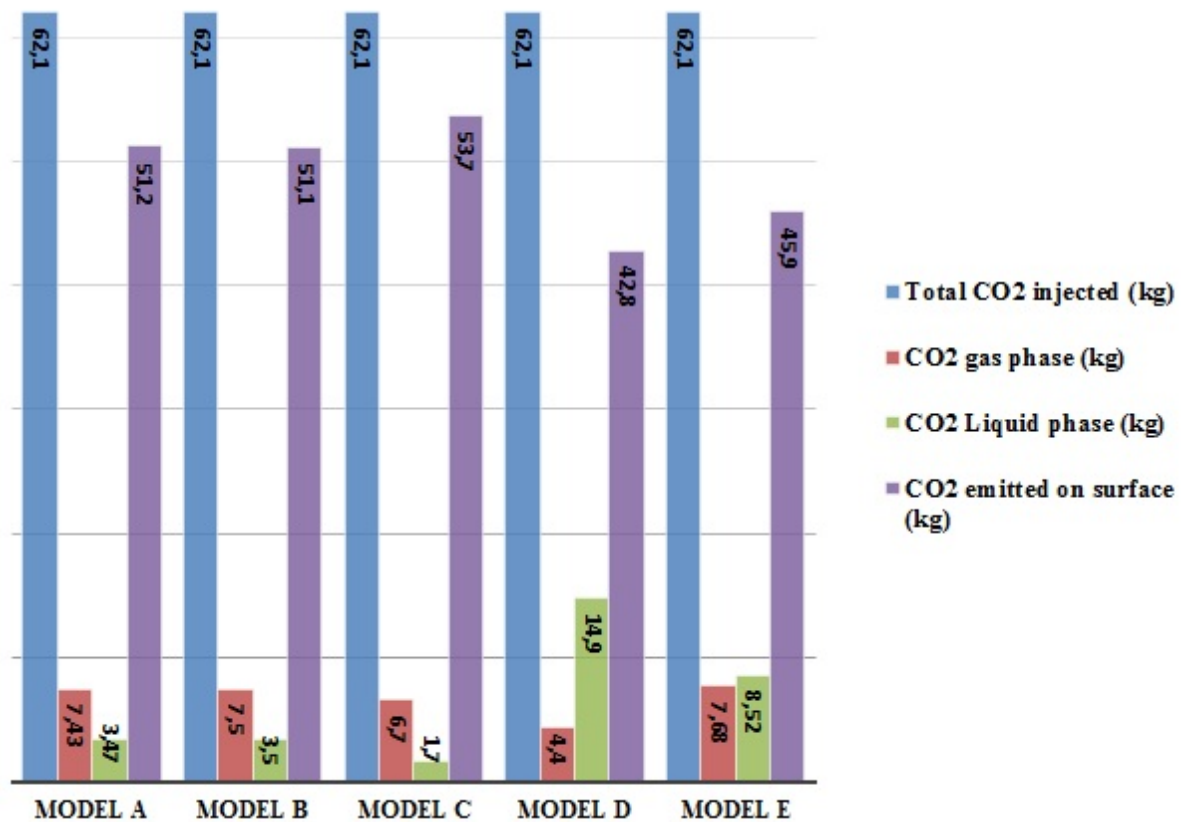


Figure 10. Mass balance comparison for the five model simulations.

### 8.3.2.2. *Model B*

Considering heterogeneities in the hydraulic properties in the coarse sand, the Model B predicts that after 4 days of injection (Fig. 11a) the CO<sub>2</sub> emission flux reached a maximum of 32 g·m<sup>-2</sup>·d<sup>-1</sup> with an injection rate of 5 L·h<sup>-1</sup>. CO<sub>2</sub> flux already appears divided into the two main sectors observed in the experimental tests. The upper left corner has emissions between 20 and 32 g·m<sup>-2</sup>·d<sup>-1</sup> and the lower right corner with emissions below 10 g·m<sup>-2</sup>·d<sup>-1</sup>. Increasing the injection rate at 20 L·h<sup>-1</sup> and after 21 days (Fig. 11b), the Model B predicts a maximum CO<sub>2</sub> emission flux reaching 112 g·m<sup>-2</sup>·d<sup>-1</sup> still in the main emission area. After 32 days (Fig. 11c), a hot spot in the upper wall comes up with an emission of 228 g·m<sup>-2</sup>·d<sup>-1</sup> and an injection rate of 40 L·h<sup>-1</sup>. In the lower right corner, CO<sub>2</sub> surface emission keeps below 56 g·m<sup>-2</sup>·d<sup>-1</sup>. The model predicts that at the end of the experiment (Fig. 11d) with an injection rate of 60 L·h<sup>-1</sup> the hot spot reaches 389 g·m<sup>-2</sup>·d<sup>-1</sup> in the upper corner. As in Model A even for this simulation a comparison between the main emission area and the lower emission area shows the latter one having a larger area.

The four zones of emission predicted in the field experiment with one hot spot of intense CO<sub>2</sub> emission and three domains with variable fluxes are also predicted in this Model B simulation.

The total amount of carbon dioxide injected in the Model B was 62.1 kg from which 51.1 kg were emitted to surface and 11.0 kg were trapped in the cell. The trapped CO<sub>2</sub> was split into 7.5 kg in the gaseous phase and 3.5 kg in the aqueous phase (Fig. 10).

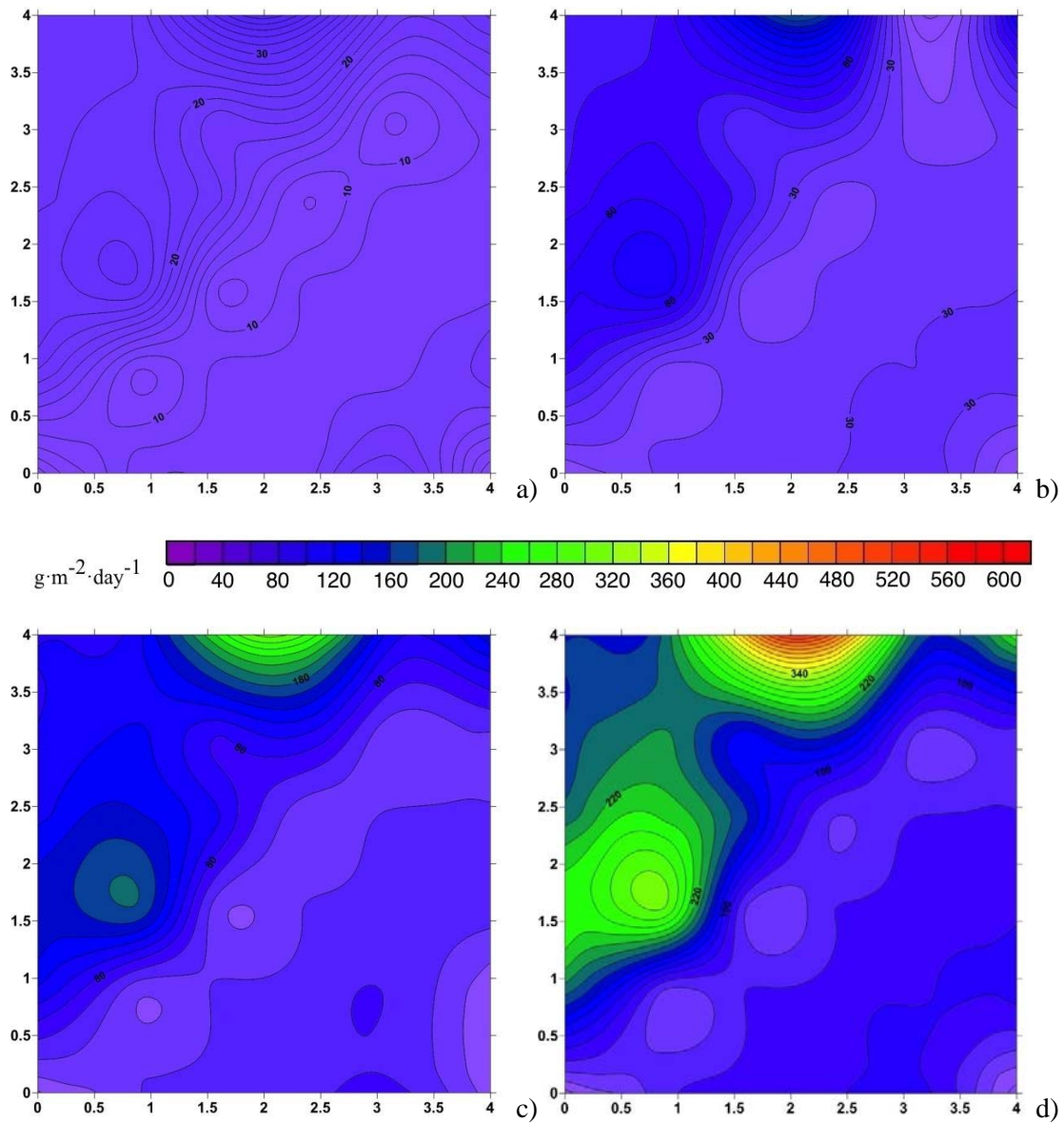


**Figure 11.** Contour mapping of surface CO<sub>2</sub> flux predicted in the model B after 4 (a), 21 (b), 32 (c), 46 (d) days.

The 3D view of the model results concerning the CO<sub>2</sub> mass fraction (represented by colours) and the CO<sub>2</sub> velocity vectors is shown in figure 12.



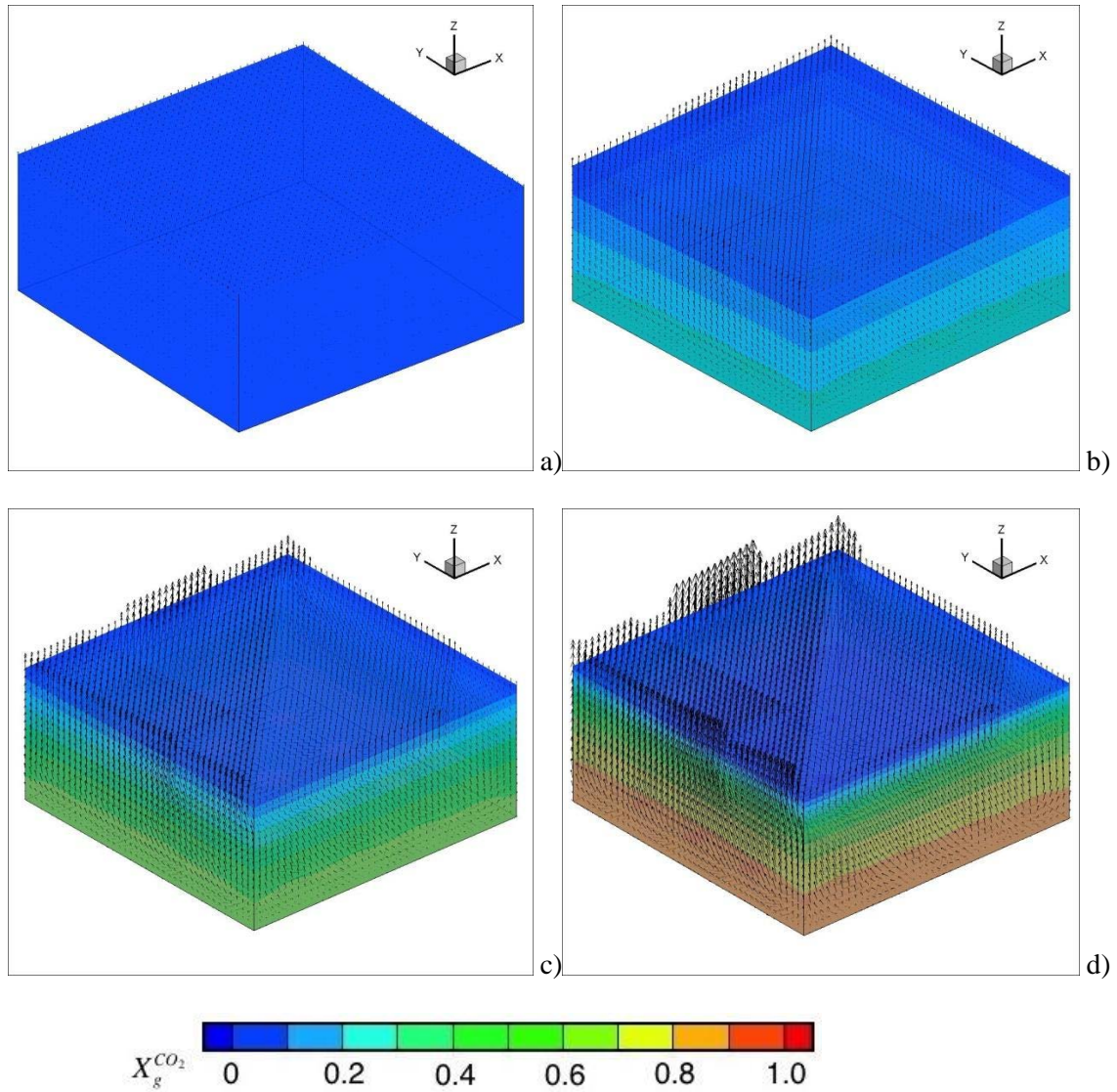


**Figure 12.** Three-dimensional view for the Model B showing the predicted gas velocity with vectors and the CO<sub>2</sub> mass fraction with colours. These parameters are drawn at 4 (a), 21 (b), 32 (c), 46 (d) days after the beginning of the injection.

### 8.3.2.3. Model C

Model C has been developed to see the effect of high ambient temperature in a leakage site; the prediction of flux emission is shown in figure 13. Emissions reach a maximum of 140 g·m<sup>-2</sup>·d<sup>-1</sup> after four days of injection at 5 L·h<sup>-1</sup> (Fig. 13a). CO<sub>2</sub> flux on surface is split into two preferential zones with the main emission in the upper left corner with the highest emission point in the upper wall. The area with lower emission is quite homogeneous. After 21 days (Fig. 13b) with an injection rate of 20 L·h<sup>-1</sup> the predicted maximum flux reaches 231 g·m<sup>-2</sup>·d<sup>-1</sup>. CO<sub>2</sub> emission on surface at this step was more heterogeneous. After 32 days (fig. 13c), with an injection rate of 40 L·h<sup>-1</sup>, the maximum flux was 350 g·m<sup>-2</sup>·d<sup>-1</sup>. The definition of two main areas of emission is clear at this step. The minimum

CO<sub>2</sub> emission is in the bottom right corner with a flux of 52 g·m<sup>-2</sup>·d<sup>-1</sup>. At the end of the simulation (Fig. 13d), the maximum emission on surface reaches 488 g·m<sup>-2</sup>·d<sup>-1</sup> in the hot spot placed in the upper wall and the minimum CO<sub>2</sub> emission reached 40 g·m<sup>-2</sup>·d<sup>-1</sup>. At the end of the simulation, carbon dioxide emission on surface fits well the CO<sub>2</sub> emission contour map obtained from the measurements in the experimental runs.

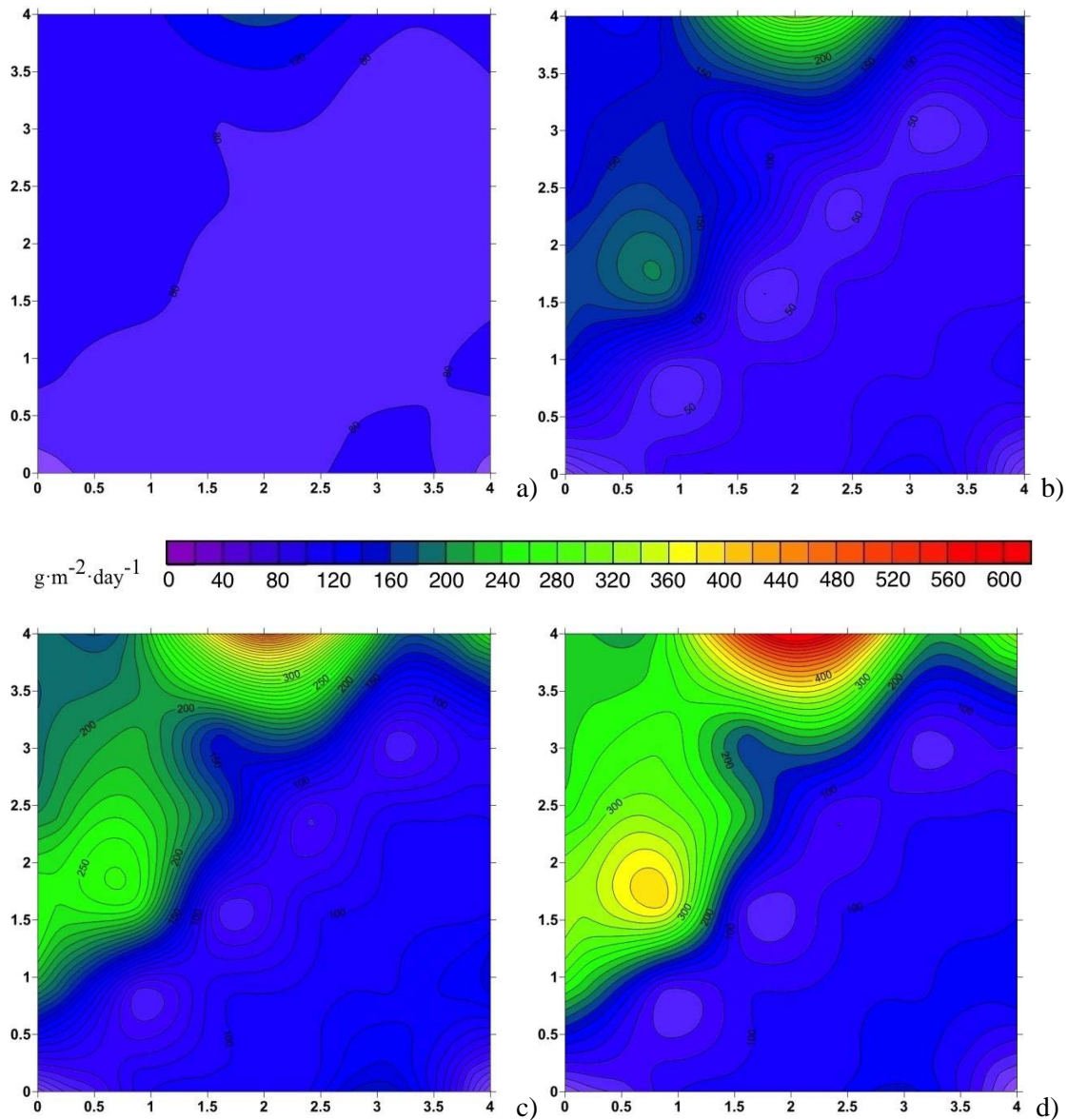


**Figure 13.** Contour map of surface CO<sub>2</sub> flux predicted in the Model C. The represented times are: 4 (a), 21 (b), 32 (c), 46 (d) days respectively.

In this model, the amount of CO<sub>2</sub> injected is 62.1 kg in 46 days (Fig. 10); 53.7 kg are emitted to atmosphere and 8.4 kg are trapped inside the cell. The trapped quantity is split into 1.7 kg in the liquid phase and 6.7 kg in the gas phase.

#### 8.3.2.4. *Model D*

Model D has been developed to see the effect of rainfall in a leakage site. CO<sub>2</sub> flux at surface predicted in the Model D is very low. From the injected 62.1 kg of CO<sub>2</sub>, 42.8 and 19.3 kg are emitted to the atmosphere and trapped inside the cell, respectively. The trapped amount of carbon dioxide is of 14.9 kg in the liquid phase and 4.4 kg in the gas phase. The numerical model predicts a maximum emission of 123.5 g·m<sup>-2</sup>·d<sup>-1</sup>, reached at the end of the simulation with an injection rate of 60 L·h<sup>-1</sup>. Surface CO<sub>2</sub> emission is homogeneous and flux maps result without any significant contour distribution. Such homogenous emission for the Model D is due to the high amount of water in the system and to the high CO<sub>2</sub> solubility (14.9 kg of CO<sub>2</sub> dissolved in water at 25 °C). As in Model A (the homogeneous model), a main emission was predicted in the centre of the experimental unit and lower emissions on the boundaries as well as in the corners and along part of the walls, this is an evidence of a lack of CO<sub>2</sub> preferential uplift effect along the walls. Such homogeneous distribution in model D ensues from the high amount of water in the soil that thwarts soil compactions. From the total amount of CO<sub>2</sub> injected, 42.8 kg are emitted to surface and 19.3 kg are trapped in the cell. The trapped CO<sub>2</sub> is split into 4.4 kg in the gaseous phase and 14.9 kg in the aqueous phase.

#### 8.3.2.5. *Model E*

The last set of simulations included the effect of initial liquid saturation on CO<sub>2</sub> transport and trapping. That model differs from the heterogeneous surface model because having a S<sub>l</sub>=0.5.

After 4 days of injection with the lowest injection rate (5 L·h<sup>-1</sup>), CO<sub>2</sub> emission on surface reaches the maximum of 11 g·m<sup>-2</sup>·d<sup>-1</sup> and the minimum of 2.5 g·m<sup>-2</sup>·d<sup>-1</sup> (Fig. 14a). The emission is so homogeneous resulting in a one-colour map. Only two sample points are predicted to exceed 10 g·m<sup>-2</sup>·d<sup>-1</sup>. After 21 days (Fig. 14b) with an injection rate of 20 L·h<sup>-1</sup>, a preferential emission area is calculated in the upper left corner with a maximum CO<sub>2</sub> surface flux of 86 g·m<sup>-2</sup>·d<sup>-1</sup> and a minimum flux of 6 g·m<sup>-2</sup>·d<sup>-1</sup>. After 32 days at an injection rate of 40 L·h<sup>-1</sup>, the maximum CO<sub>2</sub> surface flux is of 200 g·m<sup>-2</sup>·d<sup>-1</sup> located in the upper wall (Fig. 14c). The minimum CO<sub>2</sub> surface flux is 11 g·m<sup>-2</sup>·d<sup>-1</sup> in the lower right corner. At this step, the higher flux keeps in the same preferential area mentioned before. At the end of the simulation after 46 days, with the highest injection rate (60 L·h<sup>-1</sup>), the surface flux was mainly divided into two preferential areas (Fig. 14d). A main emission area in the upper left

corner is identified with a maximum CO<sub>2</sub> emission flux of 405 g·m<sup>-2</sup>·d<sup>-1</sup>; that area is actually divided into two point-sources without any connection. The other main CO<sub>2</sub> surface flux point was of 310 g·m<sup>-2</sup>·d<sup>-1</sup>. The lower emission area was in the lower right corner with a minimum CO<sub>2</sub> emission flux of 16 g·m<sup>-2</sup>·d<sup>-1</sup> placed in the right corner (Fig. 14).

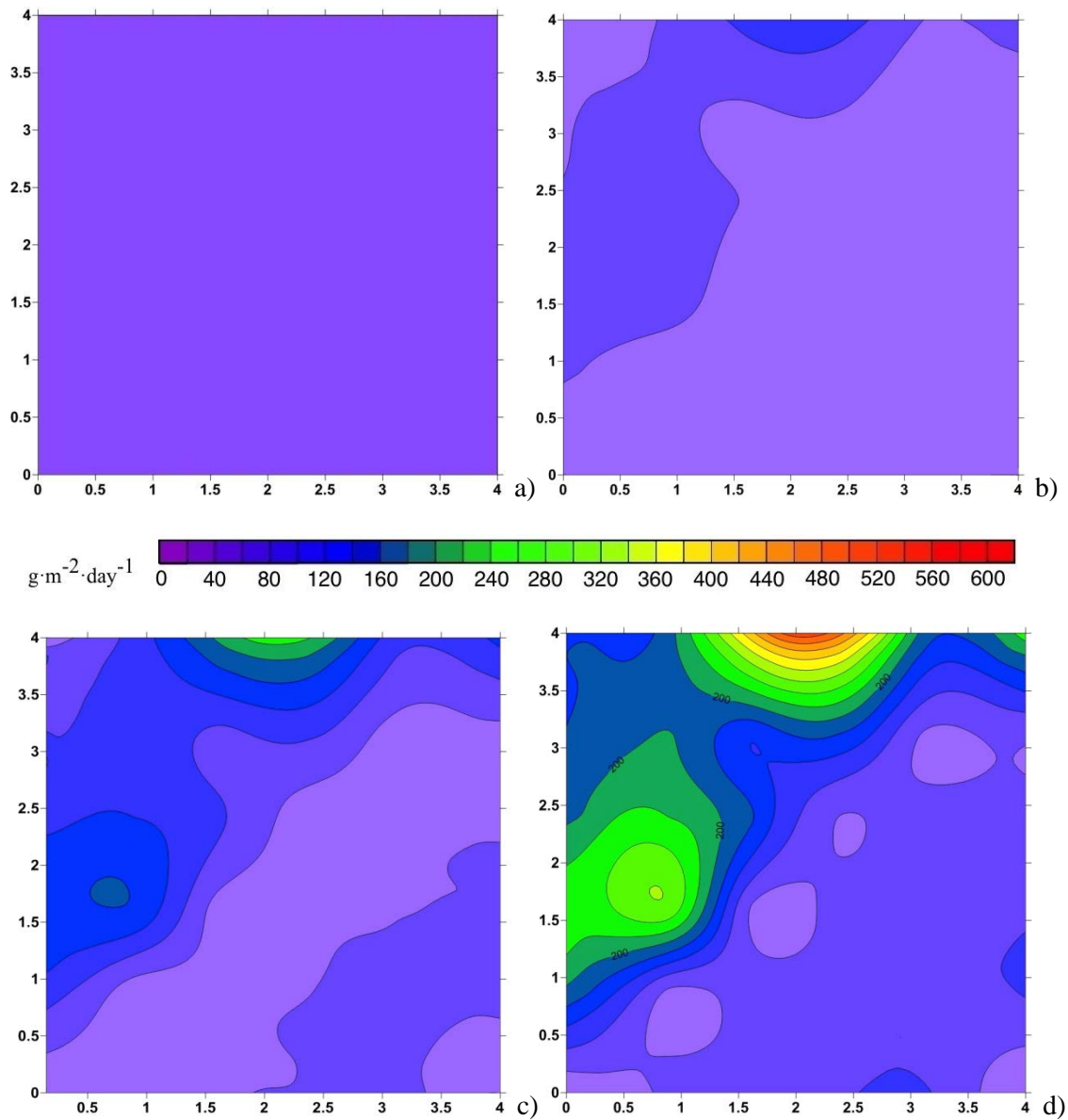


**Figure 14.** Contour mapping of surface CO<sub>2</sub> flux predicted in the Model E. The represented times are 4 (a), 21 (b), 32 (c), 46 (d) days, respectively.

In this Model E, a total amount of 62.1 kg of carbon dioxide is injected from which 45.9 kg were emitted to atmosphere and 16.2 kg were trapped in the cell. The trapped CO<sub>2</sub> was split into 7.7 kg in the gaseous phase and 8.5 kg in the aqueous phase.

### 8.3.3. Pressure and liquid saturation evolution

The analysis of the simulated pressure evolution for each model shows, as expected, that a greater amount of water in the system increases the pressure, even keeping the same atmospheric pressure. However, the impact on pressure is not significant if water is added in the system via rainfall. In figure 15, the pressure variation in depth are shown for each model simulation after the experimental period (46 days), Apart from Model E, the model simulations predict a liquid saturation of 0.3. An increase of 0.2 units in the liquid saturation (Model E) causes an increase of 30 Pa in the cell compared with the Model A, while for Model D the increase is 340 Pa.

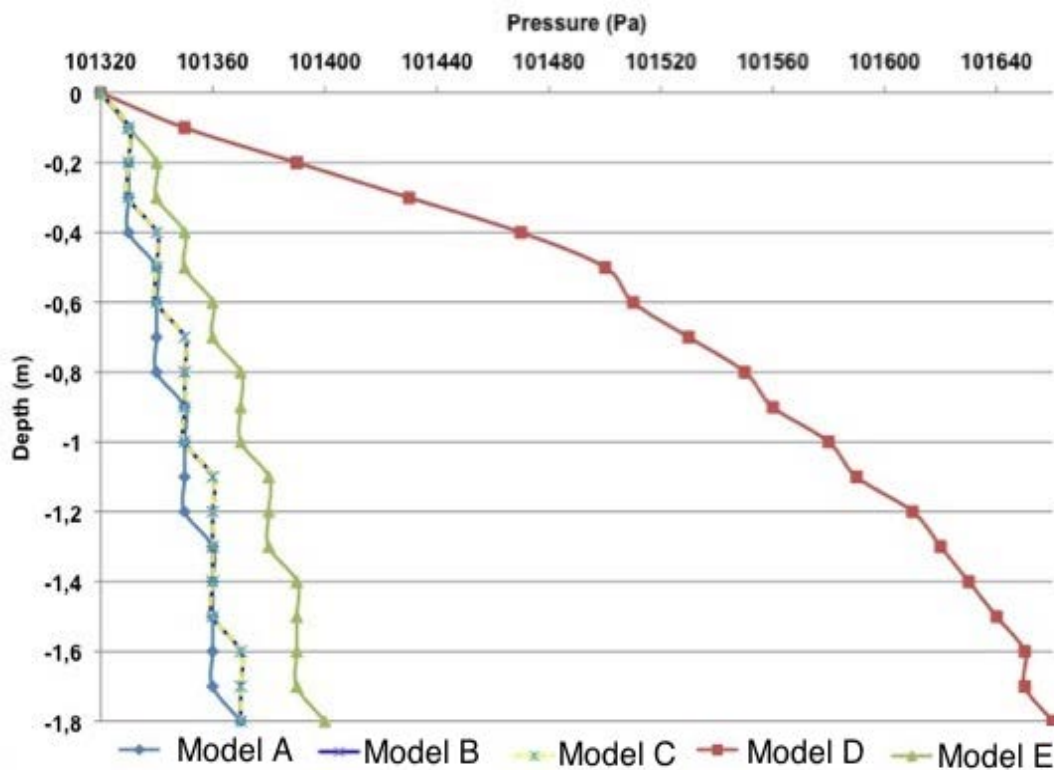


**Figure 15.** Pressure variations in depth predicted in the numerical simulations. Note that Model B and Model C show the same trend.

Concerning the evolution of the liquid saturation (Table 7), all simulations having the same initial liquid saturation show similar evolution even considering different permeability and porosity. In the Model D, the system contains the higher amount of water with a saturation that varies between

0.75 and 0.78. In the Model A, the initial liquid saturation is 0.3 and reaches a maximum value of 0.4. Similar numbers are computed Model B (from 0.3 to 0.37).

**Table 7.** Final liquid saturation predicted in each simulation.

Model Simulation	Liquid Saturation
Model A	0.3-0.4
Model B	0.3-0.37
Model C	0.3-0.35
Model D	0.75-0.78
Model E	0.5-0.53

### 8.3.4. Quantitative representation of model calibration to field data

In figure 16 the root mean square errors for the field experiment (red line) and the five numerical models (model A, B, C, D, E, green line, purple line, sky blue line, orange line, blue line respectively) are shown, using the equation:

$$RMSE = \sqrt{\frac{\sum_{i=1}^n a_i^2}{n}} \quad \text{eq. (6)}$$

The standard deviation trend of the field experiment is crescent and a similarity is found with three models out of five. Models A and D are those outermost from field model deviation trend, the first has a flat trend and the deviation error never raises over 3 g·m<sup>-2</sup>·d<sup>-1</sup>, the second with a maximum deviation of 148.07 g·m<sup>-2</sup>·d<sup>-1</sup> follows the general ascending trend of the field model but with a visible error oscillation.

As said, the numerical models that best fit the field experiment standard deviation are model B, C and E. Between those three models, model C is the one that moves away from the field experiment trend having higher deviation errors. Errors for models B and E are very similar to field experiment errors.

The values of the root mean square errors for the field experiment and for each model are reported in Table 8.

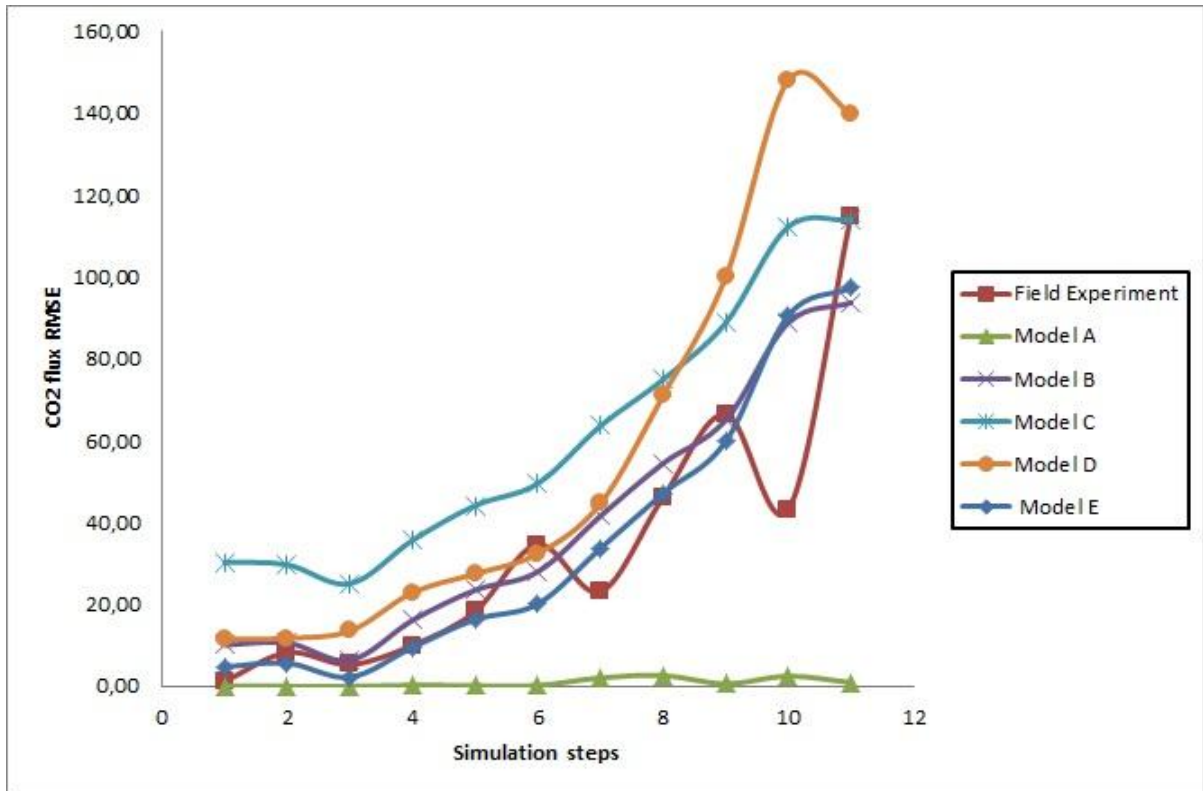


**Figure 16.** Root mean square error for the field experiment (red line) and the numerical models (model A green line; model B purple line; model C sky blue; model D orange line; model E blue line).

**Table 8.** Root mean square errors data for the field experiment and each simulation model.

Field experiment	Model A	Model B	Model C	Model D	Model E
1.20	0.13	10.10	30.34	11.50	4.81
8.27	0.05	10.66	29.71	11.76	5.69
5.33	0.01	6.38	25.09	0.01	2.26
10.07	0.32	16.15	35.70	22.92	9.51
18.31	0.18	23.51	44.18	0.23	16.36
34.67	0.23	28.01	49.57	32.40	20.15
23.12	2.10	41.60	63.63	44.65	33.71
46.17	2.69	54.47	74.59	0.78	47.15
66.53	0.64	65.05	88.79	99.94	59.81
43.21	2.53	88.81	112.25	148.07	90.59
114.83	0.96	93.79	114.03	1.09	97.37

## **8.4. Discussion**

In the PISCO2 experimental unit, the original filling material, basically coarse sand, was well sorted and no major differences in the hydraulic properties were initially expected. However, measurement of soil gas during the experiments revealed the formation of preferential pathways and channelling even at early times. The reason behind can be found in the coarse sand displacement related to water injection-pumping tests performed before CO<sub>2</sub> injection experiments to check equipment. In one of these tests, the cell was quickly dried likely causing coarse sand movement and slight changes in permeability and porosity leading to preferential migration pathways. The amount of injected CO<sub>2</sub> on surface is the same in all model calculations (62.1 kg) as well as the amount of CO<sub>2</sub> in gas and aqueous phases, respectively 7.5 and 3.5 for the homogeneous models, 7.43 and 3.47 for the heterogeneous models. However, the CO<sub>2</sub> flux patterns are notably modified as well as the time needed to reach the surface. In fact, after 4 days of injection, model calculations predict large changes in the maximum surface flux (Model A had a maximum emission of 16 g·m<sup>-2</sup>·day<sup>-1</sup> while in the Model B was of 32 g·m<sup>-2</sup>·d<sup>-1</sup>). The latter are close to the maximum emission of 27 g·m<sup>-2</sup>·d<sup>-1</sup> recorded in the experimental runs. At the end of the simulation, the model predicts a preferential emission area smaller than that mapped in the experiments that may be related to a continuous emission on surface since the beginning of the injection. This is supported by the hot spot that had a final emission value of 600 g·m<sup>-2</sup>·d<sup>-1</sup> for the field experiment and 389 g·m<sup>-2</sup>·d<sup>-1</sup> for the heterogeneous model (Fig. 17).



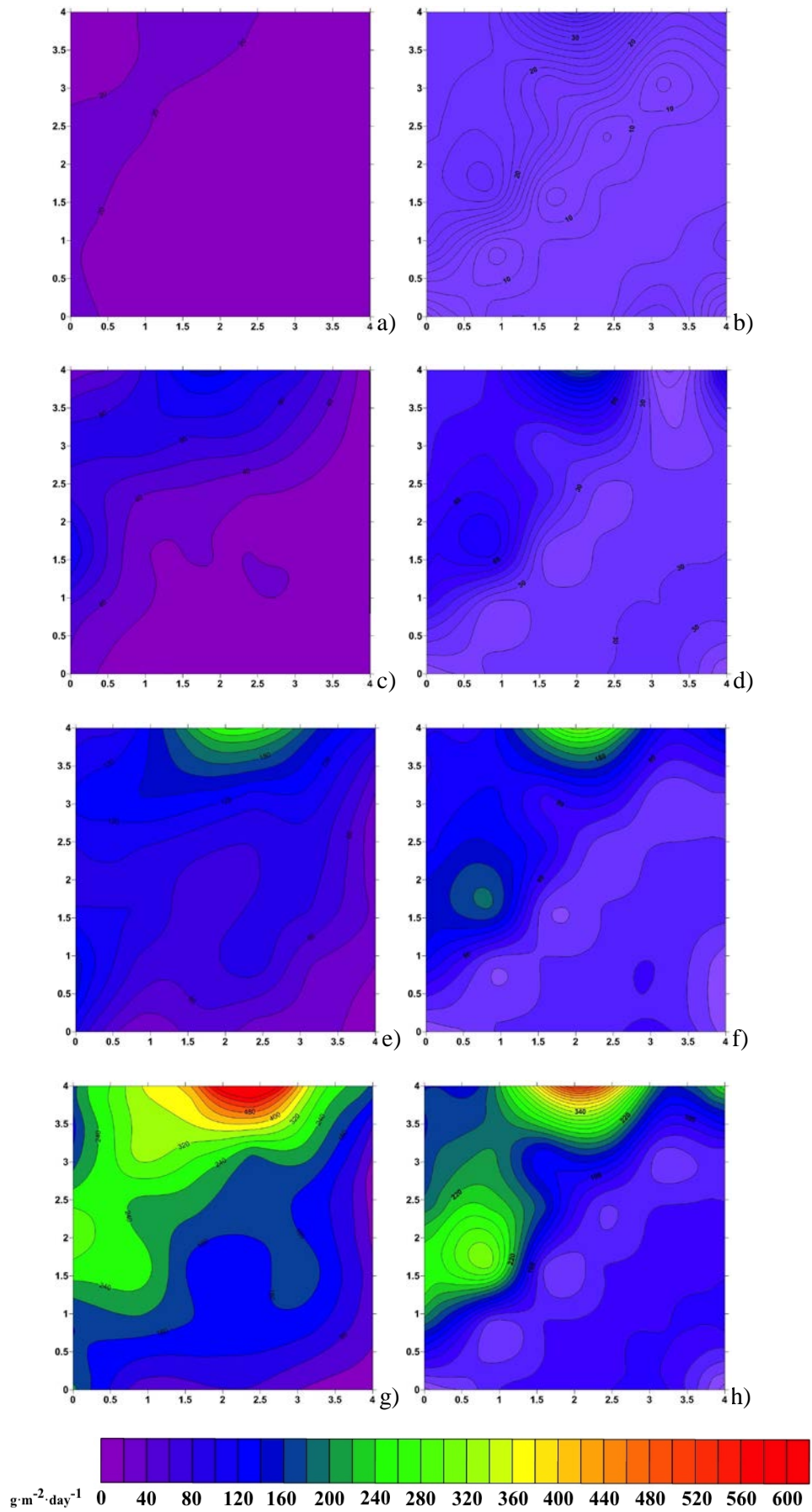


**Figure 17.** Comparison of experimental CO<sub>2</sub> flow map (on the left) and predicted flows in Model B (on the right). The represented times are 4 (a, b), 21 (c, d), 32 (e, f), 46 (g, h) days, respectively.

Table 9 shows the maximum, minimum and mean value of CO<sub>2</sub> surface flux for the field experiment and the five numerical models.

As predicted in the numerical simulations, the heterogeneity on permeability and porosity can modify the pattern of carbon dioxide degassing velocity both in vertical and in horizontal axes. From the CO<sub>2</sub> transport point of view, the consideration of soils with higher and lower permeability and porosity does imply significant changes in the surface emission times compared with the model with homogeneity. With layered soils, it is conditionally possible to detect CO<sub>2</sub> leakage away from the leakage source (tens of meters) than in unlayered soils (Ogretim et al., 2012). This finding could potentially help reducing the cost and density of surface monitoring networks (Yang et al., 2011), which are imperative for a successful CO<sub>2</sub> sequestration project (Pollak and McCoy, 2011).

**Table 9.** Maximum, minimum and mean value of CO<sub>2</sub> surface flux for the field experiment and the five numerical models.

CO <sub>2</sub> (g·m <sup>-2</sup> ·d <sup>-1</sup> )	Experimenta I model	Model A	Model B	Model C	Model D	Model E
Maximum value	600.84	123.27	389.11	487.82	123.28	405.19
Average value	195.23	121.59	127.18	176.56	121.18	127.24
Minimum value	26.61	120.06	19.49	39.85	118.37	16.23

### ***Effects of soil compaction***

The results obtained from the numerical-simulated scenarios show the important role of soil compaction (Model B) in the behaviour of CO<sub>2</sub>. Soil compaction is the term for the determination of soil structure by mechanical pressure resulting in air expulsion from the pores and as water as well. Thus, such stress produces a change in soil permeability, porosity and liquid saturation. Model B shows that the presence of soils with different compaction at surface influences the CO<sub>2</sub> dispersion. The inclusion of soils with different permeability, porosity and liquid saturation results in preferential pathways. The formation of preferential pathways in the soil and hot spots on the surface has

commonly been observed in natural systems where deep CO<sub>2</sub> fluxes interact with shallow aquifers (Fig. 18) (Costa et al., 2008; Agnelli et al., 2013).



**Figure 18.** Example of channelled emission and flow through very small spots in the Campo de Calatrava natural analogue (central Spain). On the bottom of the picture two spots (red circles) of high CO<sub>2</sub> (trace gases) flux (>5000 g·m<sup>-2</sup>·d<sup>-1</sup>); background emission (<20 g·m<sup>-2</sup>·d<sup>-1</sup>) related to biological activity found in the surrounding area.

This behaviour has important implications in the monitoring strategies of commercial CO<sub>2</sub> storage. In general, potential leakage can be detected by a number of methodologies, including fluid geochemistry, geophysics and biotracers. One of the conventional techniques is the mapping of soil gas fluxes by using an accumulation chamber during the operational and closure stages (Beaubien et al., 2013, Quattrocchi et al., 2008), comparing the data with the background fluxes (baseline maps) (Elío et al., 2012). The combined results from modelling, experimental injection and natural system observations suggest that the detection of “hot spots” can be extremely difficult due to its small emission areas. Normally, the extension to be monitored is of several km<sup>2</sup> and monitoring meshes

draw distances between measurement stations around 50-100 m or more (Elío et al., 2012). Such distances are by far longer than the potential emission areas implying a high chance of no detection.

In addition, the patterns of emission at surface can significantly change through time due to weather conditions (soil saturation or drying), making difficult the monitoring of leakage spots (see below).

As seen in figure 9 each sample value keeps the same ranking. This means that channelling or preferential pathways are developed early in time during a leakage and in absence of tectonic activity (as active fault or thrust and earthquakes) those last in the same place.

### ***Effects of water infiltration***

The Model D predicts the effects of a large amount of water inside the cell during the injection period for a total amount of 276 mm of rainfall. The presence of water percolating inside the cell caused a delay in CO<sub>2</sub> emission on surface as well as a net increase of CO<sub>2</sub> dissolved in water. The carbon dioxide trapped in the gas phase predicted by the Model D is the smallest quantity (4.4 kg) in all simulations. An important result is the CO<sub>2</sub> emission homogeneity on surface for the entire simulation due to the high amount of water percolating despite the presence of compacted soils. This simulation is important because it shows how the presence of water in the first centimetres not only increases the CO<sub>2</sub> water dissolution but also tends to homogenize the surface emission.

### ***Effects of weather conditions***

Soil temperature and water content (due to initial liquid saturation and/or rainfall and infiltration effect) play an important role in soil degassing. In Model C, the temperatures used for the simulation were of 15° C in the soil volume and of 40° C for the atmosphere. That test on the environmental temperature at 40° C has shown how the amount of carbon dioxide emitted on surface is the highest (53.7 kg) and the amount of CO<sub>2</sub> dissolved in the aqueous phase is the smallest (1.7 kg) in all the tests (see Fig. 10). Furthermore, emission times were speed up. Already at day 4 the main emission area had a flux of 80 g·m<sup>-2</sup>·d<sup>-1</sup> and 140 g·m<sup>-2</sup>·d<sup>-1</sup> in the hot spot. That rapid emission trend kept during all the simulation with the largest preferential emission area between all simulations (see fig. 13) and a second hot spot was observed close the left wall with a value of 350 g·m<sup>-2</sup>·d<sup>-1</sup>.

### ***Effects of initial water saturation***

A different behaviour was predicted from the model with the highest initial saturation (Model E) as seen in figure 14. In this simulation, the initial liquid saturation leads to a decrease in the CO<sub>2</sub> surface emission compared with others models because carbon dioxide is firstly trapped in the liquid phase. Even in this model, a channelling effect is observed in the main emission area. In fact, in that area, two hot spots were predicted with the surrounding area with very low emissions.

The PISCO2 facility is a closed system opened only at surface. As described in figure. 3 rainfalls produced only 18 mm during the experiment period so we can assert no variation in water content happened.

### *Effects of atmospheric agents*

Barometric pumping effect and wind effect could also influence CO<sub>2</sub> flux in the soil-atmosphere interface. The barometric pumping effect relates to the diurnal changes of ambient pressure due to change in the temperature, as well as pressure changes due to weather systems such as mid-latitude cyclones. This variation in pressure at the surface acts as a suction-pump on the underground (Carrigan, 2010). The wind effect drives to an enhanced mixing layer due to its turbulent character, which increases the rate of seepage into the atmosphere (Oldenburg and Unger, 2004). Low-frequency atmospheric motions are less effective than higher-frequency motions at trace gas transport (Waddington et al., 1996).

Oldenburg and Unger (2003) have investigated the effects of barometric pumping on the seepage and near-surface mole fraction of CO<sub>2</sub> using TOUGH2 numerical code with the research module EOS7CA, resulting that barometric pumping has a negligible effect on the time-averaged seepage flux and near-surface CO<sub>2</sub> concentration because of the cyclic nature of the pressure-induced flows.

Comparing leakage rate used in Oldenburg and Unger (2004) with leakage recorded at PISCO2 experimental unit (Table 10) we can assert that PISCO2 has a low leakage rate so barometric pumping effect is negligible.

**Table 10.** Comparison between the leakage rate used by Oldenburg and Unger (2004) and those obtained at the PISCO2 experimental unit and from our Model B.

	Leakage rate (g·m <sup>-2</sup> ·d <sup>-1</sup> )
Oldenburg and Unger (2004)	143 - 1432 - 14318

---

PISCO2	600
Model B	389

---

To make a comparison with other similar projects is not so direct because of a lack of data like soil characteristics or due to a different injection setting.

As described above, leakage rate of PISCO2 experimental facility and modelling results are similar to the ZERT release facility where localized high-flux regions (called patchy emission) were observed. The patchy emission pattern appears to result from the packer blocking dang-pipe flow and causing an effective point-source release (Oldenburg et al., 2010a). In comparison with PISCO2, permeability at the ZERT is one order of magnitude higher, and the main difference is the CO<sub>2</sub> source that is punctual in PISCO2 and is linear for the ZERT experiment. Same result was observed at the CO<sub>2</sub> Field Lab where areas of highest flux at surface were spatially limited to few m<sup>2</sup> (Jones et al., 2014).

Similar results were obtained at the RISCS project with a CO<sub>2</sub> leakage spatially heterogeneous. Flux distribution was spatially uneven with several zones of moderate and high flux, as well as some irregularly shaped low flux regions (Moni and Rasse, 2014).

According to Hinkle (1994) rainfalls infer to act as a physical barrier to follow and, in larger amounts, cause dissolutions and displacement of gases. Such result was seen in our results for Model D and E (respectively with continuous rainfall and higher liquid saturation) and at the CO<sub>2</sub> Field Lab. Heavy rain had a significant effect on the soil gas concentrations and reduced the flux of CO<sub>2</sub> for several hours, even in such high permeability and free-draining substrate (Jones et al., 2014).

At PISCO2 facility, water displacement is restricted for the boundary concrete walls and in the numerical models water saturation changed in the order of  $\pm 0.1$  from more to less compacted soils (Fig. 19), in accord with what seen by Oliva et al., (2014) at Ressaccada Pilot Test where fluids movements through porous media lead to the occurrence of areas that serve as preferential paths for the gas displacement.



## **8.5. Conclusions**

Coupled experimental and modelling study has been performed to better understand CO<sub>2</sub> migration in the vadose zone in case of failure of a geological storage. Results of monitoring of CO<sub>2</sub> fluxes in the ground/atmosphere interface in PISCO2 experimental platform are in good agreement with the range of CO<sub>2</sub> fluxes measured in natural analogues showing spots of higher surface leakage. Numerical models were performed to simulate CO<sub>2</sub> transport in the unsaturated zone of PISCO2 experimental unit from 16 micro-injectors until the surface for 49 days.

A good accuracy has been obtained for surface CO<sub>2</sub> fluxes location and intensity between experimental and modelling results taking into account the selected equation of state, the soil characteristics and the operational conditions. Phenomena of compaction and preferential pathways located only in the first centimetres of the soil can explain the heterogeneity of CO<sub>2</sub> fluxes in the 16 m<sup>2</sup> surface area of PISCO2 experimental platform. Increase of ambient temperature increases CO<sub>2</sub> fluxes intensity whereas rainfall decreases CO<sub>2</sub> emission in gas phase and trap it as aqueous species in the porous media of the soil.

Design of long-term monitoring campaign of large-scale commercial CO<sub>2</sub> storage site has to consider spots of CO<sub>2</sub> emission in the meter scale along the large area of potential leakage. With the results obtained in this study about the soil compaction effect on carbon dioxide migration, two techniques of monitoring can be suggested for a CCS site. Soils with different compaction levels can be used to identify preferential emission areas where the possible leakage from the reservoir can concentrate and where the monitoring effort should be focused on. On the other hand, non-invasive geotechnical surveys can be performed, as geoelectrical analysis, seismic tomography, georadar, geochemical analysis, etc.), to recognize soils properties and split areas with different soil compaction in order to highlight areas favourable to CO<sub>2</sub> emission.

## **8.6. Acknowledgements**

We are thankful for the technical support to Curtis Oldenburg from the Berkeley University for the use of the research module. Also, we are grateful to CIUDEN for the funding of the project. This study is part of the OXYCFB 300 “Compostilla” EEPR project.



## **9. Research article 2: Atmospheric dispersion modelling of a natural CO<sub>2</sub> degassing pool from Campo de Calatrava (central Spain) natural analogue. Implications for carbon storage risk assessment.**

This article has been published in **International Journal of Greenhouse Gas Control**, **47**, 38-47. DOI:[dx.doi.org/10.1016/j.ijggc.2016.01.033](https://doi.org/10.1016/j.ijggc.2016.01.033), with the title “**Atmospheric dispersion modelling of a natural CO<sub>2</sub> degassing pool from Campo de Calatrava (northeast Spain) natural analogue. Implications for carbon storage risk assessment**”. In the title of the manuscript there is an error regarding the geographical position of the site, which is placed in central Spain not in the northeast as written.

In the manuscript, the article “TWODEE-2: A shallow layer model for dense gas dispersion on complex topography. *Computers and Geosciences*, 35, 3, 667-674” is reported as Folch et al., (2008) and Folch et al., (2009). The right reference is Folch et al., (2009).

### **9.1. Introduction**

Carbon Capture and Storage (CCS) has been deployed in recent times as a technology to reduce CO<sub>2</sub> emissions into the atmosphere from anthropogenic activities such as power plants, cement production and refineries. After been captured, carbon dioxide is injected into deep geological formations that are able to store it under different mechanisms (physical, residual, solubility and mineral trapping). In case of leakage, carbon dioxide could reach the ground surface jeopardising natural and anthropogenic environments.

Natural systems provide evidences of the impact of CO<sub>2</sub> leakage on vegetal cover and wildlife (Bateson et al., 2008; Carapezza et al., 2003; Farrar et al., 1995). Root asphyxia due to O<sub>2</sub> displacement in soil and acidification lead to localised loss of vegetation. Release of high amounts of minor and trace metals due to the dissolution of iron (III) oxi-hidroxides (Bruno et al., 2009; Agnelli et al., 2013) may cause significant changes in the shallow and surface waters and related living organisms. A less known process is the formation of a CO<sub>2</sub>-rich air related to high leakage rates. The higher density of CO<sub>2</sub>-enriched air promotes its accumulation near the ground, leading to the so-called “CO<sub>2</sub> lakes” (see Fig. 21, 22). Under stable atmospheric conditions and/or in presence of

topographic depressions, CO<sub>2</sub> concentrations can reach high values resulting in lethal effect to living organisms. The distribution of denser-than-air gases released from the underground is governed by gravity, turbulence and dispersion. Once emitted, the gas distribution is initially driven by buoyancy and a gas cloud accumulates on the ground (gravitational phase); with time the density gradient becomes less important due to dispersion or mixing, and gas distribution is mainly governed by wind and atmospheric turbulence (passive dispersion phase) (Costa et al., 2008; Folch et al., 2009).

The formation of CO<sub>2</sub>-rich plumes may play a significant role on the risk assessment of carbon storage as it could represent the highest hazard for human beings. De Lary et al., (2012) have reported the impact of CO<sub>2</sub> concentration in air on human beings; they summarize the effects of its inhalation as a function of the concentration and duration of exposure. A number of studies about the effects of respiratory exposure to carbon dioxide has been reported (Baxter et al., 1999; Faivre-Pierret and Le Guern, 1983 and references therein; NIOSH, 1981), showing the hazardous levels of CO<sub>2</sub> concentration in air for humans:

- 2-3% Unnoticed at rest, but on exertion there may be marked shortness of breath;
- 3-5% Breathing becomes noticeably deeper and more frequent at rest;
- 5% Breathing becomes extremely laboured, occurrence of headaches, sweating and bounding pulse;
- 7.5% Rapid breathing, increased heart rate, occurrence of headaches, sweating, dizziness, shortness of breath, muscular weakness, loss of mental abilities, drowsiness, and ringing in the ears;
- 8-15% Headache, vertigo, vomiting, loss of consciousness and possibly death if the patient is not immediately given oxygen;
- 10% Respiratory distress develops rapidly with loss of consciousness in 10-15 minutes;
- >25% Convulsions occur and rapid loss of consciousness ensues after a few breaths. Death will occur if level is maintained.

High, dangerous CO<sub>2</sub> concentration in atmosphere (>1% CO<sub>2</sub>) related to natural or industrial underground emission has been occasionally reported (Chiodini et al., 2010; Carapezza et al., 2012) although the conditions favouring the persistence of such a concentration are barely studied.

In this work, the dynamics of CO<sub>2</sub> in the atmosphere after ground emission is assessed to quantify their potential risk. Two approaches have been followed: (1) direct measurement of air concentration in a “natural analogue”, where formation of a “CO<sub>2</sub> lake” is common and (2) numerical atmospheric modelling. Conclusions from this work provide clues on whether leakage may be a real

risk for humans and under which conditions this risk needs to be included in the risk assessment of geological storage of CO<sub>2</sub>.

The studied site is located in the Campo de Calatrava region in central Spain, which is known for a widespread degassing of mantle-derived CO<sub>2</sub>. According to Elío et al., (2015), the CO<sub>2</sub>-rich emissions at Campo de Calatrava Volcanic Field are mainly associated with fracture systems and the gas discharge are regarded as point-source seepage, being occasionally characterized by relatively high flow (>1 t·m<sup>-2</sup>·d<sup>-1</sup>).

## **9.2. Natural CO<sub>2</sub> emission from underground. Examples from the Campo de Calatrava Volcanic Field**

The Volcanic Field of Campo de Calatrava (CCVF) is an area of 5000 km<sup>2</sup> with around 240 volcanic structures, located in central Spain (Fig. 20) between Toledo and Sierra Morena ranges, on the eastern edge of the Tertiary Tajo Basin. This area is composed of a Hercynian basement with late Cenozoic sedimentary cover. The CCVF area recorded three different tectonic episodes during the Neogene (IGME, 1998) and it is characterized by a Plio-Quaternary volcanic activity with strombolian and hydromagmatic eruptions dated between 8.7 and 1.75 Ma ago (Ancochea, 1999; Gonzalez et al., 2007), composed by mafic lavas of alkali composition (Cebriá and Lopez-Ruiz, 1995; Lopez-Ruiz et al., 2002). The CCVF, along with La Selva-Empordà basins (NE Spain), are the regions with the largest natural CO<sub>2</sub> degassing in the whole continental Spain (Martin-Serrano et al., 2009; Vaselli et al., 2013).

The Cañada Real site has the largest point-source degassing rate of the CCVF, and is found in Bolaños de Calatrava municipality, close to the city of Ciudad Real. This site is an almost circular pool of 10 meters of diameter with maximum depth of around 6 meters (Fig. 21). Its present-day shape is interpreted from three electrical resistivity tomography profiles as a sinkhole due to dissolution and collapse of a top calcarenitic formation (Agnelli et al., *submitted*). Early results have shown the presence of an aquifer with different levels of permeability. In particular, a low resistivity level is present above the carbonate formation, and the CO<sub>2</sub> dissolution has favoured the sinkhole formation.

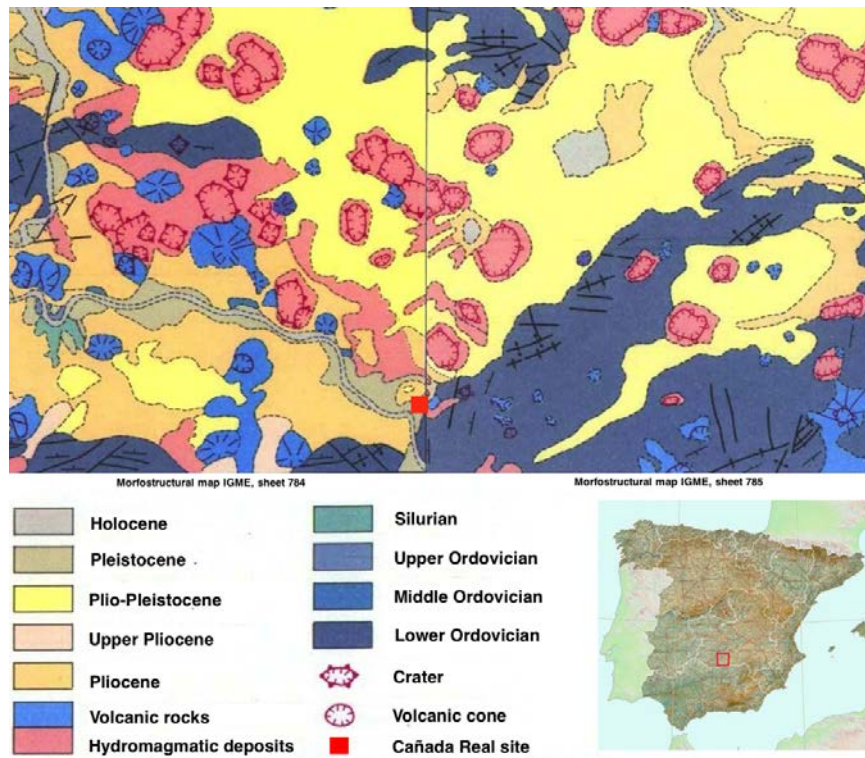


**Figure 20.** Morfostructural map of the area around Cañada Real; location of the investigation site is marked by the red square (from IGME, 1998).

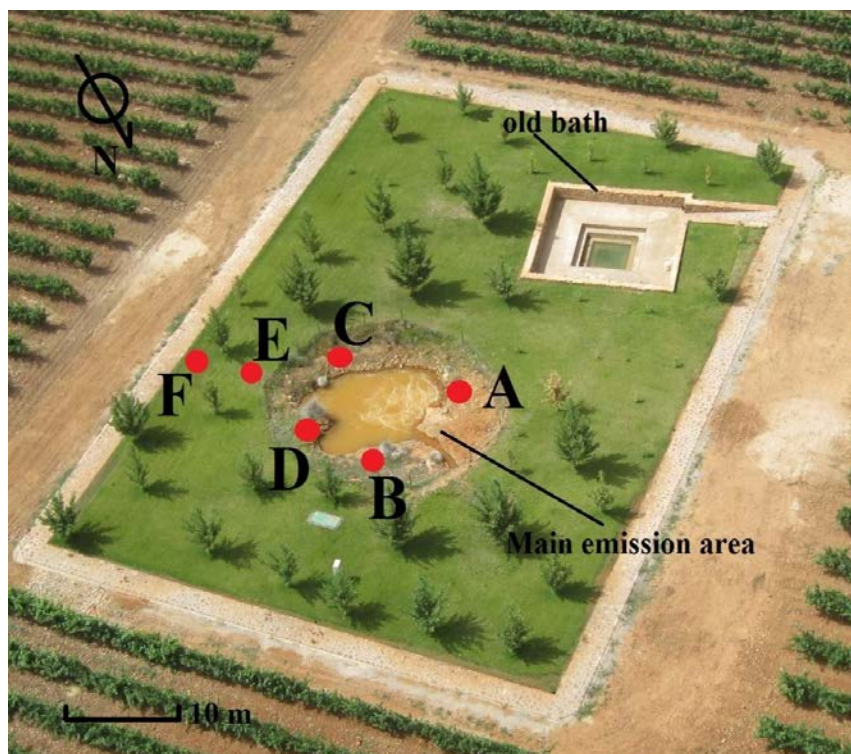


**Figure 21.** Aerial view of the Cañada Real site, showing the location of the air CO<sub>2</sub> concentration measurement stations (denoted as A to F).

From the geological point of view the pool is found in Lower Pliocene calcarenites overlaid by hydromagmatic deposits from Upper Miocene to Lower Pleistocene. The pool shows a continuous gas bubbling due to high CO<sub>2</sub> flux ( $>20,000 \text{ g}\cdot\text{m}^{-2}\cdot\text{d}^{-1}$ ). Like other emission point-sources in the CCVF (Elío et al., 2015; Vaselli et al., 2011; Vaselli et al., 2013), CO<sub>2</sub> is predominant in the gas phase ( $>98\%$  wt), with very high radon concentration in soil (up to  $453 \text{ kBq}\cdot\text{m}^{-3}$ , Elío et al., 2015). Gas temperature is around 45 °C.

When atmospheric conditions are quite stable (calm days without wind), the formation of a blanket of CO<sub>2</sub>-enriched air is visible at naked eye reaching up to 50 cm high (Fig. 22a). A much clearer observation is obtained when a smoke flare is lighted (Fig. 22b). Under these conditions, the concentration of CO<sub>2</sub> in air is high enough in air to kill animals approaching to the pool, like small birds, reptiles and mammals; vegetation is also absent in the area with high gas flux.



**Figure 22.** a) Formation of a CO<sub>2</sub> lake visible in the Cañada Real site, b) View of the Cañada Real site after lighting a smoke flare. The smoke (yellow) is not able to rise due to the denser blanket of the CO<sub>2</sub>-enriched air.

The pool has generally a constant water level with an average water discharge of 50 L·min<sup>-1</sup>. However, due to episodic water production from a well located in the vicinity of the pool, the water level decreases down to 7-8 cm when the well pumps out water. This behaviour suggests a direct connection between the pool and the aquifer beneath.

Similar scenarios are found in central Europe as Laacher See (Germany), Montmiral (France), Mihalyi-Repcelak (Hungary), Florina (Greece) (Pearce et al., 2016), Vorderrhon (Germany, Ginggenbach et al., 1991), Solforata di Pomezia (Italy, Carapezza et al., 2012), and Latera (Italy, Annunziatellis et al., 2008). Those natural analogues are linked to natural gas reservoirs connected to surface through extensional basin areas, rift systems, hydrothermal fields, active or recent active volcanic areas.

### **9.3. Measurements of CO<sub>2</sub> flow from underground and CO<sub>2</sub> concentration in air**

The CO<sub>2</sub> concentration in air has been measured in the surrounding of the Cañada Real pool with a Telaire sensor. The underground emission has been determined with a Sistema Alta Portata (SAP) system (see description below), evaluating the total gas flow from the pool.

#### **9.3.1. *Telaire***

The Telaire 7755 is a portable tool that measures CO<sub>2</sub> concentration, air temperature, dew point, wet bulb temperature and humidity. The portable CO<sub>2</sub> meter uses a non-dispersive infrared (NDIR) sensor to ensure reliability and long-term stability. This sensor detects carbon dioxide concentration in air up to 10,000 ppm (1% air concentration) that can be recorded continuously. An anemometer recording wind speed and direction was coupled to the Telaire during the sampling.

Air concentration was measured during 400 seconds at different heights from ground (10, 50, and 100 cm) mainly under very low wind conditions (less than 1 m·s<sup>-1</sup>) and stable atmospheric conditions in 6 stations: four were located on the shore of the pool (stations A, B, C, and D), and two were installed more distant (stations E and F) (Fig. 21). Sampling stations A, B, C and D were located equidistant on the shore around the pool to capture the distribution of CO<sub>2</sub> in a wide range of directions, being station A the nearest to the main emission source. Stations E and F were thought to observe the CO<sub>2</sub> distribution far from the emission point and were located 5 and 10 meters

respectively far from the pool to the southeast, as the predominant wind direction in the area is NW to SE (see section 9.6.1.).

### 9.3.2. *Sistema Alta Portata (SAP)*

This technique called Sistema Alta Portata (High Discharge System) has been used to estimate the gas flux from a large emission pool and was previously used by Siracusa and Quattrocchi (2007), who in turn improved a method first developed by Rogie et al., (2000). It is made up of a circular impervious plastic blanket, 8-m in diameter, with a pipe in its centre (Fig. 23). Once installed, the blanket has to be fixed on the ground by stakes and sealed on the edge with sand and clay. The sealing is to avoid major leakage from the soil/blanket interface.

The aim of this method is to fill the blanket with the emitted gas (as shown in Fig. 23), concentrating all the gas flow through the pipe. Depending on the flux, the pipe can be adapted to show a range of diameters. In this case we used a pipe with a diameter of 10 cm. Once the steady state is reached, it is possible to measure the gas flux at the pipe outlet using an anemometer.



**Figure 23.** The SAP system installed and working at Cañada Real site. Note the pipe connected to the centre of the blanket to determine gas flux.

As described by Siracusa and Quattrocchi (2007), the gas flow can be estimated as (eq. 7):

$$\phi_{CO_2} = \phi \cdot C_{CO_2} = \frac{\pi \cdot r^2 \cdot v \cdot P}{R \cdot T} \cdot C_{CO_2} \quad (\text{eq.7})$$

where  $r$  is the radius of the pipe (cm),  $v$  is the flux velocity at the outlet tube (L min<sup>-1</sup>),  $P$  is the atmospheric pressure (atm),  $R$  is the ideal gas constant (82.057 cm<sup>3</sup> atm mol<sup>-1</sup> L<sup>-1</sup>),  $T$  is the gas temperature (K), and  $C_{CO_2}$  is the carbon dioxide concentration (mol min<sup>-1</sup>).

## 9.4. Atmospheric dispersion modelling

Atmospheric dispersion modelling allows the prediction of air composition through time, taking into account the effects of gravity and turbulence. In this work, modelling provides numerical quantification of the extent and intensity of CO<sub>2</sub> concentration in the atmosphere emitted from an underground source. The final goal is to compare model prediction with field measurements and to provide clues for the related risk assessment.

To model gas emission and accumulation in the Cañada Real site, the TWODEE2 code (Costa et al., 2008) has been used. This code is based on shallow layer time-dependant Eulerian approach for dispersion of heavy gases, and it is an updated version of the TWODEE code (Hankin and Britter, 1999a, b, c). TWODEE2 is based on depth-averaged equations obtained by interpreting mass, density and momentum equations over the fluid depth, from the bottom up to free surface. Such approach is able to describe the time evolution of gas concentration, depth-averaged velocity, and averaged cloud thickness. The input data include the topography, ground roughness, wind measurements and gas flow rate from the ground sources (Folch et al., 2007). The wind and its effects can be dealt following two approaches: (1) a uniform wind and (2) a spatially variable wind, resulting from a meteorological processor. In the first option wind is considered horizontally uniform and data should be provided by a ground-based station. For the second option the model can be coupled with the output of a meteorological processor that generates a zero-divergence wind field incorporating terrain effects (Folch et al., 2009). In this study all simulations considering wind were developed using the meteorological processor DIAGNO (Folch et al., 2009) coupled with TWODEE2. DIAGNO uses wind data at a point of the domain and, assimilating terrain information, generates a zero-divergence wind field.



## 9.5. Model set-up

The gas emission at Cañada Real covers an area of 1500 m<sup>2</sup> at 600 meters above sea level with a gentle slope to north-west. In order to reproduce the formation of a gas cloud and to predict its atmospheric dispersion, the numerical model is based on a 2D mesh of regular quadratic elements of 1 m<sup>2</sup> and a difference in elevation of 0.1 m to NW, covering a total ground surface of 10000 m<sup>2</sup>. The degassing pool is placed at the centre of the mesh, and a gas emission of 3 t·d<sup>-1</sup> is considered (see section 9.6.2).

Two sets of simulations have been carried out: with and without wind effect (Table 11). Atmospheric pressure conditions ranges from cyclone to anticyclone (980 to 1040 hPa), while soil and atmosphere temperatures were kept unchanged and equal to 20°C and 30°C, respectively. Wind influence was implemented considering two different speeds, 1 and 10 m·s<sup>-1</sup>. The wind blows from the NNW, the main wind direction in the area (see section 9.6.1.). No flow conditions at the boundary were imposed and an initial CO<sub>2</sub> concentration of 400 ppm, the atmospheric background concentration, was considered. Boundary conditions are necessary to define how the site-specific model interacts with entire flow system. The planning of “no boundary condition” was imposed in order to generate an open system. To have no boundary conditions means that the system is open, the simulated plume is free to expand even out of the grid, and its concentrations can change without having to comply with mass conservation, so that there can be flow along the model’s boundary.

**Table 11.** List of simulations with the corresponding features.

Simulations	1	4a	4b	2	5a	5b	3	6a	6b
Atmospheric Pressure (hPa)	980			1010			1040		
Wind speed (m·s <sup>-1</sup> )	0	1	10	0	1	10	0	1	10

Simulations accounting for wind effects, i.e., 4 (a, b), 5 (a, b), and 6 (a, b), to allow an initial gas accumulation in the area start with a period of 12 hours without wind. This condition resembles a windy morning after a calm night, which is in fact a common situation in the area.

## 9.6. Results

### 9.6.1. CO<sub>2</sub> concentration in air

The atmospheric conditions during the CO<sub>2</sub> concentration measurements were stable with mild wind from NE and NNW (Fig. 24). Early in the morning, a calm period with absence of wind was observed. Such calmness period lead to the formation of a CO<sub>2</sub> blanket on the top of the pool (see Fig. 22). Along the day, wind was blowing at speeds ranging between 0 and 12 m·s<sup>-1</sup>.

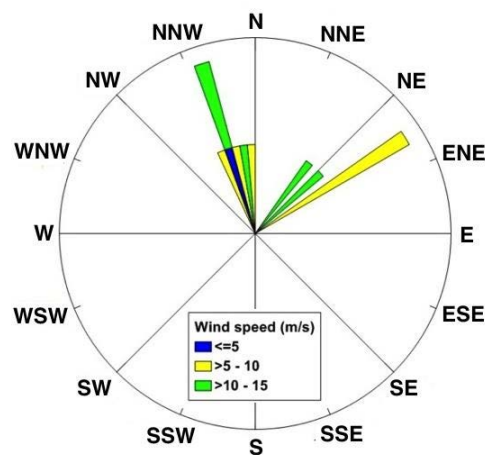


**Figure 24.** Rose diagram of dominant hourly winds. Wind directions that were dominant during one hour are plotted by short triangles, bigger triangles show wind directions that were dominant twice.

Data recorded with the Telaire sensor in stations along the shore (A, B, C and D) (see Fig. 21 to see where stations are located) show the highest values of CO<sub>2</sub> concentration (Fig. 25). Stations A, C and D have reached the sensor saturation limit, with more than 10000 ppm in air at 10 cm, while in station B the sensor did not saturate, reaching a maximum concentration of 8000 ppm. This station is located windward from the dominant wind direction and, therefore, the values recorded are lower.

At 50 cm from surface, stations A and D keep reaching the sensor limit registering concentration from 1800 ppm to more than 10000 ppm, while station C reached a maximum of 8000 ppm. At 50 cm from surface there is a lack of data for station B due to a technical problem occurred on the laptop and data were not saved. At 100 cm from surface the sensor achieved saturation for a short time only in station D, probably due to a decrease of the wind speed or a temporary change in wind direction. Concentrations recorded in stations A, C and D at 100 cm height range between 2000 and 4000 ppm, while in station B never exceeded 2000 ppm. Station A, located in a small depression and the closest to the main bubbling area of the pool, showed higher CO<sub>2</sub> concentrations.

At larger distance from the pool (stations E and F) CO<sub>2</sub> concentrations were lower, with a maximum value of 4200 ppm for station E and around 2000 ppm for station F. Data in both stations are quite similar at different heights pointing out a vertically homogeneous CO<sub>2</sub> plume along wind direction.

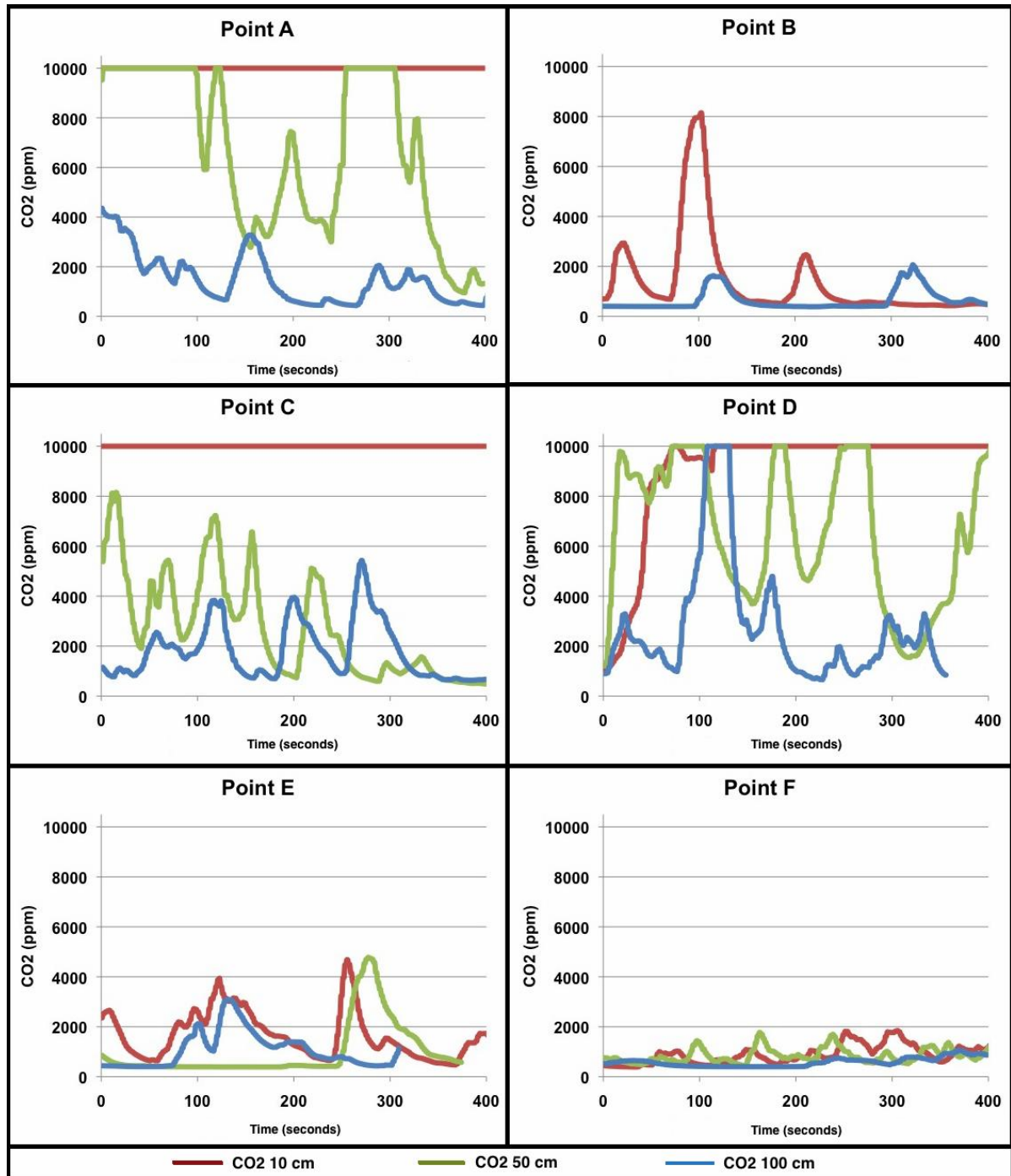


**Figure 25.** Air CO<sub>2</sub> concentration (ppm) recorded at stations A, B, C, D, E and F (see Fig 21) around the pool at different heights (10, 50 and 100 cm). The detection limit of the Telaire is 10000 ppm.

### 9.6.2. SAP system

The data treatment of the measurements from SAP using eq. 7 reveals that the flow from the degassing pool ranged from 1.1 to 3.1 t·d<sup>-1</sup> (equivalent to 2.2·10<sup>4</sup> g·m<sup>2</sup>·d<sup>-1</sup> and 6.1·10<sup>4</sup> g·m<sup>2</sup>·d<sup>-1</sup>) (Table 12). These data are comparable to that from a previous study in this site made by Vaselli et al., (2012) using an IR laser based on the Differential Absorption Spectroscopy. They estimated the overall emission rate in the range of 5-20 t·d<sup>-1</sup> with a mean value around 10 t·d<sup>-1</sup> with horizontal wind of about 4-5 m·s<sup>-1</sup>.

**Table 12.** Data of flow speed (maximum and average), humidity and temperature at the SAP's outlet. The uncertainty for each measurement is also shown.

Measurements	Temperature (°C)	Humidity (%)	Avg. flux (t·d <sup>-1</sup> )	Max. flux (t·d <sup>-1</sup> )	σ <sub>max</sub>
W1	42.2	29	1.12	1.85	0.092
W2	45.5	35	1.50	1.98	0.099
W3	44.0	36	1.76	3.10	0.155
W4	50.3	34	1.73	2.75	0.137

### 9.6.3. Numerical modelling results

Simulations considering air conditions without wind are driven by gravitational forces and topography and predict a preferential expansion toward NW (the more depressed area) of the CO<sub>2</sub>-enriched plume. The lateral spreading of the gas plume is fast and after a couple of hours the plume reaches a steady state and its maximum expansion. Figure 26 shows the maximum concentration predicted at 10, 50 and 100 cm height for simulations with an atmospheric pressure of 980 and 1040 hPa.

As can be seen the atmospheric pressure is not relevant for the distribution of the CO<sub>2</sub> concentration. Models yield similar results for the three different atmospheric pressures, with small variations on the time when the maximum concentration is reached.

At 10 centimetres from surface the plume is predicted to reach a high CO<sub>2</sub> concentration (65000 ppm) in the centre of the pool. The area with a concentration higher than 20000 ppm extends laterally

between 10-20 m occupying the whole extension of the pool. Out of the pool, the concentration is lower and diminishes with distance, reaching a value around 500 ppm close the borders of the domain.

At 50 centimetres high, the CO<sub>2</sub> plume decreases its width. CO<sub>2</sub> concentration is always higher above the pool reaching maximum values around 22000 ppm, while out of the pool only traces of CO<sub>2</sub> with values below 7000 ppm (0.7%) are predicted.

At 100 centimetres high, the plume is much smaller and restricted mainly to the pool limits, reaching 11000 ppm (1.1 %) above the pool. The presence of CO<sub>2</sub> out of the pool is not significant and with low values (less than 2500 ppm).

Simulations that take into account wind (simulations 4, 5 and 6) perform similarly, showing a fast expansion reduction of the gas plume and forming an elongated cloud along the wind direction. At each different atmospheric pressure, the plume follows wind direction and lateral expansion is hindered. Due to the similarity of results only the outputs for simulation S4a at 10, 50 and 100 cm (Fig. 27 a, b, c, respectively) are shown.

At 10 cm high CO<sub>2</sub> concentration over the emission area is predicted to reach 43000 ppm (4.3%) and the plume is continually visible for more than 50 meters long with CO<sub>2</sub> concentration under 8500 ppm. At 50 cm height the maximum CO<sub>2</sub> concentration decreased under 4100 ppm and it is located over the pool, with lower and punctual presence of CO<sub>2</sub> in its vicinity. At 100 cm high, the plume has mostly disappeared with highest concentration below 1500 ppm.

Simulations with a wind speed of 10 m·s<sup>-1</sup> (4b, 5b, 6b) predict the vanishing of the plume, even over the pool, as wind starts to blow. Such occurrence was observed on field while recording wind data and air concentration.

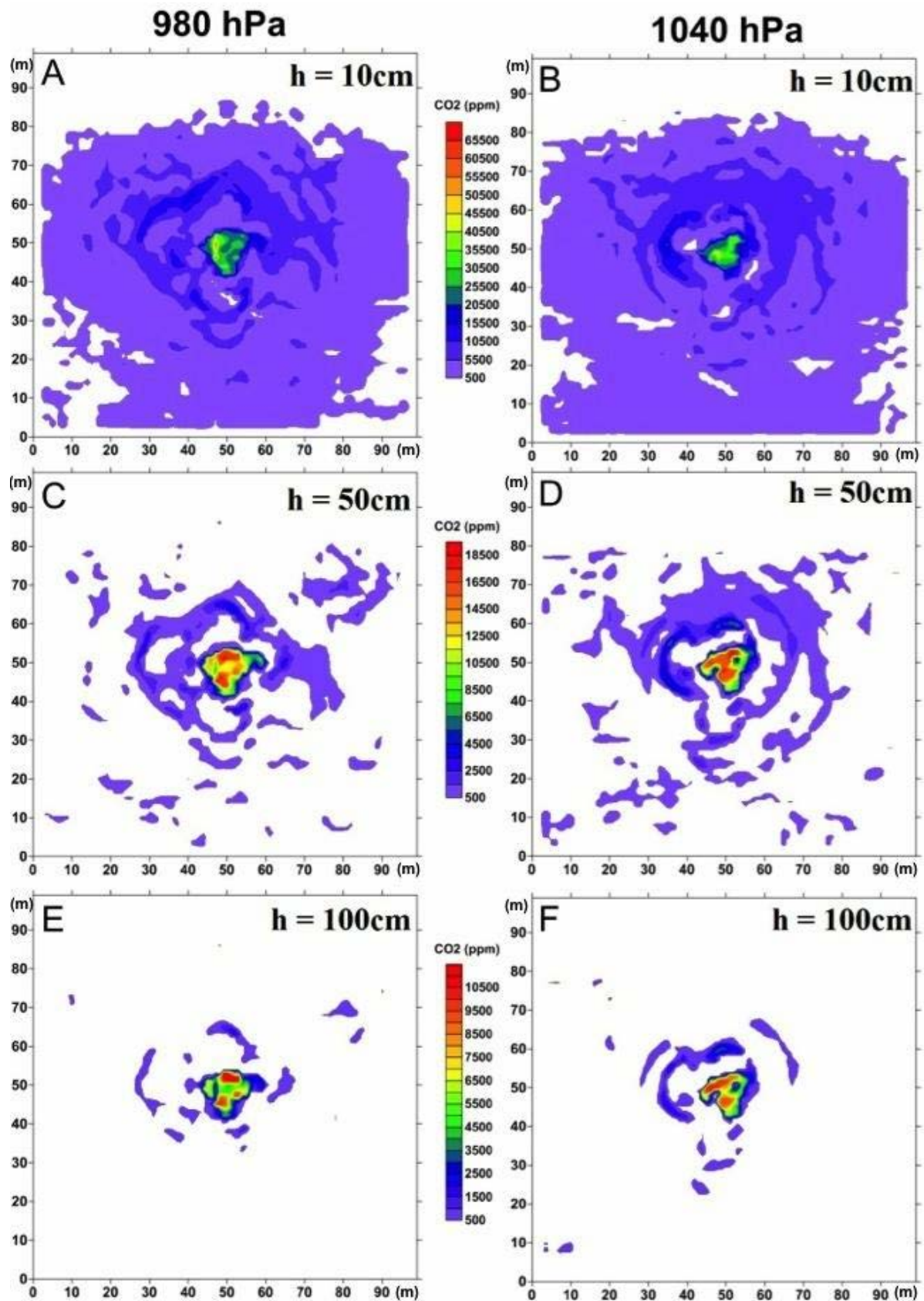


**Figure 26.** Map of the air CO<sub>2</sub> concentration for simulation S1 and S3 with an emission rate of 3 t·d<sup>-1</sup> at 980 and 1040 hPa respectively. Outputs are at 10 cm (A, B), 50 cm (C, D), 100 cm (E, F) high.

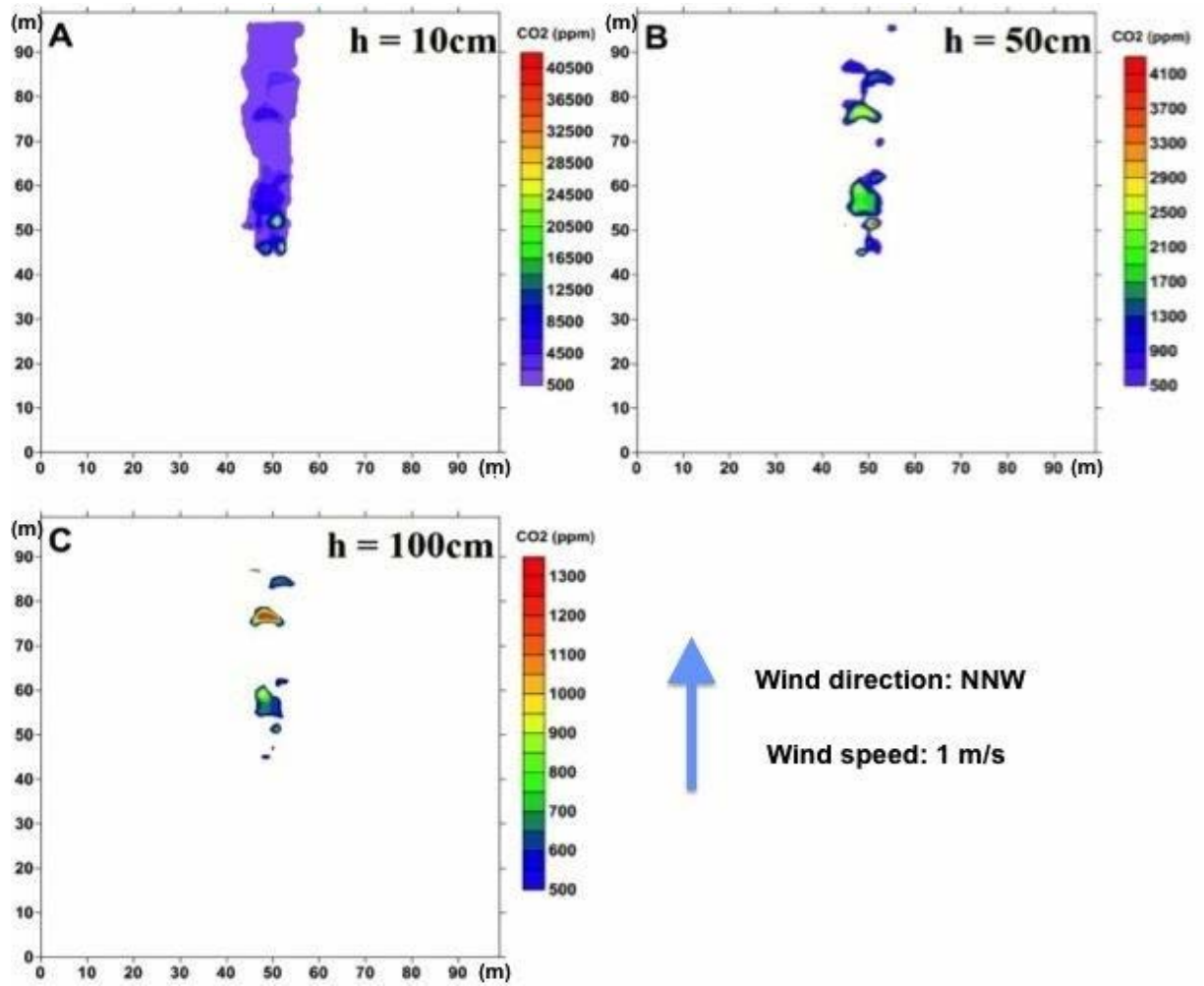


**Figure 27.** Map of the air CO<sub>2</sub> concentration for simulation S4a with an emission rate of 3 t·d<sup>-1</sup> at 980 hPa and with a wind speed of 1 m·s<sup>-1</sup>. Outputs are at 10 cm (A), 50 cm (B), 100 cm (C) high.

## 9.7. Discussion and interpretation for risk assessment

The four stations (A, B, C, D) close to the emission source present elevated CO<sub>2</sub> concentrations. However, in presence of wind, even with low wind velocity (1 m·s<sup>-1</sup>), the CO<sub>2</sub> plume is dispersed, both vertically and horizontally, reducing drastically the CO<sub>2</sub> concentration. The relevant role of the wind can also be seen in the continuous and sharp variations of the recorded concentration at 50 and 100 cm in all four stations (Fig. 25). Attending to air concentration in stations E and F, it can be concluded that once outside of the emission bubbling area the plume has a uniform vertical concentration. Both stations show a homogeneity of concentrations for the three different heights. The measurements in these stations show, also, that far from the source the plume has a much lower concentration at all heights.

Numerical modelling can be a valuable supporting tool for risk assessment. To evaluate the feasibility of the numerical simulations to predict the plume dispersion, a comparison exercise between the data acquired by the Telaire sensor and the modelling results has been carried out. During fieldwork pressure sensors recorded an atmospheric pressure of 970 hPa so that results from S1 has been compared with data from the six Telaire monitoring stations. The boxplot charts for CO<sub>2</sub> concentrations at A, B, C and D stations have been calculated for heights at 50 and 100 cm. The comparison at 10 cm from surface has been discarded due to the almost continuous saturation of the instrument (10000 ppm is the tool's detection limit), while predicted concentrations reached 70000 ppm. Numerical results are in good agreement with the recorded data at 50 and 100 cm high (Fig. 28 and 29). In each station, simulated values are in the same range as the concentration measured in field survey. It has to be noticed that there are stations where the saturation limit of the Telaire was reached (A and D at 50 cm above the surface).

As already mentioned in the Introduction section, the impacts on human health due to CO<sub>2</sub> inhalation are entirely defined by the concentration and the duration of exposure. CO<sub>2</sub> concentration of 3% produces breathing problems, considering the 10% threshold as the minimum threshold dangerous for human beings, the extent and height of the gas plume above this threshold was evaluated (Fig. 30). It can be observed that predicted values are similar (differs in only 1 centimetre) for simulations without wind: S1 (Fig. 30a) and S3 (Fig. 30b); consequently, atmospheric pressure does not play a significant role. For simulation S4a, the 3% threshold map shows a more limited extent of the plume due to the presence of wind (Fig. 30c). In the case in this study, the warning level of 10% is not reached even above the emission area. Table 13 summarizes the maximum concentration and heights above 3% threshold estimated in simulations S1 and S4a.



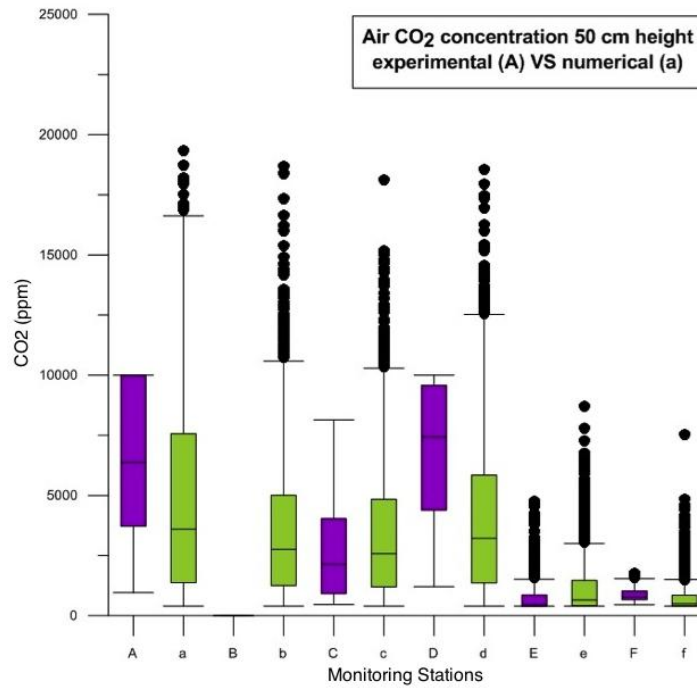


**Figure 28.** Comparison between box plot diagrams of CO<sub>2</sub> concentration measured on the field (purple) and that predicted by the simulation S1 (green), for the six monitoring stations at 50 cm above the ground surface. Black dots are the outliers.

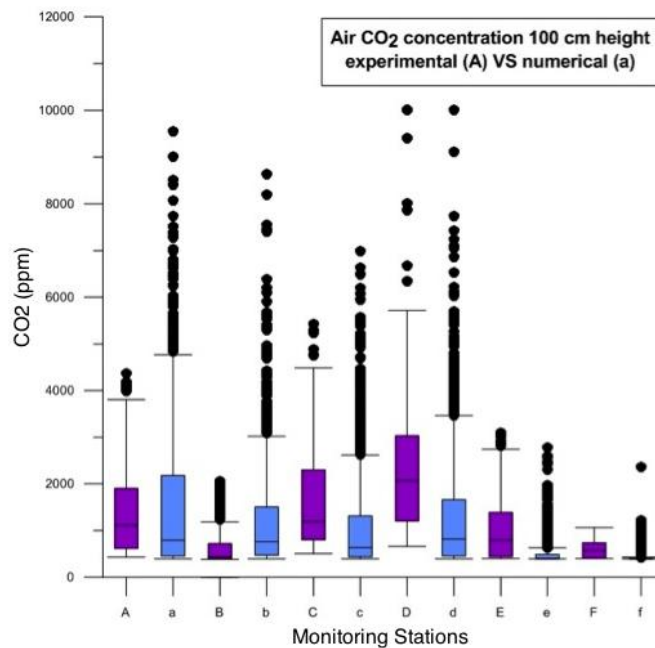


**Figure 29.** Comparison between air CO<sub>2</sub> concentration measured on the field and that predicted by the simulation S1 for the six monitoring stations at 100 cm from surface. Experimental data have capital letters and purple boxes, numerical data have lowercase letters and blue boxes. Black dots are the outliers.

**Table 13.** Predicted maximum air CO<sub>2</sub> concentration in the Cañada Real site for simulations S1 and S4a, and calculated elevation reaching hazardous 3% CO<sub>2</sub> concentration threshold.

Simulation	S1	S3	S4a
Max concentration (ppm)	70000	45000	41000
3% threshold height (m)	0.290	0.210	0.131

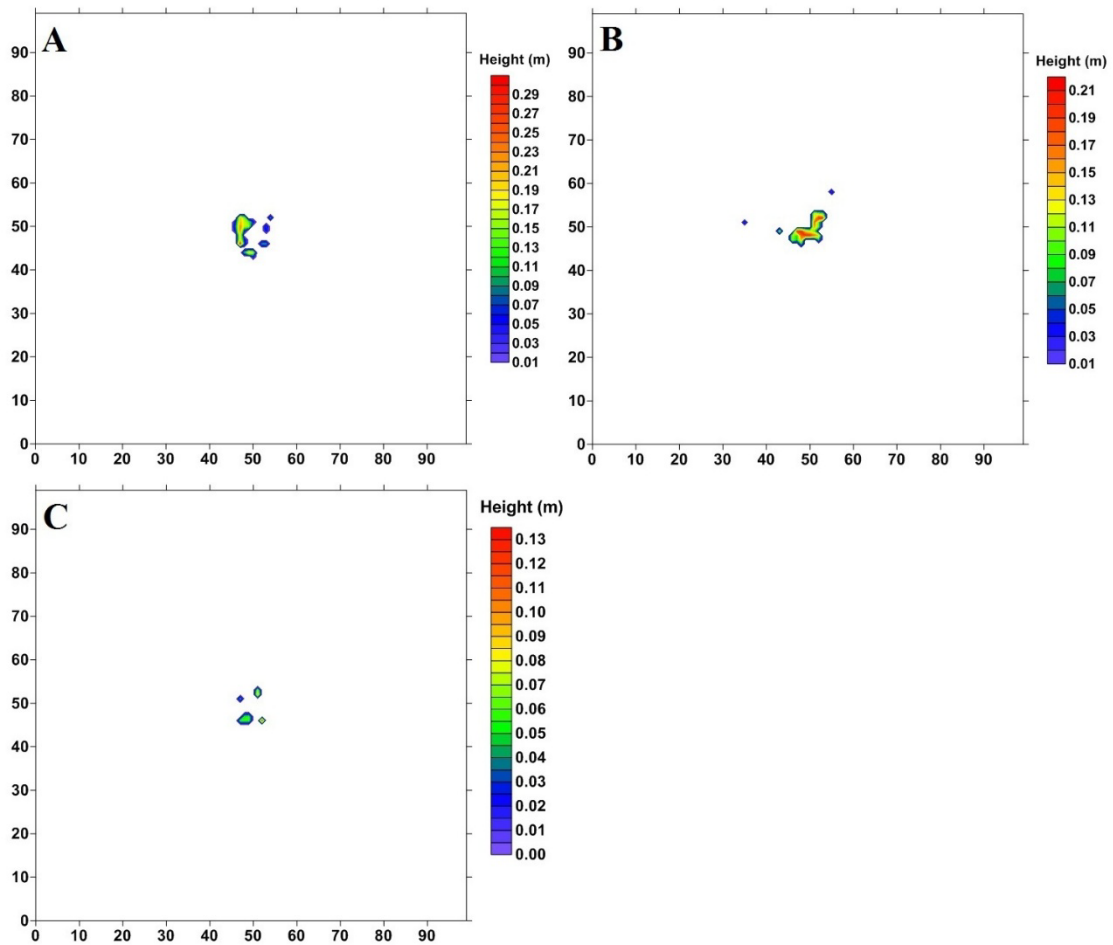


**Figure 30.** Extension and maximum height of the plume with a CO<sub>2</sub> concentration above the 3% threshold for simulations S1 (a), S3 (b), and S4a (c).

## **9.8. Conclusions**

The comparison between field data and model calculations reveals that numerical dispersion models are capable of predicting the formation of CO<sub>2</sub> accumulation over the ground as a consequence of underground gas emission. Therefore, atmospheric modelling could be included as a valuable methodology in the risk assessment of leakage in CCS projects. CO<sub>2</sub> accumulation (also called “CO<sub>2</sub> lakes”) is predicted and observed to occur only under stable, calm atmospheric conditions, without wind speed; otherwise, the plume quickly disperses into the surrounding atmosphere. From a relatively intense point-source emission, as the one studied in this work in Cañada Real, the concentration of CO<sub>2</sub> in air can be extremely high (>30,000 ppm), exceeding the limit of safety for humans. However, these concentrations are only found above the emission source and at less than 30 cm high and, consequently, the risk is small unless a person lays down on the ground. These model predictions match very well with the observations at Cañada Real, where only small animals are dead due to asphyxia.

The SAP system has been revealed a good method to evaluate high gas emissions from underground. The blanket installation is easy and only requires a small amount of soil (sand, clay or even in situ material) to seal the blanket-ground contact to avoid gas leakage. Contrary to other techniques like laser detection for air concentration, the SAP system is not affected by weather activity, so that measurements can be done even in presence of wind and rain.

## **10. Research article 3: Atmospheric dispersion modelling of CO<sub>2</sub> emission in the Colli Albani volcanic district (central Italy)**

This article has been published in **Annals of Geophysics**, **60-5**, with the title “**Atmospheric dispersion modelling of CO<sub>2</sub> emission in the Colli Albani volcanic district (central Italy)**”.

### **10.1. Introduction**

The study of CO<sub>2</sub> emissions in natural systems provides a valuable information on the assessment and quantification of potential risks related to underground carbon storage leakage. Emissions of CO<sub>2</sub> are studied in a large variety of geological environments, i.e., sedimentary basins, active and non-active volcanic areas, seismically-active regions, and geothermal fields. Because of the physics of carbon dioxide gas, e.g., colourless, odourless, higher density compared to air, its accumulation may result hazardous and even lethal for life. The impact of CO<sub>2</sub> concentration in air on human beings has recently been reported by De Lary et al., (2012), who summarized the effects of its inhalation as a function of the concentration and duration of exposure. Being denser than air, CO<sub>2</sub> tends to accumulate on the ground filling depressions and forming the so-called CO<sub>2</sub> lakes, which could represent a serious hazard for human beings. This accumulation is governed by gravity, turbulence and dispersion.

This article deals with the CO<sub>2</sub> emissions from a geological site located in Pomezia, a municipality in the province of Rome, central Italy. The site is called Solforata di Pomezia, taking its name by the typical smell of rotting eggs and bright yellow crystalline solids, and is known for a widespread degassing of mantle-derived CO<sub>2</sub> (Chiodini et al., 2004) (Fig. 31). The objective of this research is to quantify the risk of CO<sub>2</sub> accumulation in leakage episodes in geological storage by using atmospheric model simulations. The robustness of these numerical calculations is based on the calibration with measurements of air composition available in the literature. The results of this numerical model may provide clues for the determination of environmental conditions under which the site and other CO<sub>2</sub>-emitting areas can host hazardous conditions for human life.



**Figure 31.** Aerial view of the Solfiorata di Pomezia, along its main axis. Picture taken from Google Maps. The red segments outline the area mined in the past for sulphur; the green circle shows an episodic flooded area.

Atmospheric dispersion modelling is a tool that provides information to know how volatile compounds disperse in the atmosphere from a source located underground or on ground. It is used to predict future air concentration under specific risk scenarios, by developing maps of possible hazardous levels for human beings, and it can be useful in the risk assessment of geological storage of CO<sub>2</sub>.

## 10.2. Geological setting

The studied site is located in the Alban Hills region, in the Tyrrhenian sector of Central Italy (Fig. 32). This area is characterised by low permeability sedimentary formations that allow the accumulation of gas at shallow depths and surface. Also, this region underwent volcanic activity during the Quaternary, related to an extensional tectonic regime whose evolution is directly controlled by primary regional structures connected to the recent geodynamic evolution of the Tyrrhenian basin-Apennine Chain system (De Rita et al., 1995). The Alban Hills volcano is one of the main volcano craters of the peri-Tyrrhenian belt, starting erupting 0.7 Ma ago (De Rita et al., 1988). Volcanic activity ended in the Holocene 2.7 ka with a phreatomagmatic phase that formed a large number of craters in the south-western part of the volcano (Selvaggi and D'Ajello Caracciolo, 1998). The origin of CO<sub>2</sub> underground emission in the Alban Hills is related to buried highs of the carbonate basement, which act as traps for the gas of deeper origin migrating through a NE-SW fault extending from the coast to Albano Lake (Chiodini and Frondini, 2001). The observable phenomena of continuous strong degassing that is widespread in Latium district, suggests that a large amount of gas is being

accumulated underground during long periods of time with short episodes of strong gas release (Voltaggio and Barbieri, 1995; Funicello et al., 1992).

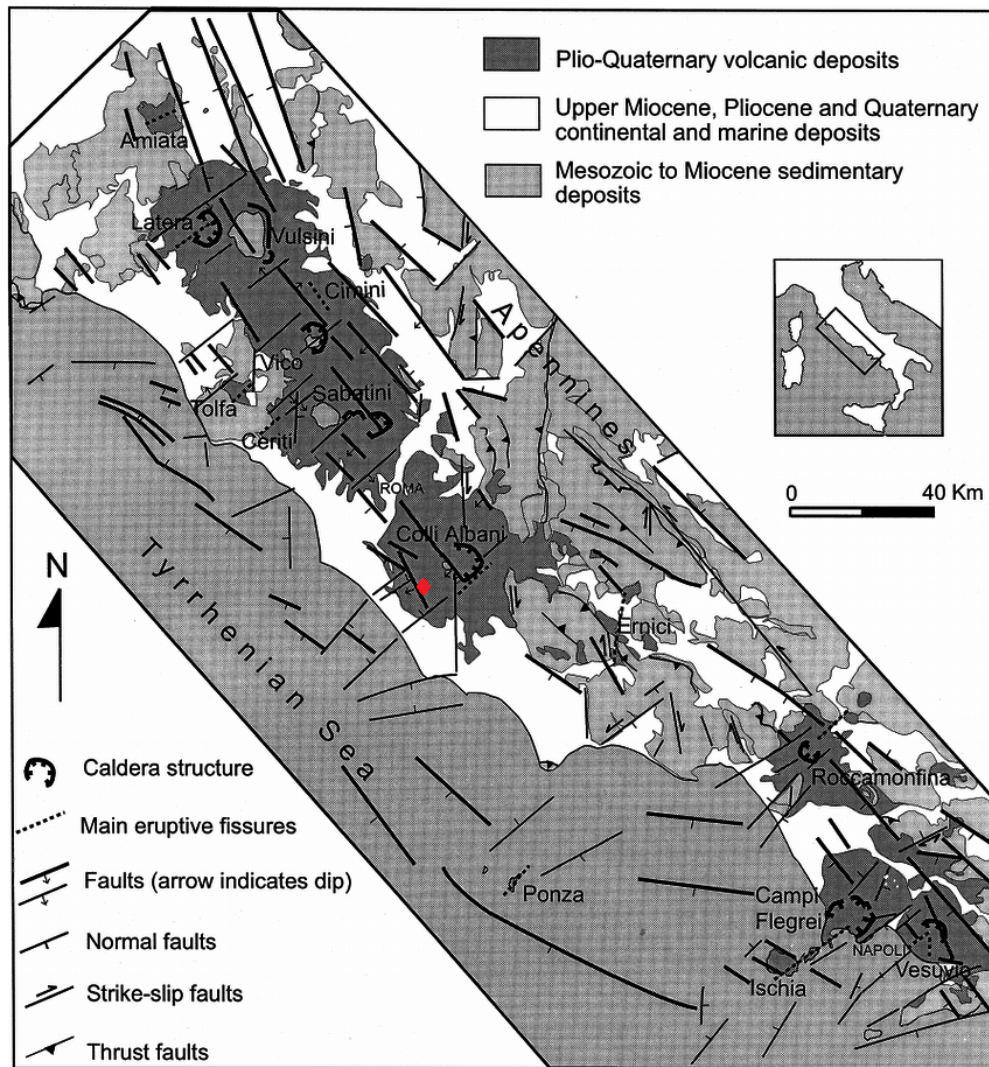


**Figure 32.** Tectonic map of the Tyrrhenian margin of the Central Italy Peninsula (from Acocella et al., 1999). The location of Solfiorata di Pomezia is highlighted by a red dot.

The Solfiorata di Pomezia is a natural degassing area located a dozen of km south-west of the city of Rome, being part of the quiescent Alban Hills Volcano district. This area is well known for the diffuse natural gas leakage and the presence of sulphide-rich waters; also, it is affected by a significant uplift rate ( $1.3 \text{ mm}\cdot\text{y}^{-1}$ ) suggesting the presence at depth of a pressurized gas source (Tolomei et al., 2003).

The morphology of the Solfiorata di Pomezia has been modified in the last century, especially when was mined for sulphur. After mining, the site was abandoned and today it is periodically flooded

during rainfall episodes. Presently, the area consists of a depression of 270,000 m<sup>2</sup> and is close to an industrial area. In the centre of the depression, there is a lake that typically dries out in summer. The site has a quite rectangular shape with an east-west orientation with a vertical difference in elevation between 20 and 30 metres. Vegetation is present all around except for the area around the lake where mud occurs. In the figure 33 the slope around the emission area, the location of the lake and the absence of vegetation around the lake are clearly observed.



**Figure 33.** Views of the Solforata di Pomezia site: vegetation, lakes and dry soil.

During the summer period, due to the drying out of the soil, main gas emission points are easily recognisable (Fig. 34).



**Figure 34.** Example of gas emission point source at the Solforata di Pomezia in the summer period.

### 10.3. CO<sub>2</sub> soil flux emissions

A first estimation of the CO<sub>2</sub> soil flux in the Solforata di Pomezia was made in 1996 by Chiodini and Frondini (2001) using an accumulation chamber, reporting 110 measurement stations over an area of 55,000 m<sup>2</sup>. In 2003, Carapezza et al., (2005) made another survey in the Solforata area covering 30,000 m<sup>2</sup> with 200 accumulation chamber measurements. Another soil flux survey was carried out in 2007 (Carapezza et al., 2012) extending the soil gas mapping to an area of 229,000 m<sup>2</sup> (356 measurements and 7 Tuneable Diode Laser, TDL, profiles). The latter set of data has been selected for this study; in particular, 278 of 356 accumulation chamber measurements were used (black dots in Fig. 35), 7 TDL profiles (black segments in Fig. 35), and the wind speed and direction data (Fig. 39). The selection of only a part of the accumulation chamber survey is due to cross-check data with the TDL profiles, the wind speed and direction data, and the atmospheric dispersion outputs over the same emission area. The diffuse soil flux of CO<sub>2</sub> has been measured by two portable accumulation chambers (Chiodini et al., 1998; Carapezza and Granieri, 2004), equipped with a Li-820 infrared CO<sub>2</sub> detector (0-2 vol.%). The final output of Carapezza et al., (2012) is the soil flux map shown in figure 35.

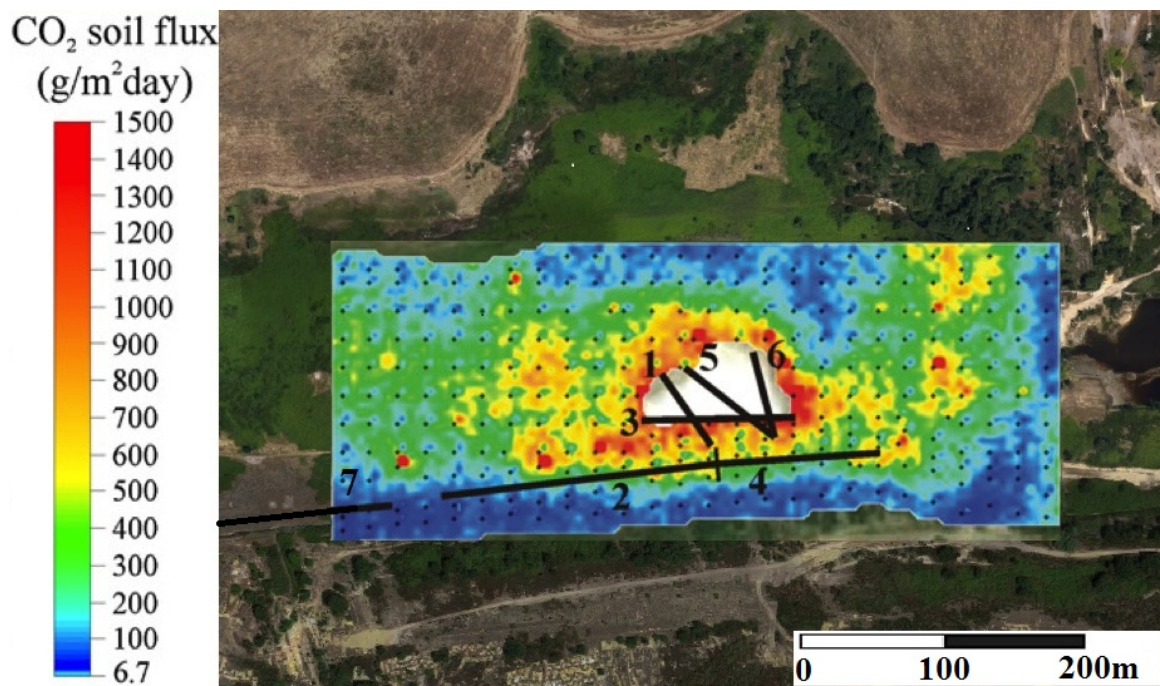


**Figure 35.** CO<sub>2</sub> soil flux map in the Solforata di Pomezia from Carapezza et al., (2012). Black dots are the 278 sampling points and numbered segments are TDL profiles. White area denotes the lake, where no measurements were performed.



The flux map clearly shows the main emission area around the pool. Moreover, other 6 emission areas, both three on the left and three on the right of the pool, can be spotted with fluxes higher than 1100 g·m<sup>2</sup>·d<sup>-1</sup> (Fig. 36). The main soil emission area is longitudinal to the valley axis.

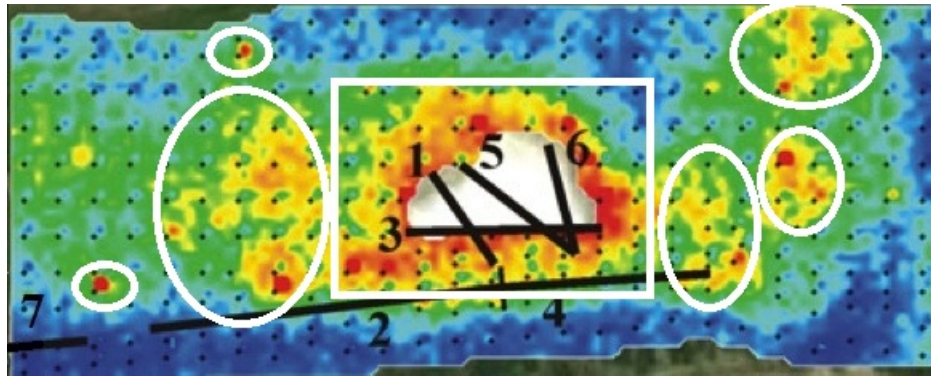


**Figure 36.** Main emission points (white ellipses) around the pool (white rectangle).

## 10.4. Field data

### 10.4.1. Air CO<sub>2</sub> concentration

Air concentration has been measured by Carapezza et al (2012) over the lake and the channel using a Tuneable Diode Laser (TDL, see Fig. 35, and Table 14). This methodology allows the measurement of the average air concentration of CO<sub>2</sub> on a profile length every few seconds (Schiff et al., 1994; Tittel et al., 2006; Weber et al., 2005); simultaneously, the wind direction and speed are recorded by a sonic anemometer (Carapezza et al., 2012). TDL profiles were recorded at two heights, 20 and 25 cm from surface; two of them were over the lake and one was along the channel. According to De Lary et al., (2012), air CO<sub>2</sub> concentration is admissible under 5% for human beings. This is considered a threshold beyond that breathing becomes extremely laboured, occurrence of headaches, sweating and bounding pulse.

Figure 35 shows the CO<sub>2</sub> soil flux map resulting from measurements and the location of 7 TDL profiles, obtained in February and May 2007, by Carapezza et al., (2012). For the present study, TDL profile on May 2007 (Table 14) will be used for a comparison with soil flux data obtained in the same period.

**Table 14.** Air CO<sub>2</sub> concentration measured by TDL profiles at Solforata di Pomezia (Carapezza et al., 2012).

Date	Location	Length (m)	Height (cm)	Duration (min)	CO <sub>2</sub> (ppm) Minimum	CO <sub>2</sub> (ppm) Average	CO <sub>2</sub> (ppm) Maximum
05/2007	Lake	68.4	20	130	139	880	3026
05/2007	Lake	58.8	20	95	n.d.	n.d.	n.d.
05/2007	Channel over night	118.0	25	1140	160	506	3384

CO<sub>2</sub> concentrations were measured by TDL and were average values on the total length of the infrared laser; consequently, some areas along the laser path could have higher concentrations than the average. Results shown in figures 37 and 38 are obtained by two measurements of 68 and 54 metres length over the lake lasting a couple of hours, CO<sub>2</sub> reached a maximum concentration of 3026 ppm and a minimum of 139 ppm. Considering the emission in Solforata di Pomezia in a steady state, concentrations recorded over the lake by TDL (Fig. 37) are indicative of the level of CO<sub>2</sub> air concentration expected over the site. The data from TDL measurements along the main channel for a length of 118 metres are shown in figure 38. For these profiles, maximum concentration reached 3500 ppm in the early morning hours while in the night maximum concentration was around 600 ppm and 360 ppm before 8 p.m., monitoring lasts almost 20 hours. These data are compared with numerical outputs of model S1 in next section. As can be observed in both plots air concentration used to vary as wind speed changes. Values for the TDL in figure 37 are higher on average than in figure 38 because the first profile is over the main emission area (the lake) while the second a profile is along the main valley axis, so a decrease of CO<sub>2</sub> in air due to dispersion is expected.

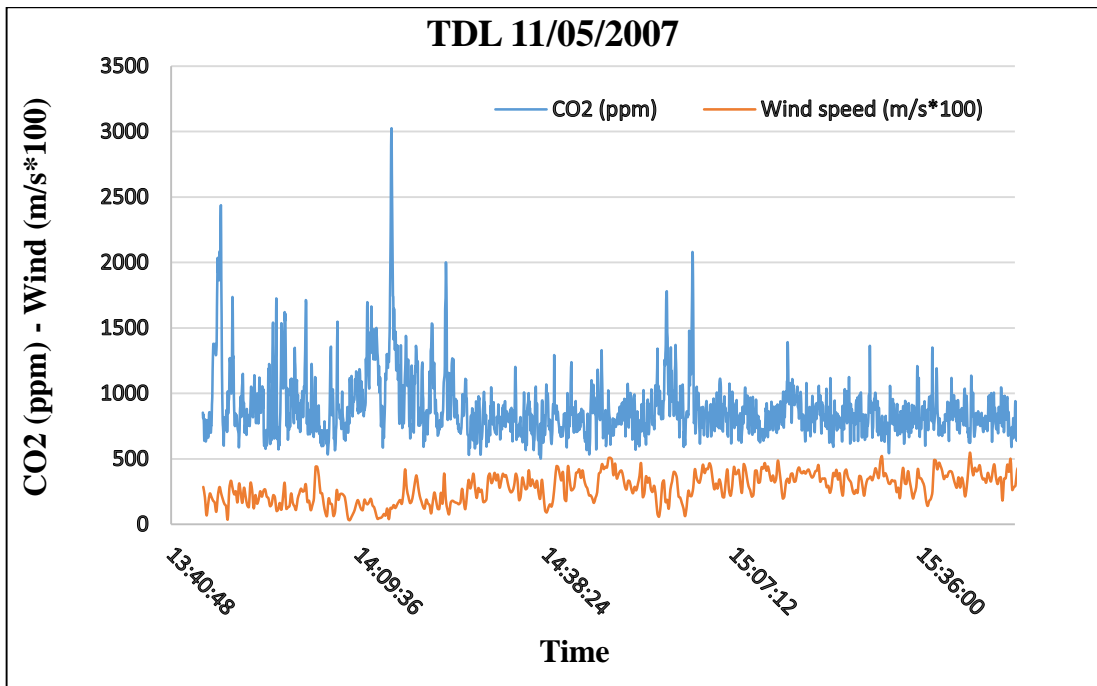


Figure 37. CO<sub>2</sub> air concentration measured by TDL (orange line) and wind speed (blue line), during May 11<sup>th</sup> - 2007 by Carapezza et al., (2012).

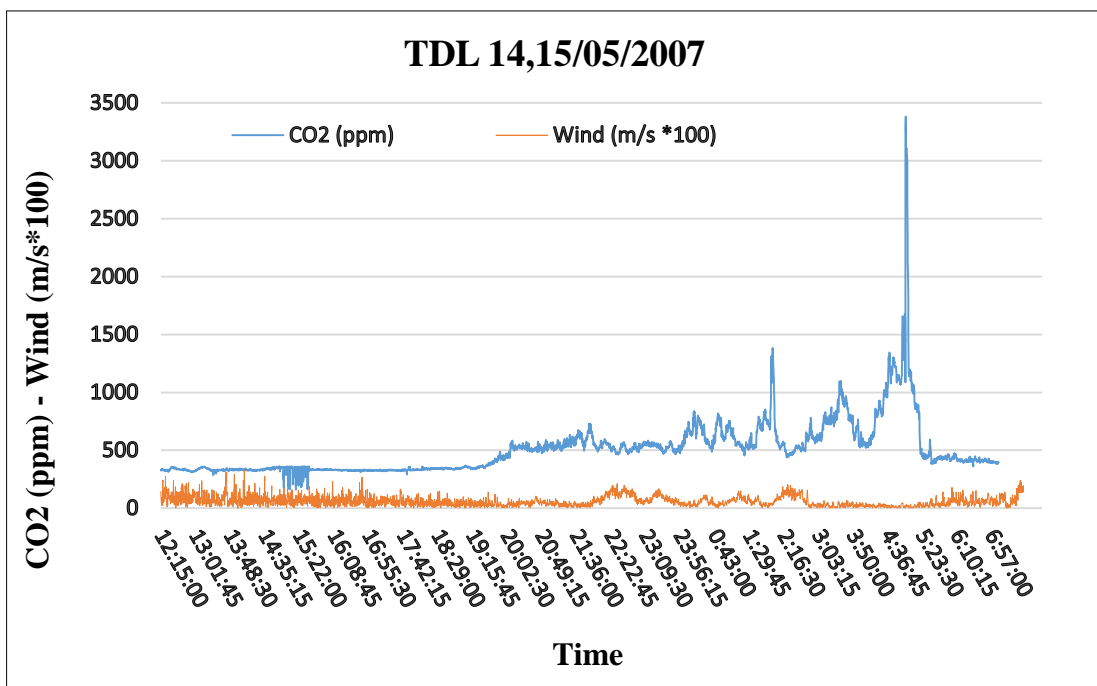
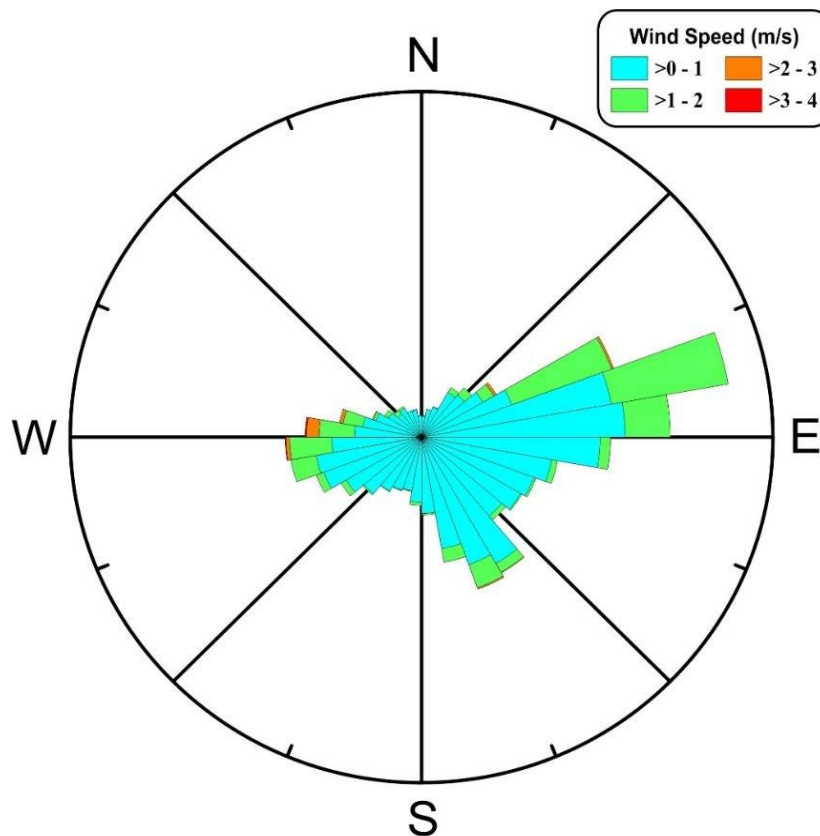


Figure 38. CO<sub>2</sub> air concentration measured by TDL (orange line) and wind speed (blue line), during May 14<sup>th</sup> and 15<sup>th</sup> 2007 by Carapezza et al., (2012).

## 10.5. Meteorological data

Carbon dioxide is a gas denser than air ( $1.976 \text{ kg}\cdot\text{m}^{-3}$ ) so that accumulates in topographic depressions like the bottom of a valley or in ditches, and under stable atmospheric conditions CO<sub>2</sub> concentrations can reach high values. Dispersion of gases denser than air is governed by gravity and by the effects of lateral eddies which decrease the plume density through the incorporation of surrounding air. In the initial phase the buoyancy controls the gas dispersion and the cloud follows the ground (gravitational phase); in contrast, when the density contrast becomes less important, gas dispersion is mainly governed by wind and atmospheric turbulence (passive dispersion phase) (Costa et al., 2005, Folch et al., 2007).

Wind speed were recorded in the Solfiorata channel for 19 hours during May 14<sup>th</sup> and 15<sup>th</sup> 2007 using a sonic anemometer every 15 seconds. The recorded wind data at 25 cm from surface are shown in figure 39. Three wind direction families are recognised: the main wind direction blew from ENE to WSW reaching a maximum speed of  $3.3 \text{ m}\cdot\text{s}^{-1}$ , and the other two blowing directions are from SSE and from W, which is the weakest family for wind speed average of these three. Other wind directions were recorded but with slower wind speeds.



**Figure 39.** Wind speed recorded at the Solforata di Pomezia during the days May 14<sup>th</sup> and 15<sup>th</sup> 2007 by Carapezza et al., (2012).

Unfortunately, the set of meteorological data does not include pressure data for the same period. This is a significant uncertainty for the input data implementation in the numerical model. As indicated in Gasparini et al., (2015), atmospheric pressure variations over a leakage gas site can move up or delay the emission from soil to atmosphere. Nevertheless, no abrupt change in pressure condition happened during measurements.

The first law of Gay-Lussac (also known as Charles's Law) says that at a constant pressure the volume of a gas is directly proportional to the absolute temperature ( $V/T=k$ ). This law describes how a gas expands as the temperature increases. Soil respiration is responsive to temperature and increases when soil temperature raised experimentally (Billing et al., 1982, Van Cleve et al., 1990). Temperature is the single best predictor of the annual soil respiration rate of a specific location, but inclusion of precipitation in the regression does increase the predictive power of the model (Raich and Schlesinger, 1992).

Air temperature was also recorded by the sonic anemometer during the TDL experiment, and ranged from 12.5 to 27 °C (Fig. 40). The highest CO<sub>2</sub> concentration is coupled with periods with lower temperature.

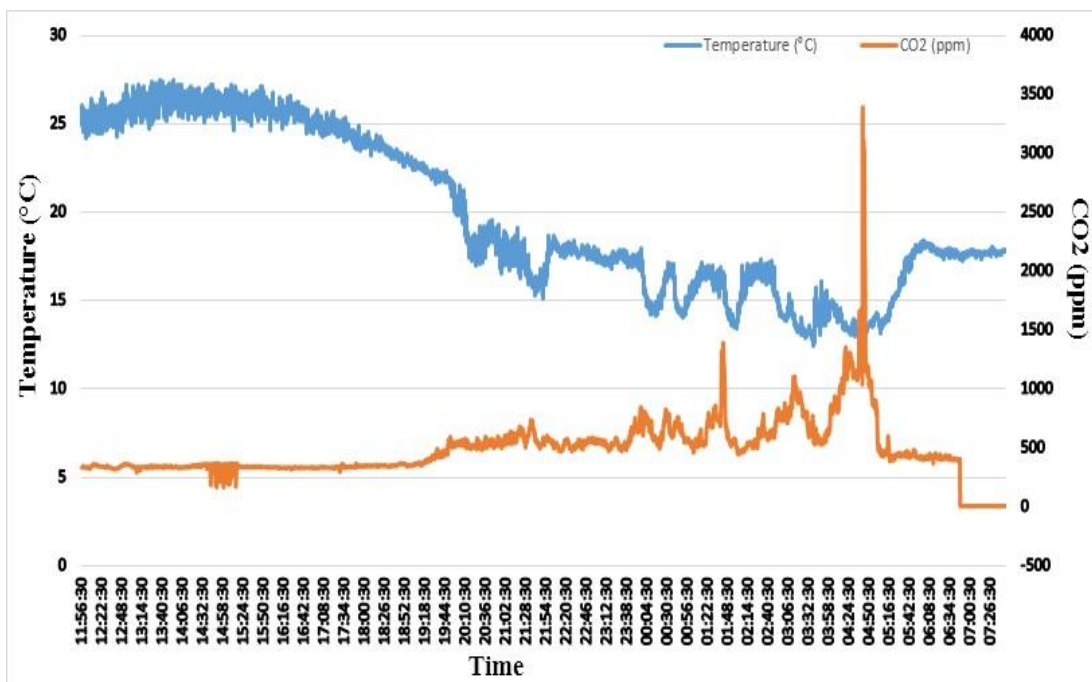


**Figure 40.** Air temperature versus CO<sub>2</sub> soil emission (data from Carapezza et al., 2012).

It is clearly visible in the figure 40 how emission is concentrated during the night time. Generally looking, temperature starts from 25° C and decreases to 20° C at dusk. During the night the temperature kept a descending trend till the early hours of the morning. In particular, during the night there are many temperature oscillations with changes of 5° C in half an hour.

In the meantime, air temperature was recorded during the TDL experiment, and ranged from 12.5 to 27 °C (Fig. 40). The highest CO<sub>2</sub> concentration is coupled with periods with lower temperature.

Comparing plots of CO<sub>2</sub> vs temperature (Fig. 40) and CO<sub>2</sub> vs wind (Fig. 38), temperature does not decrease when wind blows up; contrary to that, CO<sub>2</sub> concentrations are greater when wind speed decreases.

In order to ascertain the relations amongst air CO<sub>2</sub> concentration and atmospheric conditions, we performed a forward-stepwise multiple regression of air (CO<sub>2</sub>) and environmental data: this is a largely applied statistical method to identify the contribution of several variables on the total variance of a dependent variable (see Laiolo et al., 2016 and references therein).

Given the horizontal wind speed, the vertical wind speed, the wind direction and the air temperature measured by the anemometer, we could estimate the contribution of each on air (CO<sub>2</sub>) and model CO<sub>2</sub> fluctuations due to variations in air temperature and wind conditions.

Results of the forward-stepwise multiple regression indicate that atmospheric variations are able to predict the 36.3% of the total CO<sub>2</sub> concentration variance, and that only air T and horizontal wind speed are statistically significant and anti-correlated, on CO<sub>2</sub> flow. The output model in figure 41 shows how air T and wind speed variations can model part of the measured CO<sub>2</sub>.

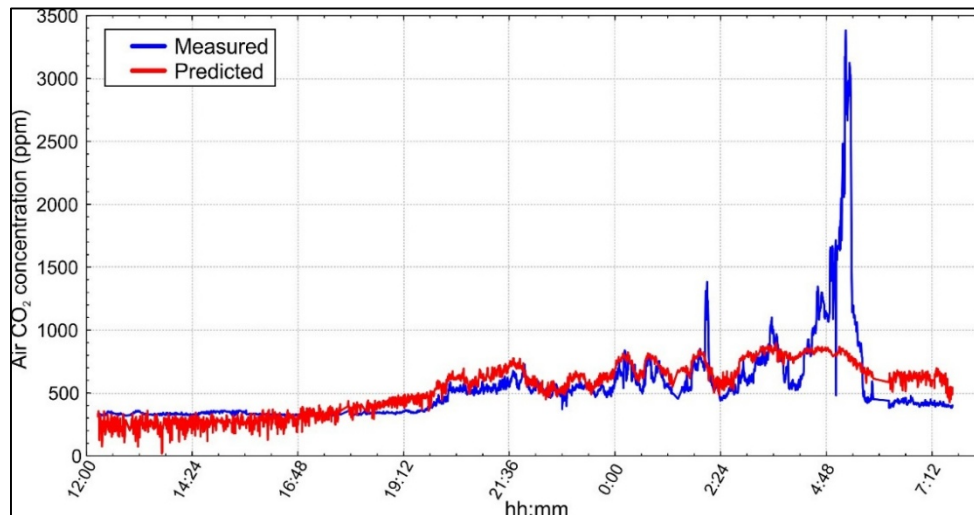


**Figure 41.** Measured (blue line) and predicted (red line) air CO<sub>2</sub> concentration.

## 10.6. Atmospheric dispersion modelling

### 10.6.1. Numerical code

The numerical simulations performed in this work were done using the TWODEE2 code (Costa et al., 2008). This code is based on shallow layer time-dependant Eulerian approach for dispersion of heavy gases, and it is an updated version of the TWODEE code (Hankin and Britter, 1999a, b, c). TWODEE2 is based on depth-averaged equations obtained by interpreting mass, density and momentum equations over the fluid depth, from the bottom up to free surface. Such approach is able to describe the time evolution of gas concentration, depth-averaged velocity, and averaged cloud thickness. The input data include the topography, ground roughness, wind measurements and gas flow rate from the ground sources (Folch et al., 2007). In this study all simulations were developed using the meteorological processor DIAGNO (Folch et al., 2009) coupled with TWODEE2. DIAGNO uses wind data at a point of the domain and, assimilating terrain information, generates a zero-divergence wind field.

### 10.6.2. Numerical model set-up

The numerical model is based on a 2D mesh of 17500 regular quadratic elements of 20×20 m, and the topography of the site has been implemented from cartographic data with a scale of 1:25000 (see Fig. 35).

No flow conditions at the boundary were imposed and an initial CO<sub>2</sub> concentration in the air of 400 ppm, the atmospheric background concentration, was considered.

All numerical simulations used wind data shown in figure 39, and as wind has been recorded for 19 hours, the simulation time had the same length.

A first simulation, called S1, was based on meteorological data and estimated emission rate (95 ton·d<sup>-1</sup>) from Carapezza et al., (2012) field data. The model S2 was built using data recorded by Chiodini and Frondini (2001), with an emission rate of 44 ton·d<sup>-1</sup>. For this simulation, the atmospheric data was that recorded by Carapezza et al., (2012). Models S3 and S4 had respectively an emission rate of five and ten times bigger than model S1.

Table 15 reports all the model features of the simulations performed.

**Table 15.** Simulation features of the four models performed.

Model	S1	S2	S3	S4
Grid Division (elements)			175×100	
Grid Spacing (m)			20×20	
Source Points			278	
Wind Speed and Direction			See Fig. 39	
Temperature			See Fig. 40	
Atmospheric Pressure (hPa)			990	
Elapsed time (h)			19	
Emission Rate (t·d <sup>-1</sup> )	95	44	500	1000

## 10.7. Results



A first significant prediction from the simulations is that the gas plume covers the emission area rapidly after short periods of time. In model S1, the gas would need 2.5 hours to cover the channel, 4.5 hours for model S2, an hour for S3 and half an hour for model S4, respectively (Fig. 42).

The predicted plume in model S1 expands towards the west side of the area steering into the left channel (Fig. 43). A small part of the plume moves to the east side remaining close the emission area. Model S1 predicts a maximum air concentration of 9000 ppm in two small areas while the average air concentration is under 2500 ppm.

Similar behaviour to S1 is predicted for model S2 but with lower gas concentrations. The plume expands mainly over the emission area and it finds its preferential way to the west side, and only a small plume goes to the east part. The plume shape is narrower than model S1. Model S2 predicts a maximum concentration of 6000 ppm but air concentration on average does not raise over 1500 ppm (Fig. 44).

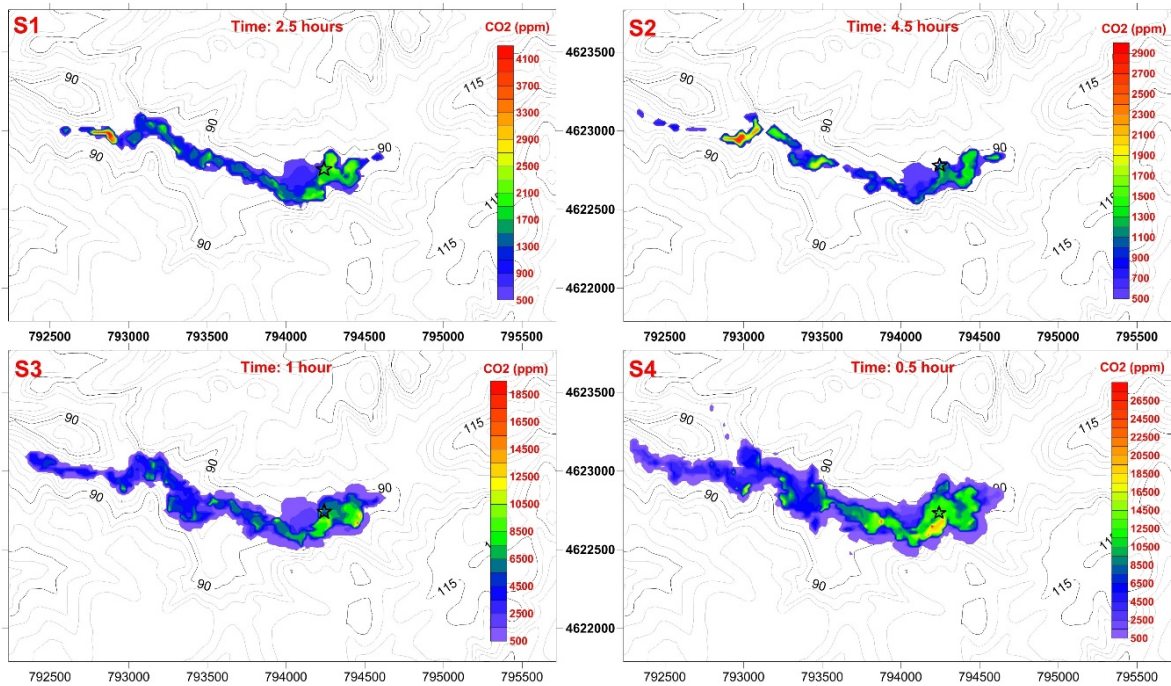


**Figure 42.** Plume dispersion at 25 cm height for S1 after 2.5 hours of simulation, for S2 after 4.5 hours, for S3 after 1 hour and for S4 after half an hour, the black star indicates the source emission.

Simulations S3 and S4 predict maximum air concentration of 15000 and 54000, respectively (Fig. 45). For those models, the predicted plumes expand along the valley's axis to the north-west part of the channel covering an area much wider than the predicted by S1 and S2. Interestingly, even

the north-east area is predicted to be affected by CO<sub>2</sub>-enriched air. Two spots are visible for S3 with concentration under 5000 ppm, while for S4 are under 13000 ppm.

Model S4 covers an area that is quite the double of S1 at 25 cm height, without reaching a dangerous level (air CO<sub>2</sub> 1.5%). Higher concentrations (5%) are reached in spot points over the emission area which is normally flooded and difficult to reach or to pass through, so that the Solforata di Pomezia is not a dangerous area even with an emission rate of ten times bigger than actual rate but always with wind activity.

In all four simulations, the CO<sub>2</sub> plume follows the longitudinal axis of the studied area with higher concentration predicted over depressions existing in the site. Plume horizontal dispersion follows the topography covering the lower area on the west side. Air concentration varied as wind intensity changes. On the other hand, areas with higher and lower CO<sub>2</sub> air concentration change location as wind changes blowing direction.

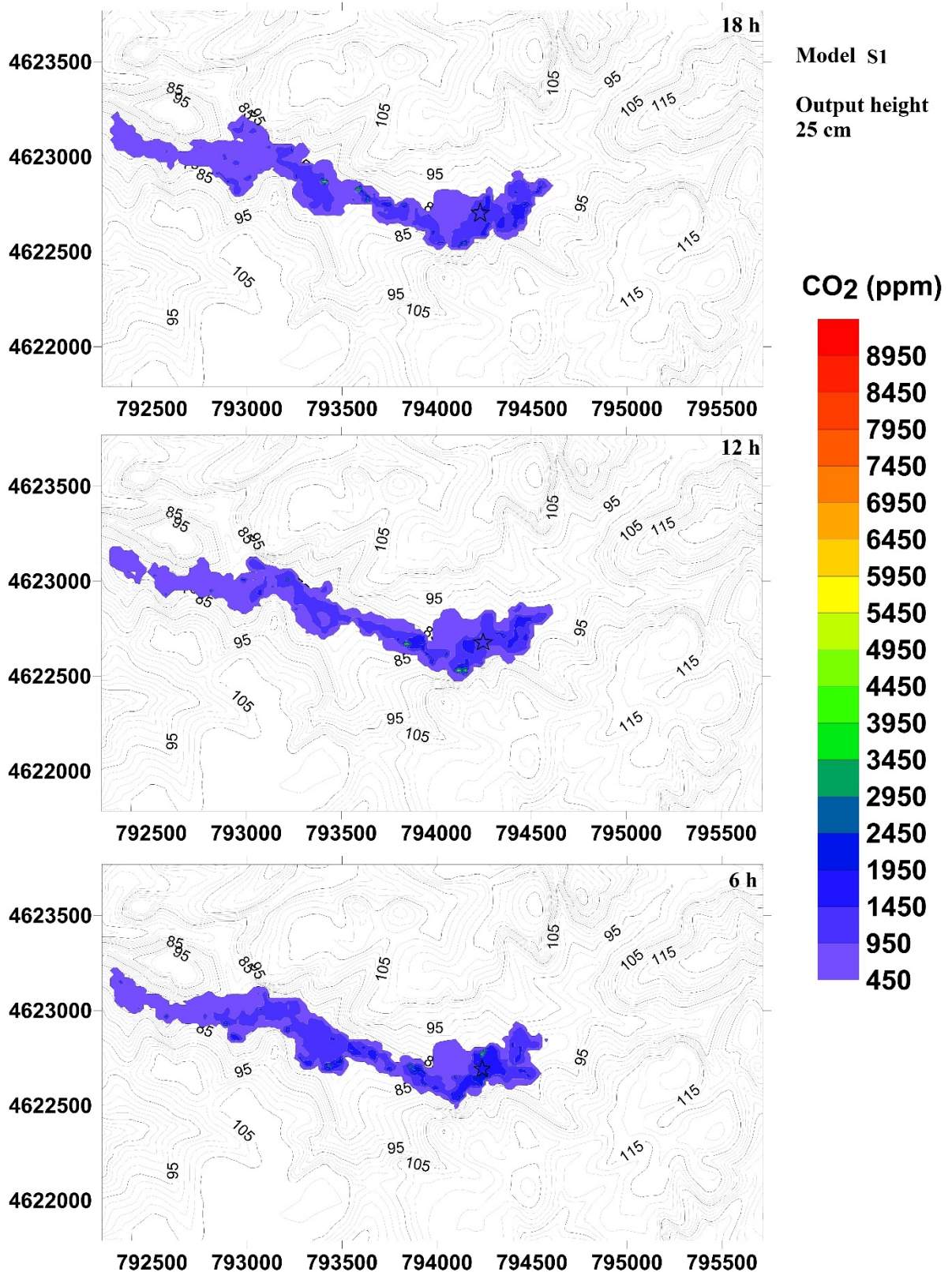
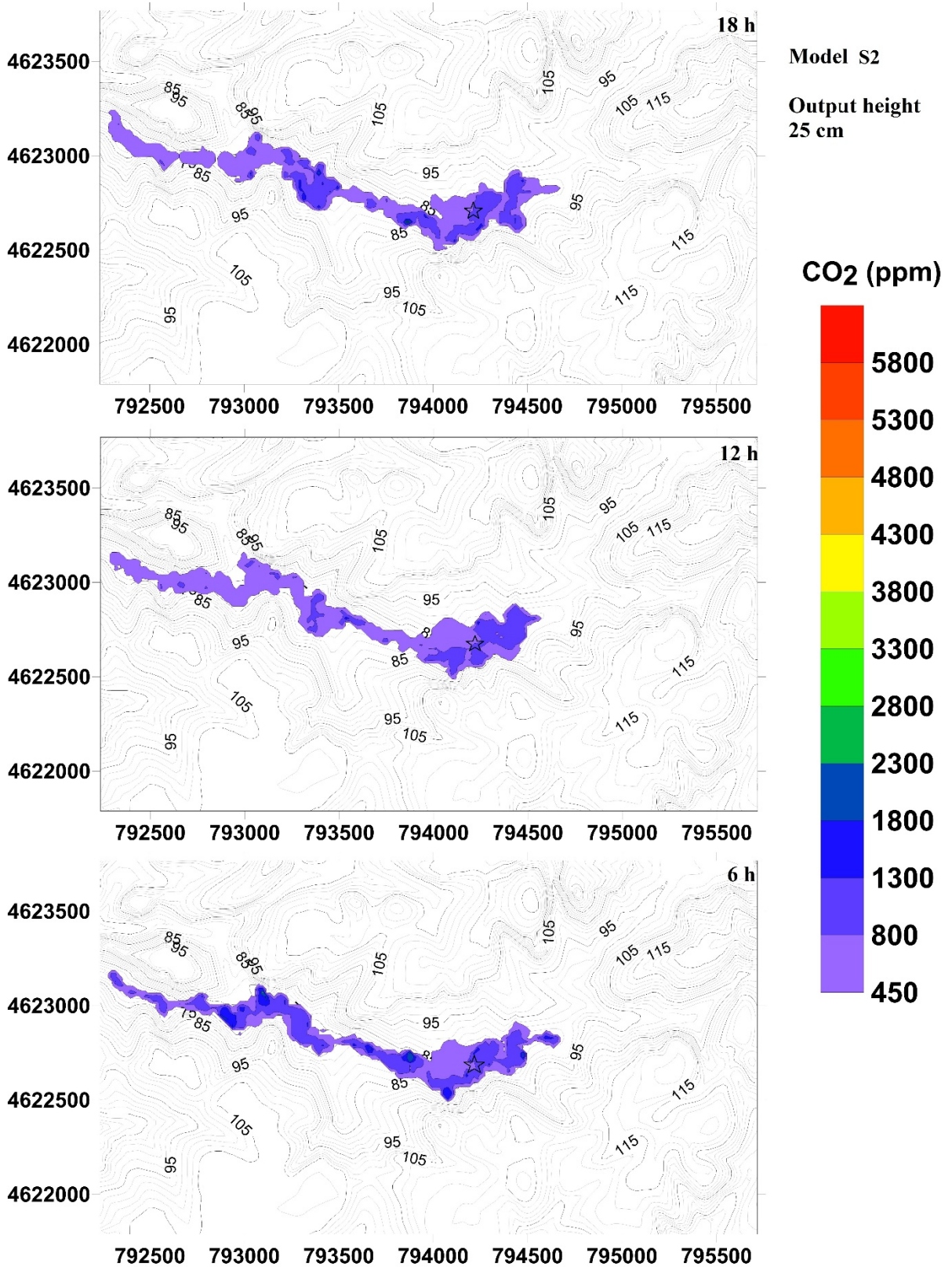


Figure 43. Prediction of the gas plume dispersion in model S1 at 25 cm high for 6, 12 and 18 h of simulation time, the black star indicates the source emission.



**Figure 44.** Prediction of the gas plume dispersion in model S2 at 25 cm high for 6, 12 and 18 h of simulation time, the black star indicates the source emission.

Comparing data from models S1, S3 and S4 at 1 m and 2m high from ground surface, a strong increase in the air CO<sub>2</sub> concentration is observed in the S3 and S4 cases (Fig. 46, Fig. 47 and Fig. 48). The predicted plume of model S1 at 1 metre has an average concentration of 470 ppm with a maximum concentration of 3895 ppm. At 2 metres, very few spots are still predicted with a high concentration (maximum up to 3353 ppm) while the minimum level decreases down to 450 ppm on average.

Models S3 and S4 show larger plumes that cover areas never reached in model S1. Concentrations are higher especially above the emission area, and in the inner part of the plume for a length of 1 km down to the bottleneck present on the middle west side; In the west side, concentrations decrease generally down to 2000/3000 ppm. Model S3 has an average value under 8000 ppm at 1 metre over the lake and 6000 ppm on the far west side (Fig. 47).

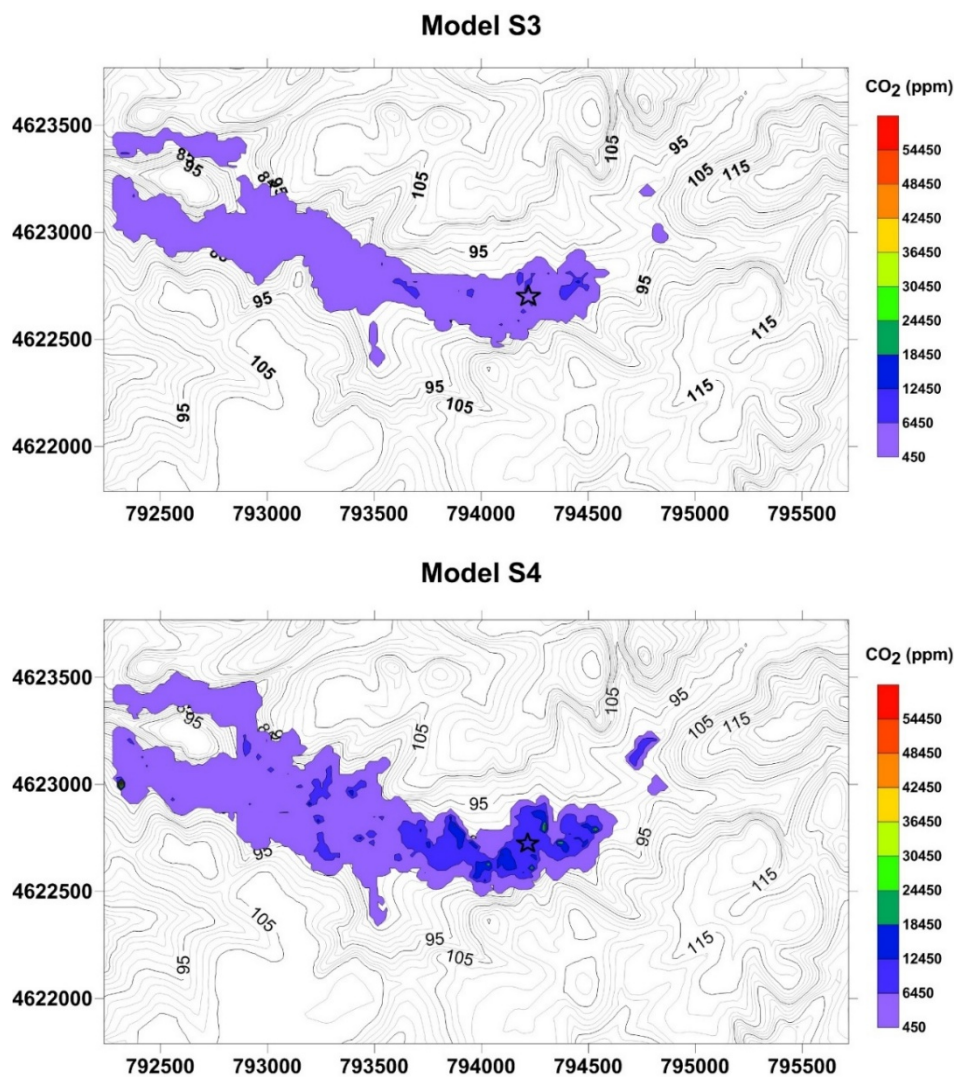


**Figure 45.** Prediction of the gas plume dispersion in models S3 and S4 at 25 cm high after 18 h of simulation time, the black star indicates the source emission.

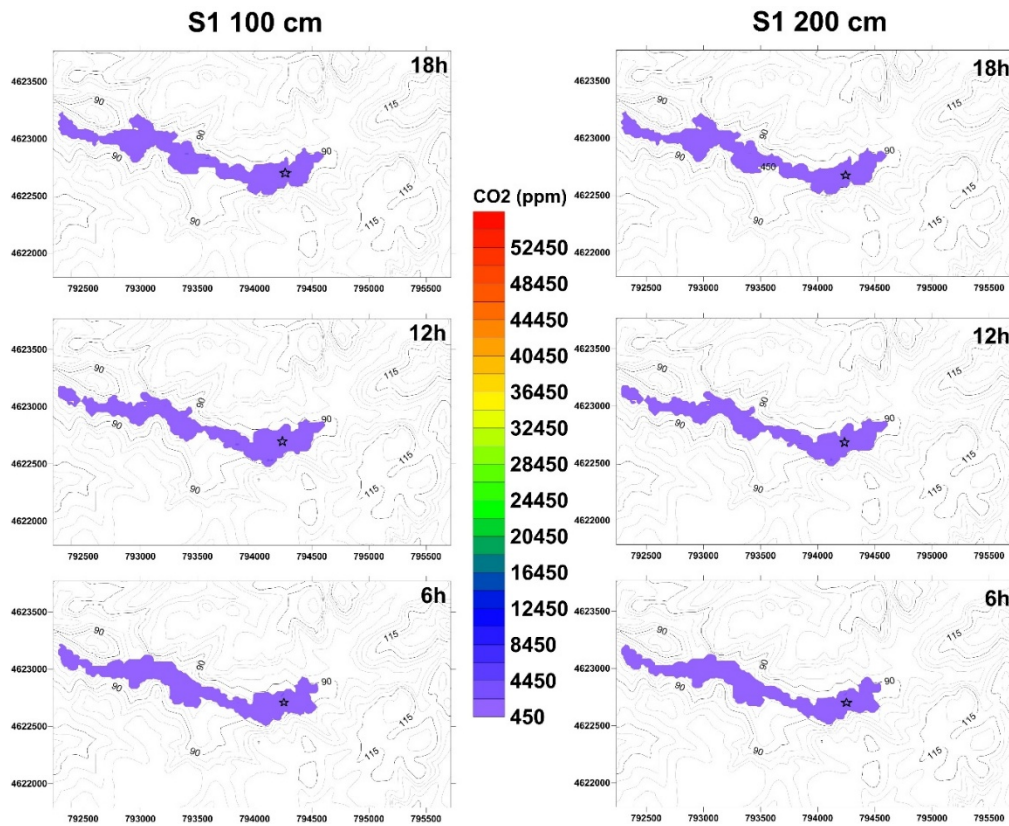


**Figure 46.** Predicted CO<sub>2</sub> air concentration for model S1 outputs at 1 metre and 2 metres high, the black star indicates the source emission.

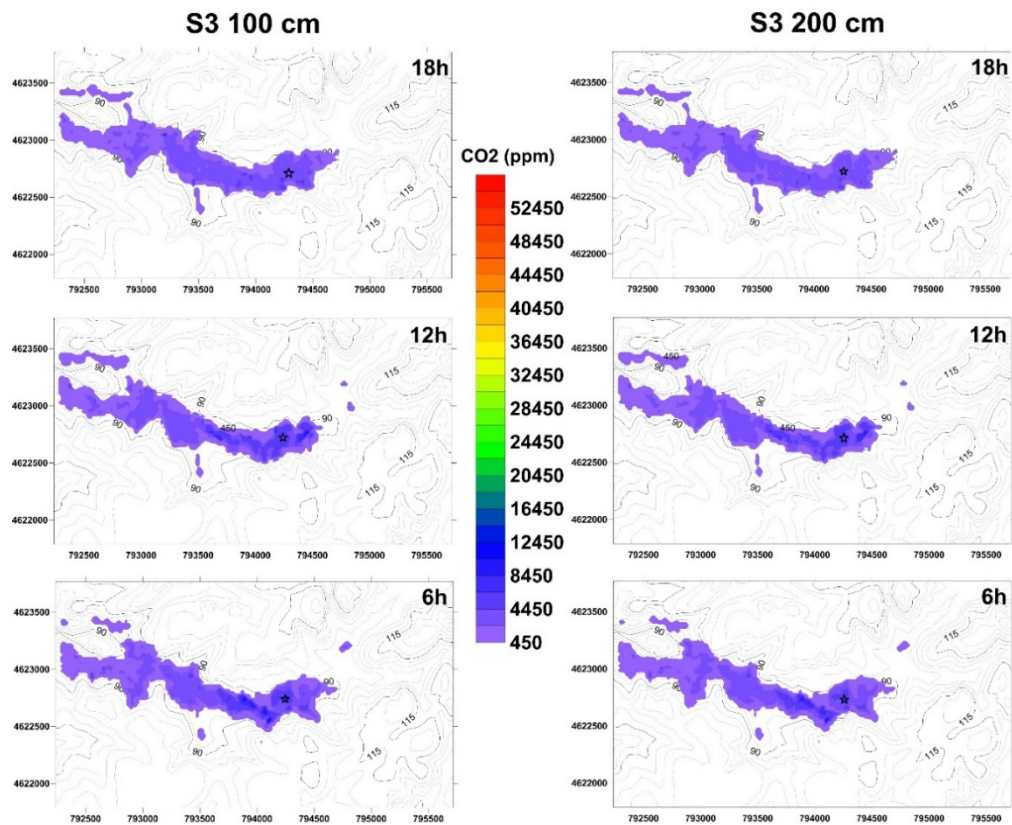


**Figure 47.** Predicted CO<sub>2</sub> air concentration for model S3 outputs at 1 metre and 2 metres high, the black star indicates the source emission.

Model S4 shows a similar behaviour as S3 with higher concentrations over the lake and a significant decrease on the west side. Interestingly, topography affects the plume dispersion in all simulations. The bottleneck area prevents plume dispersion sideways and makes the plume reach higher elevations arriving at 90 metres a.s.l. Concentration in model S4 reaches 16000 ppm over the lake and decreases down to a maximum of 7000 ppm on the west side at 1 metre high. At 2 metres high concentration over the lake has an average value of 9000 ppm and 4500 ppm on the west side.

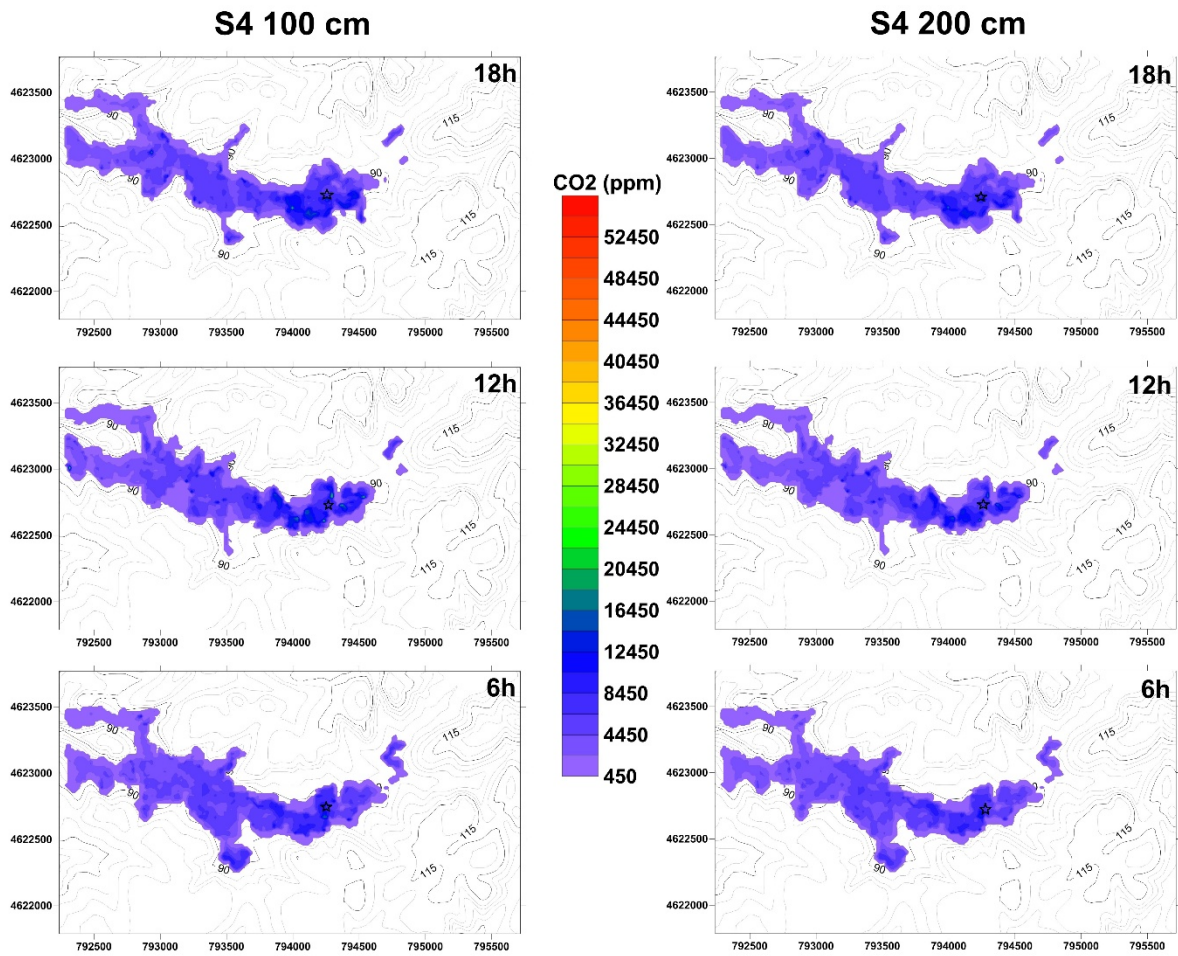


**Figure 48.** Predicted CO<sub>2</sub> air concentration for model S4 outputs at 1 metre and 2 metres high, the black star indicates the source emission.

## 10.8. Discussion

The model predictions yield a significant difference on the plume size between simulations S1 and S2 outputs (see Fig. 43 and 44). Also, a higher average air concentration is predicted in S1 due to the greater amount of emitted CO<sub>2</sub>. If the model data from S1 is compared to TDL data from measurements by Carapezza et al., (2012), it is concluded that the experimental data are always between the predicted minimum and maximum concentration and that the numerical model well reproduces the concentration changes caused by wind activity.



The mapping of risk assessment in geological active regions and areas affected by underground storage of CO<sub>2</sub> is useful to forecast which zones would be more impacted in case of episodic emission. In this respect, simulations S3 and S4 were performed to predict possible hazardous scenarios with higher emission rate than nowadays, five and ten times greater than model S1, respectively. As reported above, the results obtained with the case using present-day conditions (model S1) are comparable to real concentration data in the site. On that basis, the risk map considering a more intense emission can be produced based on atmospheric dispersion models at different heights.

Model predictions show that under some emission conditions air concentration can reach values higher than 1%. However, even in the worst scenario the concentration is below 10 % at heights of 1m or higher so that major impact on human beings (emission rate of 1000 t·d<sup>-1</sup>) vertigo, headache, vomiting, shortness of breath, loss of mental ability, muscular weakness, drowsiness would not be expected.

Due to the lack of atmospheric pressure data each simulation has considered a constant atmospheric pressure of 990 hPa disabling the suction-pump effect. The barometric pumping effect relates to the diurnal changes of ambient pressure due to change in the temperature, as well as pressure changes due to weather systems such as mid-latitude cyclones. This variation in pressure at the surface acts as a suction-pump on the underground (Carrigan, 2010). The wind effect drives to an enhanced mixing layer due to its turbulent character, which increases the rate of seepage into the atmosphere (Oldenburg et al., 2010a). Low-frequency atmospheric motions are less effective than higher-frequency motions at trace gas transport (Waddington et al., 1996). According to Oldenburg and Under (2003) barometric pumping has a negligible effect on the time-averaged seepage flux and near-surface CO<sub>2</sub> concentration because of the cyclic nature of the pressure-induced flows.

From Oldenburg and Unger (2003), the unsaturated zone can attenuate until 96% of CO<sub>2</sub> after 100 years with a leakage rate of  $4 \cdot 10^4$  kg·yr<sup>-1</sup>, while with a rate of  $4 \cdot 10^6$  kg·yr<sup>-1</sup> the attenuation efficiency decreases to 19%. The attenuation efficiency of the unsaturated zone decreased with increasing leakage rate because the higher pressure surrounding the source zone caused more vertical migration of the CO<sub>2</sub> relative to lateral migration, which is more strongly affected by infiltration. According to Oldenburg and Unger (2003) for a CO<sub>2</sub> plume present in the unsaturated zone with no continuous replenishment, dissolution into infiltrating water causes relatively rapid attenuation. Comparing Solfiorata di Pomezia data with Oldenburg and Unger (2003) results, it enhances the equilibrium reached in the Italian volcanic area. The Solfiorata di Pomezia has a soil flux of 1500 g·m<sup>-2</sup>·d<sup>-1</sup> with a leakage rate double than Oldenburg and Unger (2003) respectively 74675 and 40000 ton·yr<sup>-1</sup>. That flux is recorded by Oldenburg and Unger (2003) with a leakage rate of a bigger order

of magnitude ( $4000000 \text{ ton}\cdot\text{yr}^{-1}$ ). Water circulation plays a great role in the Solforata di Pomezia site but is not always present, as explained before in the summer period. Atmospheric pumping can favour the emission especially in the winter, due to the changes of high and low atmospheric pressure; while water content favour dissolution in the winter period due to amount of water circulating.

Comparing leakage rate used in Oldenburg and Unger (2004) with Solforata di Pomezia data it can be stated that Solforata di Pomezia has a low leakage rate so barometric pumping effect is negligible.

The diurnal temperature changes generate changes in ambient pressure. The permeable soil subsurface “breathes” in response to changes in atmospheric pressure through a process called barometric pumping (Carrigan et al., 1996; Massmann and Farrier, 1992; Auer et al., 1996). This variation in pressure at the surface acts as a suction-pump on the underground, also called barometric pumping.

Pirkle et al., (1992) studied barometric pumping of subsurface gas from a landfill at the Savannah River Site near Aiken.SC in 1990. The authors noted that methane flux into the atmosphere “is maximised during periods of falling barometric pressure and ceases or is minimised during periods of rising or stable barometric pressure”. Barometric pumping is “the primary force which causes the migration of buried volatile organics in and above the water table into the atmosphere” and its effect can extend to a few hundred feet below the surface (Pirkle et al., 1992).

The migration of air in the subsoil becomes more pronounced as the thickness and permeability of the vadose zone increase. Weeks (1978) observed barometric pressure fluctuations at depths up to hundreds of feet in deep unsaturated zones. As the subsurface pressure re-establishes equilibrium with the atmospheric pressure, air is “breathed” in and out of the unsaturated zone. Such phenomena will cause vertical transport in systems with an open ground surface (Massmann and Farrier, 1992).

During periods of decreasing atmospheric pressure, soil gas flows vertically toward and into the atmosphere in order to restore pressure equilibrium. As atmospheric pressure increases, gas from the atmosphere flows into the soil profile to reach equilibrium. Barometric pumping causes an up and down motion of subsurface air and facilitates the escape of gaseous soil contaminants in two ways. First, barometric pumping “sweeps out (soil) pore gases near the surface” and thus, contaminants in this zone escape to the atmosphere in a shorter time than they would by diffusion alone (Auer et al., 1996). Volatile species were found to migrate through the soil-atmosphere boundary during periods of rapidly decreasing barometric pressure. Short periods of stable pressure during overall declining pressure regimes were sufficient to temporarily halt the vertical migration of gases. This suggest the

importance of soil permeability and possibly soil moisture content to the overall rate of vertical migration (Wyatt et al., 1995).

According to Norstadt and Porter (1984), Xu and Qi (2001) and Gasparini et al., (2015), an increase of ambient temperature increases CO<sub>2</sub> soil fluxes intensity. Instead, for this case study, an inverse correlation is found between CO<sub>2</sub> soil flux and temperature (Fig. 40), the plot shows data of carbon dioxide soil concentration versus air temperature and is clearly visible as CO<sub>2</sub> concentration increases when temperature drops.

## **10.9. Conclusions**

The comparison between experimental data and numerical calculations of gas dispersion for the CO<sub>2</sub> natural emission site of Solforata di Pomezia shows a good reasonable fit between both set of data. The predicted data comply with experimental data both for air concentration and plume size. This suggests that numerical modelling of atmospheric dispersion of CO<sub>2</sub> plumes emitted from underground can be a valuable tool to develop risks maps in natural emission sites or in areas affected by underground storage.

Atmospheric dispersion maps predicted from numerical modelling using sampling gas data recorded in 2007 do not show hazardous conditions at 25, 100 and 200 cm from surface.

Modelling of critical scenarios of large gas leakage in the same site (five and ten times larger than the present-day emission) does not predict lethal gas concentration at least for human beings at heights 1 and 2 m above the ground, concentrations are largely under 3%. The presence of wind is important because it favours dispersion avoiding CO<sub>2</sub> accumulation at dangerous levels

## **11. General discussion**

A CCS project is targeted to store carbon dioxide deep underground in a safe reservoir through different trapping methods. The safest state of CO<sub>2</sub> once stored is the mineralisation, i.e., the precipitation as carbonate minerals (calcite, dolomite, siderite and related solid solutions); however, mineralisation is not expected in the early stages of the storage and model predictions indicate that it could occur after some thousands of years. This is true for projects in sedimentary basins injecting

CO<sub>2</sub> as supercritical state; in other options, such as the storage in basalts and ultramafic rocks, mineralisation is expected to occur much faster, within the operational time of the project. Other trapping mechanisms in storage in sedimentary basins are sensitive to leakage if integrity of some structural (faults) or engineering components (wells) fails. In this case, CO<sub>2</sub> may migrate upwards and reach shallower aquifers and even the ground surface. Therefore, in order to predict potential hazards, it is important to understand CO<sub>2</sub> behaviour from deep underground to up the vadose zone and even its atmospheric dispersion.

Risk is defined as the probability of occurrence of a process or event that can cause damage. Presently, the risk of CO<sub>2</sub> leakage on surface ecosystems has been based on impacts on shallow aquifers and surface waters. The real likelihood of more severe events such as gas accumulation into the vadose zone and its release on the ground was not well constrained. The work performed in this PhD. project has provided new insights on such a probability.

From PISCO2 experiment (Chapter 1), it is observed that CO<sub>2</sub> path to surface from the vadose zone is highly sensitive to changes in soil compaction, leading to hot spots where gas is preferentially emitted to the atmosphere. In these hot spots, gas flow is higher than the average flow reaching the vadose zone from underground. This “funnel” effect has been also observed in natural analogues like in Campo de Calatrava and Pomezia (chapter 2 and 3, respectively) where surface emission is dominated by spot emissions. Same result has been reported by Oldenburg et al., (2010a) with the patchy emission at ZERT CO<sub>2</sub> release test.

The occurrence of enhanced flows in the interface between the soil and the atmosphere has implications for the risk assessment. First, impact on ecosystems must be reassessed since it would affect to smaller areas but the affectation would be stronger in the spots. Second, the enhanced flows may favour the local accumulation of gas leading to potential formation of CO<sub>2</sub> “lakes”. Finally, the likelihood of lethal gas accumulation has proved to be very low even considering high gas flow from underground. Duration of weather conditions sustaining gas lake formation is generally short and the real impact on ecosystems and humans is predicted to be small. This does not rule out cases of asphyxia in humans as reported from some very high-flow natural analogues, although the gas fluxes in these sites could be much higher than potential leakage from CO<sub>2</sub> storage sites.

The “channelized” pattern of surface emission of underground gases has also implications for monitoring. Baseline studies to characterise the pre-operational gas flows in the area potentially affected by leakage are based on measurements by accumulation chamber following regular meshes of some tenths of metres between measurement stations (Elío et al., 2012 and 2013). According to

the observations in this PhD. work, there will be a high chance of not detecting emission spots following the officially proposed strategy.

## **12. Conclusions and key messages from this PhD.**

This PhD. work has provided new evidences of the gas behaviour in the soil-atmosphere interface. Detailed conclusions have been reported in each chapter but, in a short, they can be summarised as follows:

- Changes in the soil properties have a strong effect on gas flows from underground. As a consequence, gas does not come out homogeneously but forming high-flow spots. This has profound implications on risk assessment and monitoring since these “hot spots” are difficult to detect.

- Water infiltration in the first centimetres has the effect of not only to increase the CO<sub>2</sub> water dissolution but also to homogenize the surface emission.

- Natural analogues are valuable areas to test gas dynamics and the results can be extrapolated (with caution) to industrial CCS projects. These systems appear to be the only places able to provide information about impacts of CO<sub>2</sub> leakage.

- Preferential pathways for gas leakage are connected to soil properties in the unsaturated zone (i.e. permeability, porosity, liquid saturation, ambient temperature).

- Soils with different compaction levels can be used to create preferential emission areas.

- The Sistema Alta Portata (SAP) is a cost-effective method to measure very large spot emissions from underground. It has been successfully used to collect flow data from CO<sub>2</sub> emitting pools in natural analogues.

- Formation of gas “lakes” is unlikely even considering high gas fluxes. Both topographic and weather conditions have a strong effect on its formation. Gas accumulation is usually restricted to the first meter of atmosphere from the ground, and it is highly sensitive to wind. This does not mean that gas accumulation on ground should not be considered in risk assessment studies.

- Numerical models (multiphase transport and atmospheric gas dispersion) are proved to be useful tools to predict gas behaviour in the vadose zone and in the near-ground atmosphere. They have been used to successfully reproduce pilot plant and field observations and help understand gas transport in the interface soil-atmosphere.

- Atmospheric dispersion models are useful to make predictive mapping of risk in areas potentially affected by natural leakage. In the risk assessment for an industrial CCS site, inspection of potential areas of gas outflow and accumulation on ground due to favourable topographic

conditions can be combined with predictive numerical modelling to determine the real risk conditions and to build risk mapping. Numerical models also showed how atmospheric effects (as rainfalls, high liquid saturation) act as physical barriers capable to reduce soil emissions.

### 13. Further work

The work in this PhD. provides new information about CO<sub>2</sub> dynamics in the vadose zone and its atmospheric dispersion. This research line, however, needs still further testing and investigation, and a number of further steps can be suggested:

(1) *Coupled underground-atmospheric modelling of a site (industrial or natural analogue).* This would require the detailed characterisation of a site from the geological and hydrogeological point of view. The multiphase gas-water transport would be coupled with an atmospheric layer in order to study and predict atmospheric dispersion (or accumulation).

(2) *Study of the soil gas emissions from volcanic rocks in the city of Rome district.* This project would consist of a series of soil gas surveys of the green areas inside the Great Ring Road. The monitoring of the CO<sub>2</sub> and Radon (Rn<sup>222</sup> – Rn<sup>220</sup>) emissions would produce a series of flux and concentration maps in order to study both natural volcanic rocks decay and to supervise areas with dangerous natural emissions for human beings coupling the research with radon indoor survey.

(3) *Study of a seismic active area in Italy with soil gas emissions.* Such study may be helpful to understand the relationship between earthquakes and gas emission along faults. Soil gas survey is already used to recognize blind faults in active areas; this work suggests the use of gas tracers as seismic precursors.

### 14. References

Acocella, V., Salvini, F., Funicello, R., Faccenna, C., 1999. The role of transfer structures on volcanic activity at Campi Flegrei (Southern Italy). *Journal of Volcanology and Geothermal Research* **91**(2), 123-139.

**Agnelli, M., Grandia, F., Credoza, A., Gasparini, A., Bruno, J., 2013.** Use of diffusive gradients in thin films (DGT) as early detection tool of low-intensity leakage from CO<sub>2</sub> storage. *Greenhouse gases: Science and Technology* **4(2)**, 163-175.

**Agnelli, M., Grandia, F., Soler, D., Sainz-Garcia, A., Brusi, D., Zamorano, M., submitted 2018.** Metal release in shallow aquifers impacted by deep CO<sub>2</sub> fluxes. Submitted to *Energy Procedia*.

**Annunziatellis, A., Beaubien, S.E., Bigi, S., Ciotoli, G., Coltella, M., Lombardi, S., 2008.** Gas migration along fault system and through the vadose zone in the Latera caldera (Central Italy): Implication for CO<sub>2</sub> geological storage. *International Journal of Greenhouse Gas Control* **2(3)**, 353-372.

**Ancochea, E., 1999.** El Campo Volcánico de Calatrava. Enseñanza de las Ciencias de la Tierra, 1999, (7.3) 237-243 I.S.S.N.: 1132-9157

**André, L., Audigane P., Azaroual, M., Menjoz, A., 2007.** Numerical modeling of fluid-rock chemical interactions at the supercritical CO<sub>2</sub>-liquid interface during CO<sub>2</sub> injection into carbonate reservoir, the Dogger aquifer (Paris Basin, France). *Energy conversion and management*, **48(3)**, 1782-1797.

**Annunziatellis, A., Beaubien, S.E., Bigi, S., Ciotoli, G., Coltella, M., Lombardi, S., 2008.** Gas migration along fault systems and through the vadose zone in the Latera caldera (central Italy): Implications for CO<sub>2</sub> geological storage. *International Journal of Greenhouse Gas Control* **2**, 353-372.

**Audigane, P., Gaus, I., Czernichowski-Lauriol, I., Pruess, K., Xu, T., 2007.** Two-dimensional reactive transport modeling of CO<sub>2</sub> injection in a saline aquifer at the Sleipner site, North Sea. *American Journal of Science*, **09/2007-307**, 974-1008.

**Auer, L.H., Rosenberg, N.D., Biordsell, K.H., Whitney, E.M., 1996.** The effect of barometric pumping on contaminant transport. *Journal of Contaminant Hydrology* **24**, 145. [https://doi.org/10.1016/S0169-7722\(96\)00010-1](https://doi.org/10.1016/S0169-7722(96)00010-1)

**Bachu, S., Gunter, W.D., Perkins, E.H., 1994.** Aquifer disposal of CO<sub>2</sub>: Hydrodynamic and mineral trapping. *Energy conversion and management* **35(4)**, 269-279.

**Bateson, L., Vellico, M., Beaubien, S.E., Pearce, J.M., Annunziatellis, A., Ciotoli, G., Coren, F., Lombardi, S., Marsh, S., 2008.** The application of remote sensing techniques to monitor CO<sub>2</sub>-storage sites for surface leakage: Method development and testing at Latera (Italy) where

naturally produced CO<sub>2</sub> is leaking to the atmosphere. *International Journal of Greenhouse Gas Control* **2**, 388-400.

**Battistelli, A., Calore, C., Pruess, K., 1997.** The simulator TOUGH2/EWASG for modeling geothermal reservoirs with brines and non-condensable gas. *Geothermics*, **26(4)**, 437–464.

**Baxter, P.J., Baubron, J.-C., Coutinho, R., 1999.** Health hazards and disaster potential of ground gas emissions at Furnas volcano, Sao Miguel, Azores. *Journal of Volcanology and Geothermal Research* **92(1-2)**, 95-106.

**Beaubien, S.E, Ciotoli, G., Coombs, P., Dictor, M.C., Kruger, M., Lombardi, S., Pearce, J.M. West, J.M., 2008.** The impact of a naturally occurring CO<sub>2</sub> gas vent on the shallow ecosystem and soil chemistry of a Mediterranean pasture (Latera, Italy). *International Journal of Greenhouse Gas Control* **2(3)**, 373-387.

**Beaubien, S.E., Jones, D.G., Gal, F., Barkwith, A.K.A.P., Braibant, G., Baubron, J.C., Ciotoli, G., Graziani, S., Lister, T.R., Lombardi, S., Michel, K., Quattrocchi, F., Strutt, M., 2013.** Monitoring of near-surface gas geochemistry at the Weyburn, Canada, CO<sub>2</sub>-EOR site, 2001-2011. *International Journal of Greenhouse Gas Control* **16(1)**, S236-S262.

**Billing, W.F.D., Lucken, J.O., Mortensen, D.A., Peterson, K.M., 1982.** Arctic tundra: a source or sink for atmospheric carbon dioxide in a changing environment? *Oecologia*, **53**, 7-11.

**Boonstra, J., De Ridder, N.A., 1981.** Numerical modeling of groundwater basins.

**Bruno J., Grandia F. and Vilanova E., 2009.** Trace element behavior in connection to the geological storage of CO<sub>2</sub>. Lessons from natural analogues. Abstracts of the Goldschmidt Conference 2009, Davos (Switzerland). *Geochim Cosmochim Acta* **73(13)**, A167.

**Carapezza, M.L., Barberi, F., Tarchini, G., Ranaldi, M., Ricci, T., 2003.** Volcanic hazards of the Colli Albani. From: Funicello, R., and Giordano, G., (eds) *The Colli Albani Volcano*. Special publication of IAVCEI, **3**, 279-297. Geological Society, London.

**Carapezza, M.L., and Granieri, D., 2004.** CO<sub>2</sub> soil flux at Vulcano (Italy): comparison between active and passive methods. *Applied Geochemistry* **19**, 73-88.

**Carapezza, M.L., Barberi, F., Tarchini, L., Cavarra, L., Granieri, D., 2005.** Le emissioni gassose dell'area vulcanica dei Colli Albani. In: Carapezza, M.L., et al. (Ed.), *Nuovi dati sull'attività recente del cratere del Lago Albano e sul degassamento dei Colli Albani*. *Atti Accad. Naz. Lincei* **218**, 229–242.



**Carapezza, M.L., Barber, F., Ranaldi, M., Ricci, T., Tarchini, G., Barrancos, J., Fischer, C., Granieri, D., Lucchetti, C., Melian, G., Perez, N., Tuccimei, P., Vogel, A., Webber, K., 2012.** Hazardous gas emissions from the flanks of the quiescent Colli Albani volcano (Rome, Italy). *Applied Geochemistry* **27**, 1767-1782.

**Carrigan, C.R., Heinle, R.A., Hudson, G.B., Nitao, J.J., and Zucca, J.J., 1996.** Trace gas emissions on geological faults as indicators of underground nuclear testing, *Nature* **382**, 528-531.

**Carrigan, C.R., 2010.** Noble gas field operations test: Towards detecting 'the smoking gun' during an on-site inspection. *CTBTO Spectrum* **15(1)**, 22–25.

**Cebriá, J.M., and Lopez-Ruiz, J., 1995.** Alkali basalts and leucitites in an extensional intra-continental plate setting: the Late Cenozoic Calatrava Volcanic Province. *Journal of Volcanology and Geothermal Research* **185**, 172-180.

**Chiodini, G., Cioni, R., Guidi, M., Raco, B., Marini, L., 1998.** Soil CO<sub>2</sub> flux measurements in volcanic and geothermal areas. *Applied Geochemistry* **13**, 543-552.

**Chiodini, G., and Frondini, F., 2001.** Carbon dioxide degassing from the Albani Hills volcanic region, Central Italy. *Chemical Geology* **177**, 67-83.

**Chiodini, G., Cardellini, C., Amato, A., Boschi, E., Caliro, S., Frondini, F., Ventura, G., 2004.** Carbon dioxide earth degassing and seismogenesis in central and southern Italy. *Geophysical Research Letters*, **31**, L07615.

**Chiodini, G., Granieri, D., Avino, R., Caliro, S., Costa, A., Minopoli, C., Vilardo, G., 2010.** Non-volcanic CO<sub>2</sub> earth degassing: case of Mefite d'Ansanto (southern Apennines), Italy. *Geophysical Research Letters* **37**, L11303.

**Chung, T.-H., Ajlan, M., Lee, L.L., Starling, K.E., 1988.** Generalized multiparameter correlation for nonpolar and polar fluid transport properties. *Ind. Eng. Chem. Res.* **27**, 671–679.

**Compton, R.R., 1985.** *Geology in the field*. John Wiley and Sons, Publishers, 628 pp.

**Costa, A., Macedonio, G., Chiodini, G., 2005.** Numerical model of gas dispersion emitted from volcanic sources. *Annals of Geophysics* **48**, 805-815.

**Costa, A., Chiodini, G., Granieri, D., Folch, A., Hankin, R., Caliro, S., Avino, R., Cardellini, C., 2008.** A shallow layer model for heavy gas dispersion from natural sources: application on hazard assessment at Caldara di Manziana, Italy. *Geochem. Geophys. Geosys.* **9(3)**, 1-13.

**Cramer, S.D., 1982.** The solubility of methane, carbon dioxide and oxygen in brines from 0 to 300 °C, U.S. Bureau of Mines Report No. 8706.

**Creoz, A., Grandia, F., Luna, M., Bayer, M., Salas, J., Jordana, S., Bruno, J., 2011a.** Simulación numérica de fugas profundas de CO<sub>2</sub> en la zona no saturada; primeros Resultados del proyecto PISCO<sub>2</sub> –Ciuden. *Estudios en la zona no saturada del suelo X*, 223 – 228.

**Creoz, A., Grandia, F., Bruno, J., 2011b.** Diseño definitivo y estrategia de validaciones de la CELDA BASE. Informe interno Fundación Ciudad de la Energía.

**D’Amore, F., and Truesdell, A.H., 1988.** A review of solubilities and equilibrium constants for gaseous species of geothermal interest. *Sci. Geol. Bull.* **41 (3–4)**, 309–332.

**Dávila Ordóñez, M.G., Luquot, L., Soler, J.M., Cama, J., 2016a.** 2D reactive transport modelling of the interaction between a marl and a CO<sub>2</sub>-rich sulphate solution under supercritical CO<sub>2</sub> conditions. *International Journal of Greenhouse Gas Control*, **54**, 145-159.

**Dávila Ordóñez, M.G., Luquot, L., Soler, J.M., Cama, J., 2016b.** Interactions between a fractured marl caprock and CO<sub>2</sub>-rich sulphate solution under supercritical CO<sub>2</sub> conditions. *International Journal of Greenhouse Gas Control*, **48**, 105-119.

**Davis, S.N. and De Wiest, R.J.M., 1966.** Hydrogeology. New York, John Wiley and Sons, Inc., 463 pp.

**De Jong, E., and Schappert, H., 1972.** Calculation of soil respiration and activity from CO<sub>2</sub> profiles in the soil. *Soil Science* **113(5)**, 328-333.

**De Lary, L., Loschetter, A., Bouc, O., Rohmer, J., Oldenburg, C.M., 2012.** Assessing health impacts of CO<sub>2</sub> leakage from a geological storage site into buildings: role of attenuation in the unsaturated zone and buildings foundation. *Int. Journal of Greenhouse Gas Control*, **9**, 322-333. DOI: 10.1016/j.ijggc.2012.04.011.

**De Rita, D., Funicello, R., Parotto, M., 1988.** Geological map of the Colli Albani volcanic complex (“Vulcano Laziale”), CNR-GNV, Joint venture ENEA-AGIP.

**De Rita, D., Faccenna, C., Funicello, R., Rosa, C., 1995.** Stratigraphy and volcano-tectonics. In Triglia, R (Ed.), *The Volcano of Alban Hills*, Rome, 33-71.

**Dillen, M., Lindeberg, E., Aagaard, P., Aker, E., Saether, O.M., Johansen, H., Lien, M., Hatzignatiou, D.G., Golmen, L., Hellevang, J., 2009.** A field laboratory for monitoring CO<sub>2</sub> leakage. *Energy Procedia* **1(1)**, 2397-2404.

**Elío, J., Ortega, M.F., Chacón, E., Mazadiego, L.F., Grandia, F., 2012.** Sampling strategies using the accumulation chamber for monitoring geological storage of CO<sub>2</sub>. *International Journal of Greenhouse Gas Control* **9**, 303-311.

**Elío, J., Nisi, B., Ortega, M.F., Mazadiego, L.F., Vaselli, O., Grandia, F., 2013.** CO<sub>2</sub> soil flux baseline at the technological development plant for CO<sub>2</sub> injection at Hontomín (Burgos, Spain). *International Journal of Greenhouse Gas Control*, **18**, 224-236.

**Elío, J., Ortega, M.F., Nisi, B., Mazadiego, L.F., Vaselli, O., Caballero, J., Grandia, F., 2015.** CO<sub>2</sub> and radon degassing from the natural analog of Campo de Calatrava (Spain): implications for monitoring of CO<sub>2</sub> storage sites. *International Journal of Greenhouse Gas Control*, **32**, 1-14.

**Faive-Pierret, R. and Le Guern, F., 1983.** Health risks linked with inhalation of volcanic gases and aerosols. In: H. Tazieff and J.C. Sabroux (Editors), *Forecasting Volcanic Events*. Elsevier Science Publishers B.V., Amsterdam, pp. 69-81.

**Farrar, C.D., Sorey, M.L., Evans, W.C., Howle, J.F., Kerr, B.D., Kennedy, B.M., King, C.-Y., Southon, J.R., 1995.** Forest-killing diffuse CO<sub>2</sub> emission at Mammoth Mountain as a sign of magmatic unrest. *Nature*, **08/1995**.

**Folch, A., Costa, A, Hankin, R.K.S., 2007.** TWODEE-2 Computer code and related documentation (for internal use only). Project INGV-DPC V5 Diffuse degassing in Italy (2005-2007).

**Folch, A., Costa, A, Hankin, R.K.S., 2009.** TWODEE-2: A shallow layer model for dense gas dispersion on complex topography. *Computers and Geosciences* **35**, 3, 667-674. doi:10.1016/j.cageo.2007.12.017.

**Freeze, R.A., and Cherry, J.A., 1979.** *Groundwater*. Prentice-Hall, 604 pp.

**Funicello, R., Mattei, M., Voltaggio, M., 1992.** Recent strike slip faulting and problems of possible reactivation in Rome area. In: Boschi, E., Dragoni, M., (Eds.), *Earthquake Prediction*, 225-236, Rome.

**Garcia-Rios, M., Cama, J., Luquot, L., Soler, J.M., 2014.** Interaction between CO<sub>2</sub>-rich sulphate solutions and carbonate reservoir rocks from atmospheric to supercritical CO<sub>2</sub> conditions: Experiments and modelling. *Chemical Geology*, **383**, 107-122.

**Gasparini, A., Credo, A., Grandia, F., Garcia, D.A., Bruno, J., 2015.** Experimental and numerical modeling of CO<sub>2</sub> leakage in the vadose zone. *Greenhouse Gas Science and Technology* **5**, 1-24.

**Gaus, I., Audigane, P., André, L., Jacquemet, N., Durst, O., Czernichowski-Lauriol, I., Azaroual, M., 2008.** Geochemical and solute transport modeling for CO<sub>2</sub> storage, what expect from it?. *International Journal of Greenhouse Gas Control* **2(4)**, 605-625.

**Gherardi, F., Xu, T., Pruess, K., 2007.** Numerical modeling of self-limiting and self-enhancing caprock alternation induced by CO<sub>2</sub> storage in a depleted gas reservoir. *Chemical geology* **244**, 103-129.

**Giggenbach, W.F., Sano, Y., Schmincke, H.U., 1991.** CO<sub>2</sub>-rich gases from Lakes Nyos and Monoun, Cameroon; Laacher See, Germany; Dineg, Indonesia, and Mt. Gambier, Australia-variations on a common theme. *Journal of Volcanology and Geothermal Research* **45**, 311-323.

**Gonzalez, C.E., Gosalvez, R.U., Becerra, R., Escobar, L.E., 2007.** Actividad eruptiva holocena en el Campo de Calatrava (Volcán Columba, Ciudad Real, España). In: XII Reunión Nacional de Cuaternario, Lario, J. and Silva, G., (Eds.), 143-144, Ávila, España.

**Grivé, M., 2005.** The linkage between uranium, iron and carbon cycling. Processes at interfaces: evidences from combined solution chemical and spectroscopic studies. *Tesis doctoral, Universitat Politècnica de Catalunya*, pp. 341.

**Hankin, R., and Britter, R., 1999 a.** TWODEE: the Health and Safety Laboratory's shallow layer model for heavy gas dispersion. Part 1: Mathematical basis and physical assumptions. *Journal of Hazardous Materials* **A66**, 211-226.

**Hankin, R., and Britter, R., 1999 b.** TWODEE: the Health and Safety Laboratory's shallow layer model for heavy gas dispersion. Part 2: Outline and validation of the computational scheme. *Journal of Hazardous Materials* **A66**, 227-237.

**Hankin, R., and Britter, R., 1999 c.** TWODEE: the Health and Safety Laboratory's shallow layer model for heavy gas dispersion. Part 3: Experimental validation (Theory island). *Journal of Hazardous Materials* **A66**, 236-261.

**Haynes, W.M., 2012.** *CRC Handbook of chemistry and physics, 93<sup>rd</sup> edition*. CRC Press, pp. 2664.

**Hinkle, M.E., 1994.** Environmental-conditions affecting concentrations of He, CO<sub>2</sub>, O<sub>2</sub> and N<sub>2</sub> in soil gases. *Applied Geochemistry* **9(1)**, 53-63.

**Hirschfelder, J.O., Curtis, C.F., Bird, R.B., 1954.** *Molecular theory of gases and liquids*. John Wiley and Sons, Inc., New York.

**IEA, 2010.** *Energy Technology perspective: Scenarios and Strategies to 2050*.

**Instituto Geológico y Minero de España (IGME), 1998.** Mapa geológico de España E: 1:50.000. Hoja n.º 784-785, Ciudad Real. I.G.M.E., Madrid.

**International Formulation Committee, 1967.** A formulation of the thermodynamic properties of ordinary water substance. IFC Secretariat, Dusseldorf, Germany.

**IPCC, 2005.** Special report on carbon dioxide capture and storage. In: Metz, B., Davidson, O., de Coninck, H.C., Loos, M., Meyer, L.A.,(Eds.), prepared by working group III of the Intergovernmental Panel on Climate Change. Cambridge University Press, Cambridge, U.K. and N.Y., New York, USA, p 442.

**Jacques, D., Šimůnek, J., Timmerman, A., Feyen, J., 2002.** Calibration of Richards' and convection- dispersion equations to field-scale water flow and solute transport under rainfall conditions. *Journal of Hydrology* **259**, 15-31.

**Jacobson, M., 1999.** Fundamentals of atmospheric modelling, 1<sup>st</sup> Edition. Cambridge University Press, New York.

**Jones. D.G., Barkwith, A.K.A.P., Hannis, S., Lister, T.R., Gal, F., Graziani, S., Beaubien, S.E., Widory, D., 2014.** Monitoring of near surface gas seepage from a shallow injection experiment at the CO<sub>2</sub> Field Lab, Norway. *International Journal of Greenhouse Gas Control* **28**, 300-317.

**Kano, Y., and Ishido, T., 2011.** Numerical simulation on the long-term behavior of CO<sub>2</sub> injected into a deep saline aquifer composed of alternating layers. *Energy Procedia* **4**, 4339-4346.

**Kharaka, Y.K., Thordsen, J.J., Kakouros, E., Ambats, G., Herkelrath, W.M., Beers, S.R., Birkholzer, J.T., Apps, J.A., Spycher, N.F., Zheng, L., Trautz, R.C., Rauch, H.W., Gullickson, K.S. 2010.** Changes in the chemistry of shallow groundwater related to the 2008 injection of CO<sub>2</sub> at the ZERT field site, Bozeman, Montana. *Environ. Earth Sci.*, **60(2)**, 273-284.

**Koerner, B., Klopatek, J., 2002.** Anthropogenic and natural CO<sub>2</sub> emission sources in an arid urban environment. *Environmental Pollution* **116(1)**, S45-S51.

**Kowalik, P.C., Barnes, J., Smiles, D.E., 1979.** Oxidation of liquid animal wastes in soil. *Soil Science Soc. Am. J.* **43(2)**, 255-260.

**Laiolo, M, Ranaldi, M., Tarchini, L., Carapezza, M.L., Coppola, D., Ricci, T., Cigolini, C., 2016.** The effects of environmental parameters on diffuse degassing at Stromboli volcano: insights from joint monitoring of soil CO<sub>2</sub> flux and radon activity. *J. Volcanol. Geotherm. Res.*, 315, 65-78. DOI:10.1016/j.vol-geores.2016.02.004.

**Lewicki, J.L., Oldenburg, C.M., Dobeck, L., Spangler, L., 2007.** Surface CO<sub>2</sub> leakage during two shallow subsurface CO<sub>2</sub> releases. *Geophysical Research Letters* **34(24)**, L24402.

**Lewicki, J.L., Hilley, G.E., Dobeck, L., Spangler, L., 2010.** Dynamics of CO<sub>2</sub> fluxes and concentrations during a shallow subsurface CO<sub>2</sub> release. *Env. Earth Sci.* **60**, 285-297.

**Loisy, C., Cohen, G., Laveuf, C., Le Roux, O., Delaplace, P., Magnier, C., Rouchon, V., Cerepi, A., Garcia, B., 2013.** The CO<sub>2</sub>-Vadose Project: dynamics of the natural CO<sub>2</sub> in a carbonate vadose zone. *International Journal of Greenhouse Gas Control* **14**, 97-112.

**Lopez-Ruiz, J., Cebriá, J.M., Doblas, M., 2002.** Cenozoic Volcanism I: the Iberian Peninsula. In: Gibbons, W., Moreno, T., (Eds.), *The geology of Spain*. Geological Society, London, 417-4383.

**Louis, J., 1979.** A parametric model of vertical eddy fluxes in the atmosphere. *Boundary Layer Meteor.* **17**, 187-202.

**Massmann J., and Farrier, D.F., 1992.** Atmospheric pressures on gas transport in the vadose zone. *Water Resources Research* **28(3)**, 777-791.

**Martin-Serrano, A., Vegas, J., Garcia-Cortes, A., Galan, L., Gallardo-Millan, J.L., Martin-Alfageme, S., Rubio, F.M., Ibarra, P.I., Granda, A., Perez-Gonzalez, A., Garcia-Lobon, J.L., 2009.** Morphotectonic setting of maar lakes in the Campo de Calatrava Volcanic Field (Central Spain, SW Europe). *Sedimentary Geology* **222(1-2)**, 52-63.

**Melo, C.L., 2012.** Técnicas de monitoramento para armazenamento geológico de CO<sub>2</sub>. I Curso basico “Compreendendo a Captura eo Armazenamento de Carbono”, PUCRS, Porto Alegre.

**Moni, C., and Rasse, D.P., 2014.** Detection of simulated leaks from geologically stored CO<sub>2</sub> with <sup>13</sup>C monitoring. *International Journal of Greenhouse Gas Control* **26**, 61-68.

**National Institute of Occupational Safety and Health (NIOSH), 1981.** Occupational Health Guidelines for Chemical Hazards, DHHS (NIOSH) Publication No. 81-123. <http://www.cdc.gov/niosh/81-123.html>.

**NIST (National Institute of Standards and Technology), 2013.** Standard Reference Database 69 – NIST Chemistry Web Book, <http://webbook.nist.gov>, (retrieved during May 2013).

**Norstadt, F.A., and Porter, L.K., 1984.** Soil gases and temperatures: a beef cattle feedlot compared to alfalfa. *Soil Sci. Soc. Am. J.* **48**, 783–789.

**Ogretim, E., Mulkeen, E., Donald, D.G., Grant, S.B., 2012.** A parametric study of the transport of CO<sub>2</sub> in the near-surface. *International Journal of Greenhouse Gas Control* **9**, 294-302.

**Oldenburg, C.M., and Unger, A.J.A., 2003.** On leakage and seepage from geologic carbon sequestration sites: unsaturated zone attenuation. *Vadose Zone Journal* **2(3)**, 287-296.

**Oldenburg, C.M., and Unger, A.J.A., 2004.** Coupled vadose zone and atmospheric surface-layer transport of CO<sub>2</sub> from geologic carbon sequestration sites. *Vadose Zone Journal* **3(3)**, 848-857.

**Oldenburg, C.M., Moridis, G.J., Spycher, N., and Pruess, K., 2004.** EOS7C 1.0: TOUGH2 Module for carbon dioxide or nitrogen in natural gas (methane) reservoirs. Earth Science Division, Lawrence Berkeley Nat. Lab., Univ. of California, LBNL-56589.

**Oldenburg, C.M., Lewicki, J.L., Pan, L., Dobeck, L., Spangler, L., 2010a.** Origin of the patchy emission pattern at the ZERT CO<sub>2</sub> release test. *Environ Earth Sci* **60**, 241–250.

**Oldenburg, C.M., Lewicki, J L., Dobeck, L., Spangler, L., 2010b.** Modelling gas transport in the shallow subsurface during the ZERT CO<sub>2</sub> Release Test. *Transp. Porous Media* **82**, 77-92.

**Oliva, A., Moreira, A.C.C.A., Chang, H.K., Rosario, F.F., Musse, A.P.S., Melo, C.L., Bressan, L.W., Ketzer, J.M.M., Contant, M-J., Lazzarin, H.S.C., Cavelhao, G., Corseuil, H.X., 2014.** A comparison of three methods for monitoring CO<sub>2</sub> migration in soil and shallow subsurface in the Ressaccada Pilot site, Southern Brazil. *Energy Procedia* **63**, 3992-4002.

**Papendick, R.I., and Runkles, J.R., 1965.** Transient state oxygen diffusion in soil, I, The case when the rate of oxygen consumption is constant. *Soil Science* **100**, 251-261.

**Papendick, R.I., and Runkles, J.R., 1966.** Transient state oxygen diffusion in soil, II, The case when the rate of oxygen consumption varies with time. *Soil Science* **102**, 223-230.

**Pearce, J., Czernichowsky-Lauriol, I., Lombardi, S., Brune, S., Nador, A., Baker, J., Pauwels, H., Hatziyannis, G., Beaubien, S., Faber, E., 2016.** A review of natural CO<sub>2</sub> accumulations in Europe as analogues for geological sequestration. From: Baines, S.J., and Worde, R.H., (eds) 2004. Geological Storage of Carbon Dioxide. Geol. Soc., London, Special Publications, 233, 29-41.

**Pirkle, R.J., Wyatt, D.E., Price, V., Looney, B.B., 1992.** National ground water association, Proceeding of the Focus Conference on Eastern regional ground water issues, 427.

**Poling, B.E., Prausnitz, J.M., O'Connell, J.P., 2000.** The properties of gases and liquids, fifth edition, McGraw Hill, New York

**Pollak, M., and McCoy, S.T., 2011.** Monitoring for greenhouse gas accounting at geologic sequestration sites: technical and policy considerations. *Energy Procedia*, **4**, 5917-5924.

**Pruess, K. and Wang, J.S.Y., 1987.** Numerical modeling of isothermal and non-isothermal flow in unsaturated fractured rock - A review, in D. Evans and T. Nicholson, (eds.), Flow and Transport Through Unsaturated Fracture Rock, American Geophysical Union, Geophysical Monograph 42, 11-21, 1987.

**Pruess, K., Oldenburg, C.M., Moridis, G., 1999.** TOUGH2 User's Guide, Version 2. Earth Sciences Division, Lawrence Berkeley National Laboratory University of California (1999).

**Pruess, K., 2005.** ECO2N: a TOUGH2 Fluid property module for mixtures of water, NaCl, and CO<sub>2</sub>. Earth Science Division, Lawrence Berkeley National University, LBNL-57952 (2005).

**Pruess, K., Oldenburg, C. Moridis, G., 2011.** TOUGH2 User's Guide Version 2. Earth Sciences Division, Lawrence Berkeley National Laboratory Report LBNL-43134 revised.

**Quattrocchi, F., Cantucci, B., Cinti, D., Pizzino, L., Sciarra, A., 2008.** Continuous/discrete geochemical monitoring of CO<sub>2</sub> Natural Analogues and of Diffuse Degassing Structure (DDS): hints for CO<sub>2</sub> storage sites geochemical protocol. *Energy Procedia* 1, 2135-2142.

**Raich, J.W., Schlesinger, W.H., 1992.** The global carbone-dioxide flux in soil respiration and its relationship to vegetation and climate. *Tellus Series B, Chemical and Physical Meteorology*, **44**, 81-99.

**Reid, R.C., Prausnitz, J.M., Poling, B.E., 1987.** Properties of gases and liquids. 4<sup>th</sup> Ed, McGraw-Hill, 768 pp.

**Rogie, J.D., Kerrick, D.M., Chiodini, G., Frondini, F., 2000.** Flux measurements of nonvolcanic CO<sub>2</sub> emission from some vents in central Italy. *Journal of Geophysical Research* **105 (B4)**, 8435-8445.

**Rogie, J.D., Kerrick, D.M., Sorey, M.L., Chiodini, G., Galloway, D.L., 2001.** Dynamics of carbon dioxide emission at Mammoth Mountain, California. *Earth and Planetary Science Letters* **188(3-4)**, 535-541.

**Rohmer J., De Lary, L., Blanc, C., Guerin, V., Coftier, A., Hube, D., Audigane, P., and Oldenburg, C.M., 2010.** Managing the risks in the vadose zone associated with the leakage of CO<sub>2</sub> from a deep geological storage. Proceedings of CONSOIL 2010 - 11th International UFZ-Deltares/TNO Conference on Management of Soil, Groundwater and Sediment, Sep 2010, Salzburg, Austria, pp. 8 (2010).



**Salomon, D.K., and Cerling, T.E., 1987.** The annual carbon dioxide cycle in a Montane soil: Observation, modelling, and implication for weathering. *Water Resources Research* **23(12)**, 2257-2265.

**Sanders, L., 1998.** A manual of field hydrogeology. Prentice-hall, 381 pp.

**Sharma, S., Cook, P., Berly, T., Lees, M., 2009.** The CO<sub>2</sub>CRC Otway Project: overcoming challenges from planning to execution of Australia's first CCS project. *Energy Procedia* **1(1)**, 1965-1972.

**Schiff, H.I., Mackay, G-I. Bechara, J., 1994.** The use of Tunable Diode Laser Absorption spectroscopy for atmospheric measurements. In: Sigrist, M.W. (ed.), *Air Monitoring by Spectroscopy Techniques*. J. Wiley & Sons, 239-333.

**Selvaggi, G., and D'Ajello Caracciolo, F., 1998.** Seismic deformation at the Alban Hills volcano during the 1989-1990 seismic sequence. *Annali di Geofisica*, **41(2)**, 225-231.

**Siracusa, F., and Quattrocchi, F., 2007.** Misure di flusso di Geo-gas (CO<sub>2</sub>, etc..) con il "Sistema SAP" con polle gassose a flusso macroscopico: i casi della Val Comino e Palidoro. INGV Technical Report, N. 45, 24 pp.

**Smith, K.L., Steven, M.D., Jones, D.G., West, J.M., Coombs, P., Green, K. A., Barlow, T. S., Breward, N., Gwosdz, S., Kruger, M., Beaubien, S. E., Annunziatellis, A., Graziani, S., Lombardi, S., 2013.** Environmental impacts of CO<sub>2</sub> leakage: recent results from the ASGARD facility, UK. *Energy Procedia* **37**, 791-799.

**Stakman, W.P, 1969.** Determination of pore size by the air bubbling pressure method. Institute for land and Water management research Wageningen, Netherlands.

**Takle, E.S., Brandle, J.R., Schmidt, R.A., Garcia, R., Litvina, I V., Massman, W.J., Zhou, X., Doyle, G., Rice, C.W., 2003.** High-frequency pressure variations in the vicinity of a surface CO<sub>2</sub> flux chamber. *Agricultural and Forest Meteorology* **114**, 245-250.

**Tittel, F.K., Weidmann, D., Oppenheimer, C., Gianfrani, L., 2006.** Laser absorption spectroscopy for volcano monitoring. *Opt. Photom. News, Opt. Soc. Am.* 24-31.

**Tolomei, C., Attori, S., Salvi, S., Allievi, J., Ferretti, A., Prati, C., Rocca, F., Stramondo, S., Feillet, N., 2003.** Crustal deformation of the Alban Hills volcanic complex (central Italy) by permanent scatterers analysis. In: Proc. FRINGE 2003 Workshop, Frascati, Italy, 1-5 December 2003 (ESA SP-550, June 2004).

**Van Bavel, C.H.M., 1951.** A soil aeration theory based on diffusion. *Soil Science* **72**, 33-46.

**Van Cleve, K., Oechel, W.C., Hom, J.L., 1990.** Response of black spruce (*Picea mariana*) ecosystems to soil temperature modification in interior Alaska. *Can. J. For. Res.*, 20, 1530-1535.

**Van Genuchten, M. Th., 1980.** A closed-form equation for predicting the hydraulic conductivity of unsaturated soils. *Soil Science Society of America* **44** (5), 892-898.

**Vaselli, O., Nisi, B., Giannini, L., Delgado Huertas, A., 2011.** Water and gas geochemistry from the CO<sub>2</sub>-rich field of Campo de Calatrava (Castilla-La Mancha). Internal report Fundación Ciudad de la Energía, , p. 39.

**Vaselli, O., Cuccoli, F., Giannini, L., Nisi, B., Sermi, F., Tassi, F., Capecchiacci, F., Capannesi, L., Nocentini, M. 2012.** Open-Path IR Laser Measurements, thermal imaging and fluid geochemistry in the Campo de Calatrava Volcanic Field. CNR-ING Report.

**Vaselli, O., Nisi, B., Tassi, F., Giannini, L., Grandia, F., Darrah, T., Capecchiacci, F., Pérez del Villar, L., 2013.** Water and gas geochemistry of the Calatrava Volcanic Province (CVP) hydrothermal system (Ciudad Real, Central Spain). *Geophysical Res. Abstract*, 10<sup>th</sup> EGU General Assembly, EGU2013-11102.

**Voltaggio, M., and Barbieri, M., 1995.** Geochronology. In: Triglia, R., (Ed.), *The Volcano of the Alban Hills*, Rome, 167-192.

**Voltattorni, N., Sciarra, A., Caramanna, G., Cinti, D., Pizzino, L., Quattrocchi, F., 2009.** Gas geochemistry of natural analogues for the studies of geological CO<sub>2</sub> sequestration. *Applied Geochemistry* **24**, 1339-1346.

**Voltattorni, N., Cinti, D., Galli, G., Lombardi, S., Pizzino, L., Sciarra, A., Quattrocchi, F., 2011.** Study of natural analogues for the comprehension of gas migration mechanisms. *Miscellanea INGV*, **12/2011**: 87-91.

**Waddington, E.D., Cunningham, J., Harder, S.L., 1996.** The effects of snow ventilation on chemical concentration, in *Chemical Exchange Between the Atmosphere and Polar Snow*, ed. by Wolff, E.W. and Bales, R.C. , Springer, New York, pp. 403–451.

**Weber, K., Bothe, K., Pistiridis, S., Laue, M., Fischer, C., Van Haren, G., Gonzales Ramos, Y., Barrancos, J., Hernandez, P., Perez, N.M., Pabel, K., Sosef, M., 2005.** Gas emission measurements from Teide volcano (Tenerife, Canary Islands, Spain) by means of optical remote sensing. In: *Proc. 99<sup>th</sup> Annual Conf. and Exhibition Air and Waste Management Association*, June 20-23, 2005, New Orleans, Louisiana, USA, A&WMA Pittsburgh, PA, 2006.

**Weeks, E.P., 1978.** Field determination of vertical permeability to air in the unsaturated zone. U.S.G.S. Professional Paper 1051, available from the Superintendent of Documents, U.S. Government Printing Office, Washington D.C., 20402 USA. Stock Number 024-001-03092-6.

**Wyatt, D.E., Richers, D.M., Pirkle, R.J., 1995.** Barometric pumping effects on soil gas studies for geological and environmental characterization. *Environmental Geology* **25**, 243-250.

**Xiao, Y., Xu, T., Pruess, K., 2009.** The effects of gas-fluid-rock interactions on CO<sub>2</sub> injection and storage: Insights from reactive transport modelling. *Energy Procedia* **1(1)**, 1783-1790.

**Xu, M., and Qi, Y., 2001.** Soil-surface CO<sub>2</sub> efflux and its spatial and temporal variations in a young ponderosa pine plantation in northern California. *Global Change Biology* **7(6)**, 667-677.

**Xu, T., Sonnenthal, E., Spycher, N., Pruess, K., 2004.** TOUGHREACT- A simulation program for non-isothermal multiphase reactive geochemical transport in variably saturated geology media: Applications to geothermal injectivity and CO<sub>2</sub> geological sequestration. *Computer and Geosciences* **32(2)**, 145-165.

**Xu, T., Apps, J.A., Pruess, K., 2005.** Mineral sequestration of carbon dioxide in a sandstone-shale system. *Chemical Geology* **217**, 295-318.

**Yang, Y.M., Small, M. J., Ogretim, E.O., Gray, D D., Bromhal, G.S., Strazisar, B.R., Wells, A.W., 2011.** Probabilistic design of a near-surface CO<sub>2</sub> leak detection system. *Environmental Science and Technology* **45(15)**, 6380-6387.

**Zhang, Y., Oldenburg, C.M., Benson, S.M., 2004.** Vadose zone remediation of CO<sub>2</sub> leakage from geologic CO<sub>2</sub> storage sites. *Vadose Zone Journal* **3**, 858-866.

## **Appendix 1**

## Definition of the 1-D mesh and discretization

The first step of a modelling task is the definition of the geometry of the experimental domain where fluid flow occurs. In the case of the vadose zone modelling in this work, the main output of interest is the spatial distribution of the gas flux at surface (way out of gas in the soil/atmosphere interface), gas pressures and saturation level in the unsaturated zone.

In this first step of the study, numerical simulations in 1-D vertical geometry have been performed to select the better intrinsic input parameters of each material and optimize the mesh discretization and the time of calculation. This study keeps on the work developed by Creodz et al., (2011a, b), in which TOUGHREACT code (Xu et al., 2004) was described and selected to perform numerical simulations of 4 different injecting scenarios in the PISCO2 cell.

In this study, it has come along with a mesh discretization keeping in mind cell characteristics like vertical dimensions of the experimental cell, 5 materials, and 2 injection points.

In the present conceptual model, PISCO2 cell consists of the following layers:

- Atmosphere;
- Coarse sand;
- Injection points;
- Gravel;
- Concrete.

The **atmosphere layer** represents the upper boundary of the model and extends down to the coarse sand layer. The first top element of this layer has a circa infinite volume (with an order of  $10^{52}$ ), that enables the infinite vertical gas flow injection and release out of the cell gas. No atmospheric or dispersive processes have been considered in the compartment at this stage of the study.

At the beginning, the soil layer will not be laid down in order to set the cell's instrumentations and for the numerical modeling calibration tests.

Physical, chemical and biological processes affect surface soils before, during and after the CO<sub>2</sub> injection, which could involve a further aliquot of CO<sub>2</sub> leaking from soils. They have a particular sensitivity to variations of capillary pressure, temperature, air pressure, grain size underground water flow, suction effects, tortuosity water infiltration and pore spaces. However, at this stage no soil layer has been considered in the numerical simulations due to the lack of reliable soil property data.

The **coarse sand layer** represents the main bulk of the cell filling where processes in unsaturated zone take place. Because of from the early stage of the project this level was always called “Sand level” even if is made up of very fine gravel, in order not to have misunderstanding between different participants of the PISCO2 project it was kept the definition of sand level.

The **gravel layer** is needed to preserve liquid flow drainage in order to maintain an unsaturated zone in the upper layers. The gravel was selected with a 10-mm average grain size and size variability of material satisfies the dry analysis for sieved UNE.

The **concrete layer** is the low permeable layer of the cell and represents a boundary. During CO<sub>2</sub> injection in PISCO2 its integrity is monitored to alert any kind of leakage, in liquid or gas phase in the original soil.

The atmosphere zone, plus the soil layer horizon, is 0.8 meters thick. For an ideal simulation, the first element of the column has a like-infinity volume value. This is because the cell is not closed volume. Also, concrete and atmosphere have been set with the same capillary function value, because in preliminary simulations was observed a capillary process with a water infiltration in the concrete layer. Mesh discretization has focused on the 80 centimeters before interface with coarse sand.

The coarse sand layer has a thickness of 1.7 meters and includes the injection point at 2.45 meters depth. This is the layer that requires more attention in discretization due the presence of two interfaces (atmosphere/ coarse sand and coarse sand/gravel), and two injection points (only one active in 1-D simulations). As said before, minding to 2-D and 3-D successive simulations the injecting point sizing was repeated at -1.3 meters depth.

The gravel layer, 0.30 meters in thickness, has a finer discretization in the first 10 centimeters. Concrete layer is 0.20 meters thick, and it does not have a particular discretization.

The picture below (Fig. 49) describes the 1-D and 2-D conceptual model.

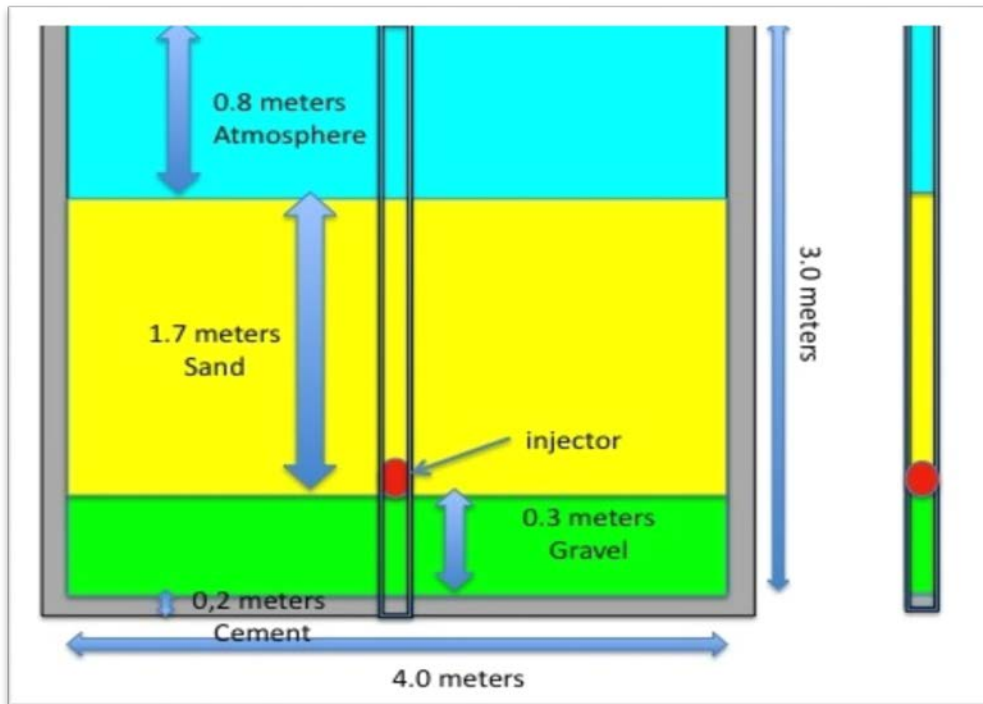


**Figure 49.** PISCO2 1-D (on the right side) and 2-D (on the left side) conceptual models.

A number of discretization tests were carried out to define the right dimension for each element regarding its position inside a layer or in the interface with two materials. Three different meshes were developed considering the above-mentioned characteristics. An interface is a crossing line between two different objects with different properties (physical and/or chemical and/or biological). Depending on the properties of such objects, a transition from an element to another can be more or less fluent by the simulation code.

In the model, there are three interfaces where discretization shows refined elements (smaller in dimensions), except for the one between gravel and concrete. This is because the concrete layer is a limiting element without water flow due to its low porosity and permeability, and where can only occur chemical reactions on the interface. Consequently, no particular discretization is needed.

In the first calculations, mesh discretization was focused on reduced number of elements. This was the starting point thinking to further modeling in 2-D and 3-D, so that not to build a model too full of elements that could generate numerical problems due to tiny elements. In this study, the elements are from 1 mm to 5 cm thick and 1 m wide.

The first generated mesh (Table 16) was made up of 169 elements and a particular attention was paid to sand and gravel layers. The second mesh had 218 elements (Table 17), since the

atmosphere/sand interface was better refined. The last mesh (Table 18) has 260 elements, with a better discretization in the atmosphere (air-soil interface) and sand layers. The sand layer has almost doubled the number of elements especially in the first centimeters after air-soil interface. The elements number of the gravel layer were halved because in this thin layer (30 cm) was not considered a need for finer discretization and the same was done with concrete elements reducing the number as in the first mesh.

**Table 16.** Mesh A: atmosphere in blue, sand in yellow, gravel in green and concrete in grey.

Cell number	Size (m)	Sub-total (m)
5	0,001	0,005
5	0,002	0,01
7	0,005	0,035
5	0,01	0,05
20	0,02	0,4
15	0,02	0,3
12	0,05	0,6
2	0,02	0,04
2	0,01	0,02
5	0,005	0,025
5	0,002	0,01
10	0,001	0,01
5	0,002	0,01
5	0,005	0,025
2	0,01	0,02
2	0,02	0,04
16	0,05	0,8
2	0,02	0,04
2	0,01	0,02
5	0,005	0,025
5	0,002	0,01
10	0,001	0,01
5	0,002	0,01
5	0,005	0,025
2	0,01	0,02
2	0,02	0,04
2	0,05	0,1
2	0,05	0,1
4	0,05	0,2
169		3



**Table 17.** Mesh B: atmosphere in blue, sand in yellow, gravel in green and concrete in grey.

Cell number	Size (m)	Sub-total (m)
5	0,001	0,005
5	0,002	0,01
7	0,005	0,035
5	0,01	0,05
20	0,02	0,4
15	0,02	0,3
12	0,05	0,6
2	0,02	0,04
2	0,01	0,02
5	0,005	0,025
5	0,002	0,01
10	0,001	0,01
5	0,002	0,01
5	0,005	0,025
2	0,01	0,02
2	0,02	0,04
16	0,05	0,8
2	0,02	0,04
2	0,01	0,02
5	0,005	0,025
5	0,002	0,01
10	0,001	0,01
5	0,002	0,01
5	0,005	0,025
5	0,01	0,05
2	0,02	0,04
3	0,01	0,03
5	0,005	0,025
5	0,002	0,01
5	0,001	0,005
5	0,001	0,005
5	0,002	0,01
5	0,005	0,025
6	0,005	0,03
7	0,01	0,07
8	0,02	0,16
218		3

**Table 18.** Mesh C: atmosphere in blue, sand in yellow, gravel in green and concrete in grey.

Cell number	Size (m)	Sub-total (m)
5	0,001	0,005
5	0,002	0,01
7	0,005	0,035
6	0,01	0,06
30	0,02	0,6
6	0,01	0,06
2	0,005	0,01
5	0,002	0,01
10	0,001	0,01
10	0,001	0,01
10	0,002	0,02
10	0,0035	0,035
13	0,01	0,13
6	0,03	0,18
4	0,01	0,04
6	0,005	0,03
5	0,002	0,01
15	0,001	0,015
5	0,002	0,01
6	0,005	0,03
4	0,01	0,04
8	0,02	0,16
16	0,05	0,8
6	0,02	0,12
2	0,01	0,02
6	0,005	0,03
5	0,002	0,01
10	0,001	0,01
15	0,001	0,015
10	0,0025	0,025
2	0,01	0,02
2	0,02	0,04
2	0,05	0,1
2	0,05	0,1
4	0,05	0,2
260		3

After some trials with different element spacing, a mesh constituted of 76 elements for the atmosphere, of 147 elements for the sand layer, of 33 elements for the gravel layer and 4 elements for the concrete layer has been obtained. Injection points are made up of six elements, 0.005 meters in length. During 1-D simulations, the deepest injector (-2,5 meters) was used as a source of CO<sub>2</sub>.

## ***Sensitivity studies***

### ***Objective***

A sensitivity study was performed to see how soil properties can affect the predicted CO<sub>2</sub> flow in the PISCO2 cell. The selected properties for this study were porosity, permeability, lambda ( $\lambda$ ), P<sub>0</sub> and gas saturation (S<sub>g</sub>). For each test a *rule* of conduct with  $a < b < c < d$  was followed, that means that each test range was carried out from lower to higher values.

Porosity and permeability are connected to water and gas saturation and to the ability of a porous media to allow fluids and gas to pass through it.

Lambda, P<sub>0</sub> and gas saturation are relative to Van Genuchten functions (Van Genuchten, 1980).

The Van Genuchten equation for predicting the hydraulic conductivity of unsaturated soil is a simple equation for the soil-water content-pressure head curve,  $\theta$  (h). The Van Genuchten parameters are used to describe soil hydraulic behavior resulting from the non-linear interactions of soil water pressure ( $\Psi$ ), saturation level ( $\theta$ ) and hydraulic conductivity (k):

$$\theta = \frac{(\theta_s - \theta_r)}{(1 + |\alpha|\psi|^n)^m} + \theta_r \quad (\psi \leq 0) \quad (\text{eq. 8})$$

$$K(\psi) = K_s \frac{|1 - (\alpha|\psi|^n)^m (1 + (\alpha|\psi|^n)^{-m})|^2}{(1 + (\alpha|\psi|^n)^m)^{ml}} \quad (\psi \leq 0) \quad (\text{eq. 9})$$

where  $\theta$ ,  $\theta_s$  and  $\theta_r$  represent the actual, saturated and residual water content (m<sup>3</sup>·m<sup>-3</sup>) respectively,  $\alpha$  is the soil retention function (m<sup>-1</sup>),  $l$  is the pore connectivity and tortuosity factor,  $\psi$  is the pressure head (m),  $K_s$  is the saturated soil conductivity (m·s<sup>-1</sup>), and  $m$  and  $n$  are water retention curve parameters (Jacques et al., 2002).

In TOUGH2 codes the parameter  $m$  is called  $\lambda$ , with  $m=(1-1/n)$ , the parameter  $n$  is often written  $\beta$  (Pruess et al., 1999).

### ***Literature search and data selection***

A literature review about soil and rock intrinsic properties both for reservoir and for caprock has been performed. Such a search has resulted in a list of articles with data that can be used in the

models. These papers are those of Sanders et al., (1998), Davis and De Wiest (1966), Boonstra and De Ridder (1981), Freeze and Cherry (1979), Compton (1985), Gherardi et al., (2007), Kano and Ishido, (2011), André et al., (2007), Audigane et al., (2007), Gaus et al., (2008), Xu et al., (2005), and Oldenburg and Unger (2004). Some of these studies are related to CO<sub>2</sub> geological storage in rock and shale reservoirs. The analysis of such papers provided soil and rock average properties of porosity, permeability, capillary and permeability functions parameters. Other papers dealt with soil classification, which can be useful for the simulation of tortuosity, saturation and grain size.

### *Sensitivity study for porosity*

Porosity is an empty bulk (or pores) volume relative to the full sample bulk. The knowledge of the porosity of a soil allows the estimation of how much fluid a reservoir can store and move, which is very relevant in hydrocarbon, water, CO<sub>2</sub> and heat storage or production.

The range of porosity found in literature for the materials used in the PISCO2 cell is presented in Table 19.

**Table 19.** Data of porosity for relevant materials in the PISCO2 project (from Sanders et al., 1998; Oldenburg and Unger, 2004).

Sanders et al., (1998)	Oldenburg and Unger (2004)
0.1 < $\phi$ < 0.28 fine sand	$\phi=0.2$ gravel
0.22 < $\phi$ < 0.35 thick sand	
0.13 < $\phi$ < 0.26 gravel	

Table 20 shows the selected values of porosity from the analyzed studies mentioned above.

**Table 20.** Porosity values selected for sensibility study.

Reference Test	Sand	Gravel
12a	0.1	0.13
12b	0.2	0.15
12c	0.3	0.2

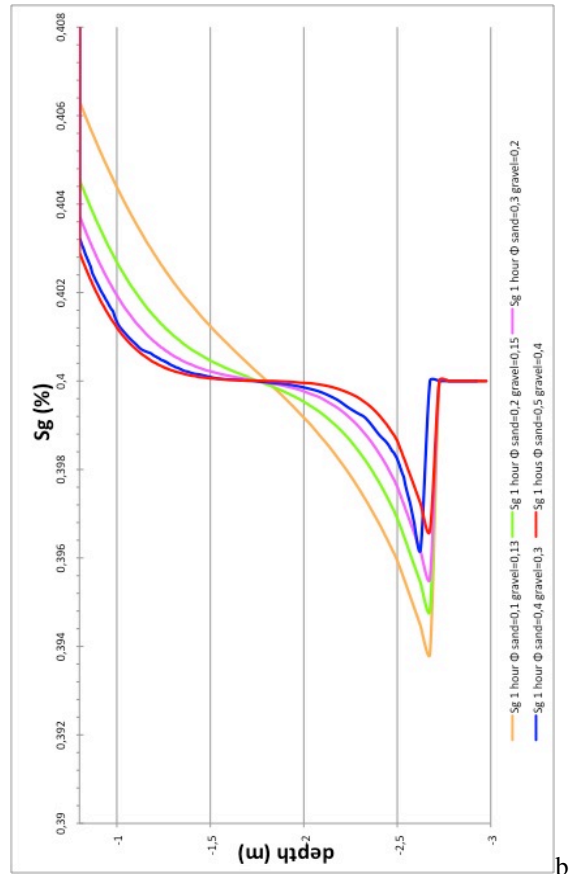
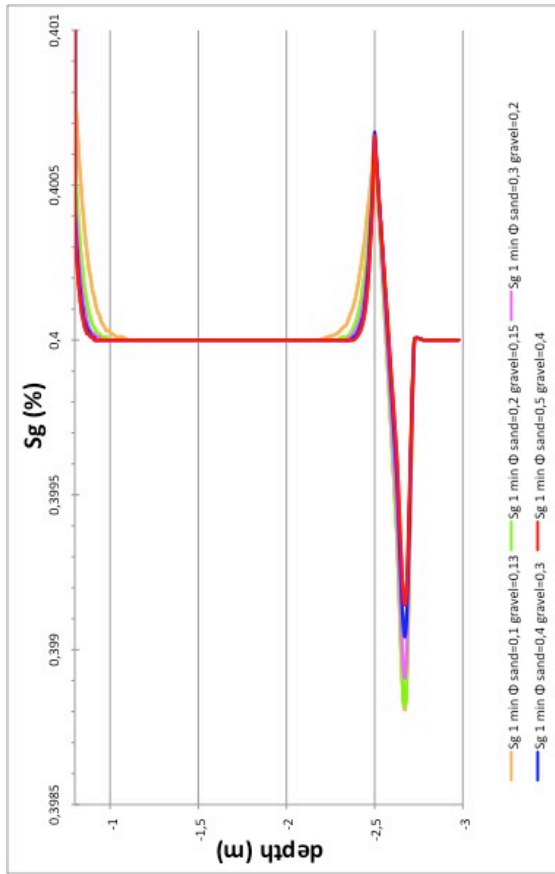
12d	0.4	0.3
12e	0.5	0.4

An inverse correlation is observed in results between porosity and gas flow during the early stage of the simulation, but in successive time-steps this ratio becomes positive. In the first minute of simulation, the inverse ratio is due to water falling/suction that with lower porosity decreases its effect. After 16 hours, gas flow is stationary.

Concerning gas saturation, two different trends are predicted before reaching a stationary stage. The main trend has a sigmoid curve with a gradual increase for lower porosity values and a bit straight (along vertical) for higher porosity. At time-step one minute, the sigmoid curve is not observed due to injection that produces a sensible effect on gas saturation. The sigmoid curve trend provides faster gas saturation for most porous media between 1.7 and 2.2 meters depth. Instead, above 1.7 meters until surface saturation is faster in lower porosity media.

In the following Gas Saturation charts (Fig. 50) the depth is cut at 0.8 meters because of in the atmosphere there are no variations from the starting value of gas saturation, so this focus permits a better view of the very low variations next to injector and sand/gravel interface. A transitory flow begins with a gradual increase of gas saturation in the upper part of the cell with loss in saturation  $S_g < 4$  ( $S_g = 4$  was the starting value) in the middle/lower part, from 1.8 to 2.7 meters depth. After 1 day from the onset of the injection an equilibrium state is reached in all cases, where the latter one to reach such equilibrium is the case with higher porosity.

Gas Flow charts (Fig. 51) confirm what said about saturation, it increases from lower porosity to higher porosity case with a transitory flow during the first day and then a stationary flow, even in the gravel layer.



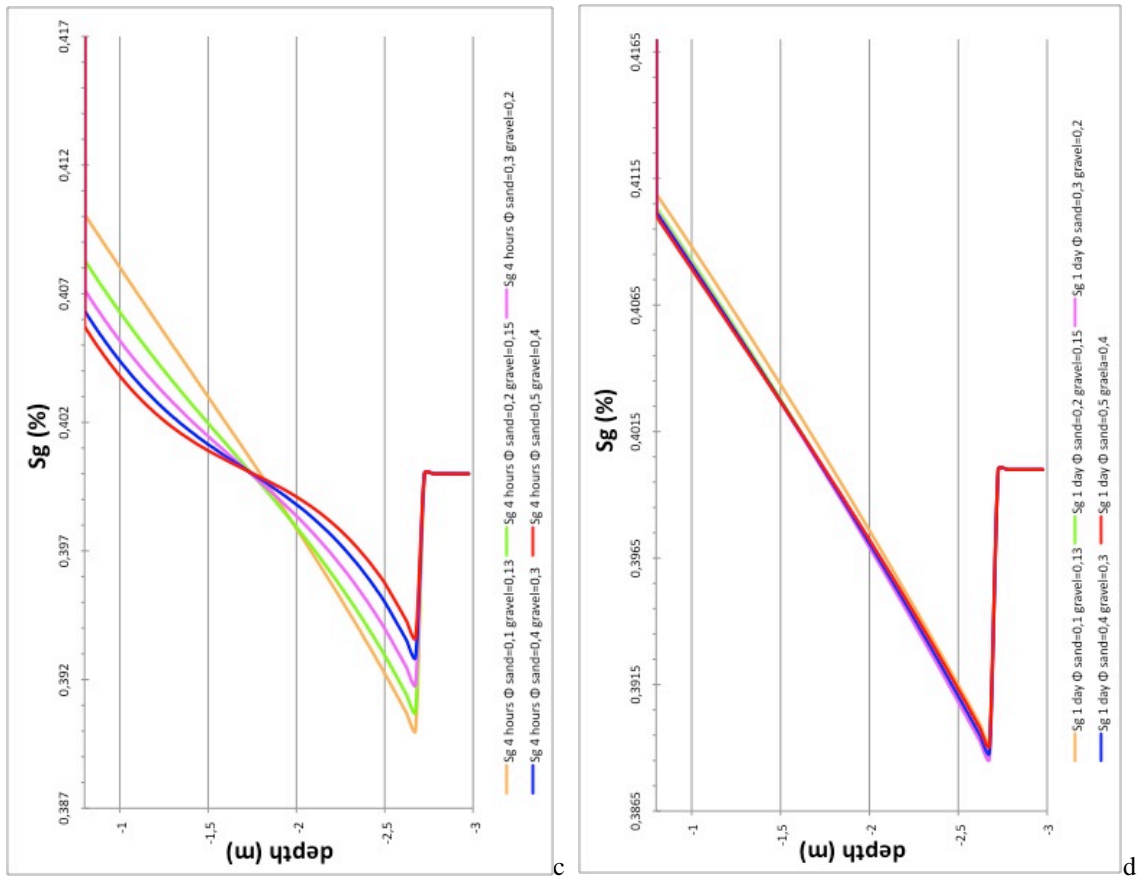
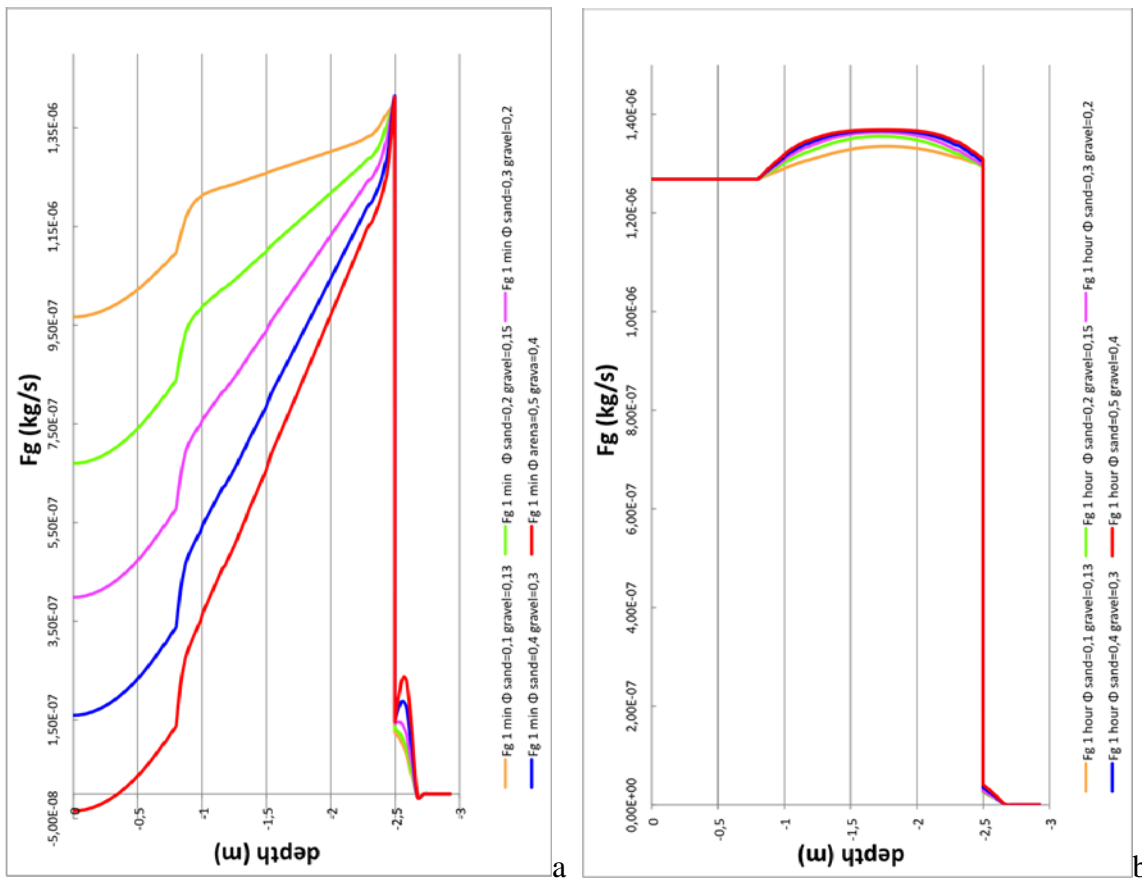


Figure 50. Gas saturation charts at 1 minute (a), 1 hour (b), 4 hours (c) and 1 day (d).



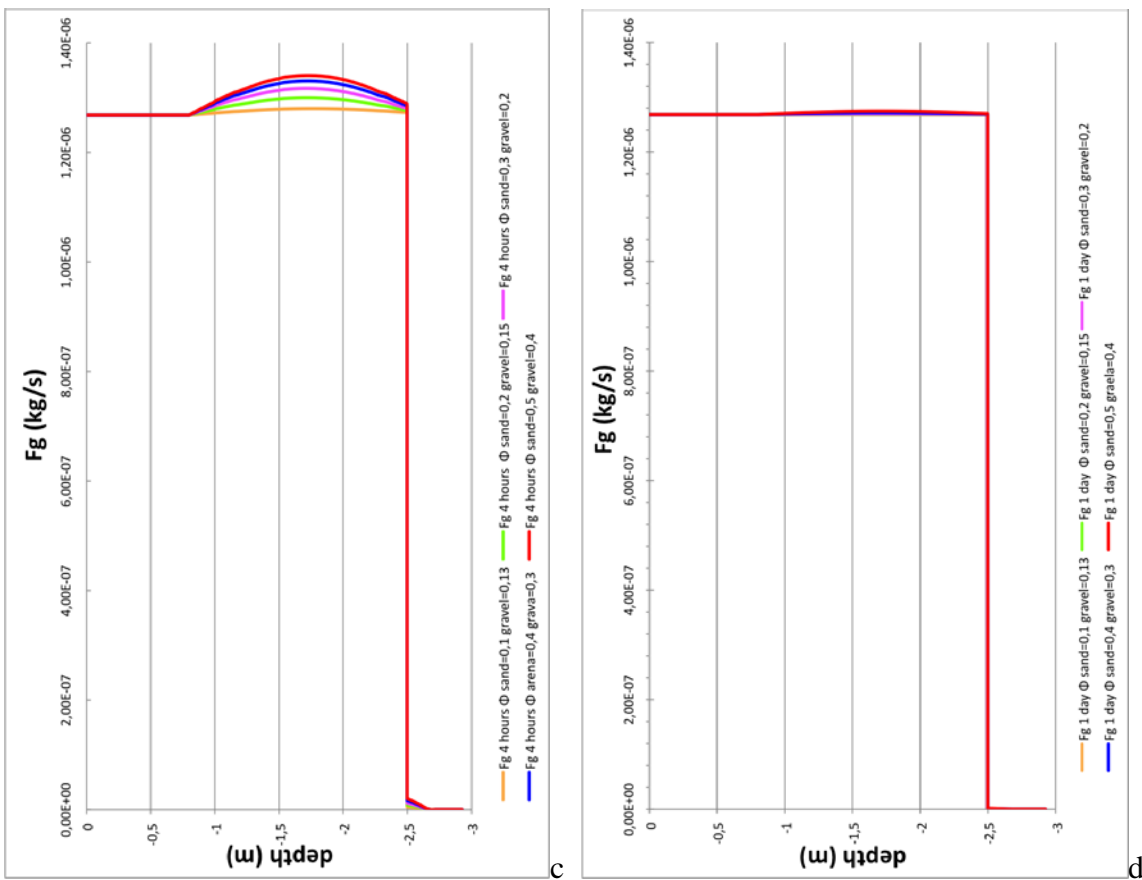


Figure 51. Gas flow charts at 1 minute (a), 1 hour (b), 4 hours (c) and 1 day (d).



### ***Sensitivity study for permeability***

Rock or soil permeability is the capacity of a medium to be passed through by a liquid.

In Table 21 a selection of the range of permeability values found from the literature is shown. Table 22 shows the selected value for the sensitivity case study.

**Table 21.** Range of permeability in literature.

<b><u>PERMEABILITY</u></b>	
Freeze and Cherry (1979)	Oldenburg and Unger (2004)
$10^{-9} < \kappa < 10^{-12}$ (m <sup>2</sup> ) sand	$\kappa = 10^{-12}$ (m <sup>2</sup> ) gravel
$10^{-7} < \kappa < 10^{-10}$ (m <sup>2</sup> ) gravel	

The numerical calculations showed some problems of convergence using permeability values over  $10^{-10}$  m<sup>2</sup> for sand and  $10^{-9}$  m<sup>2</sup> for gravel (tests 13a and 13b) and after 1 day of time simulation both tests stopped. Test 13c shows a linear growing saturation from bottom to top of the cell (Fig. 52). On the contrary, test 13d shows a different behavior in gas saturation between sand and gravel. It is worth mentioning that those tests differ on gas saturation only in the gravel layer.

**Table 22.** Permeability values for sensibility study.

<b>Test case</b>	<b>Sand (m<sup>2</sup>)</b>	<b>Gravel (m<sup>2</sup>)</b>
13a	$10^{-8}$	$10^{-7}$
13b	$10^{-9}$	$10^{-8}$
13c	$10^{-11}$	$10^{-10}$
13d	$10^{-12}$	$10^{-11}$

Gas flow plots (Fig. 53) show a similar trend for test 13 c and d, and they only differ at the early beginning of the injection in the gravel layer. Just after an hour of injection a stationary flow is reached.

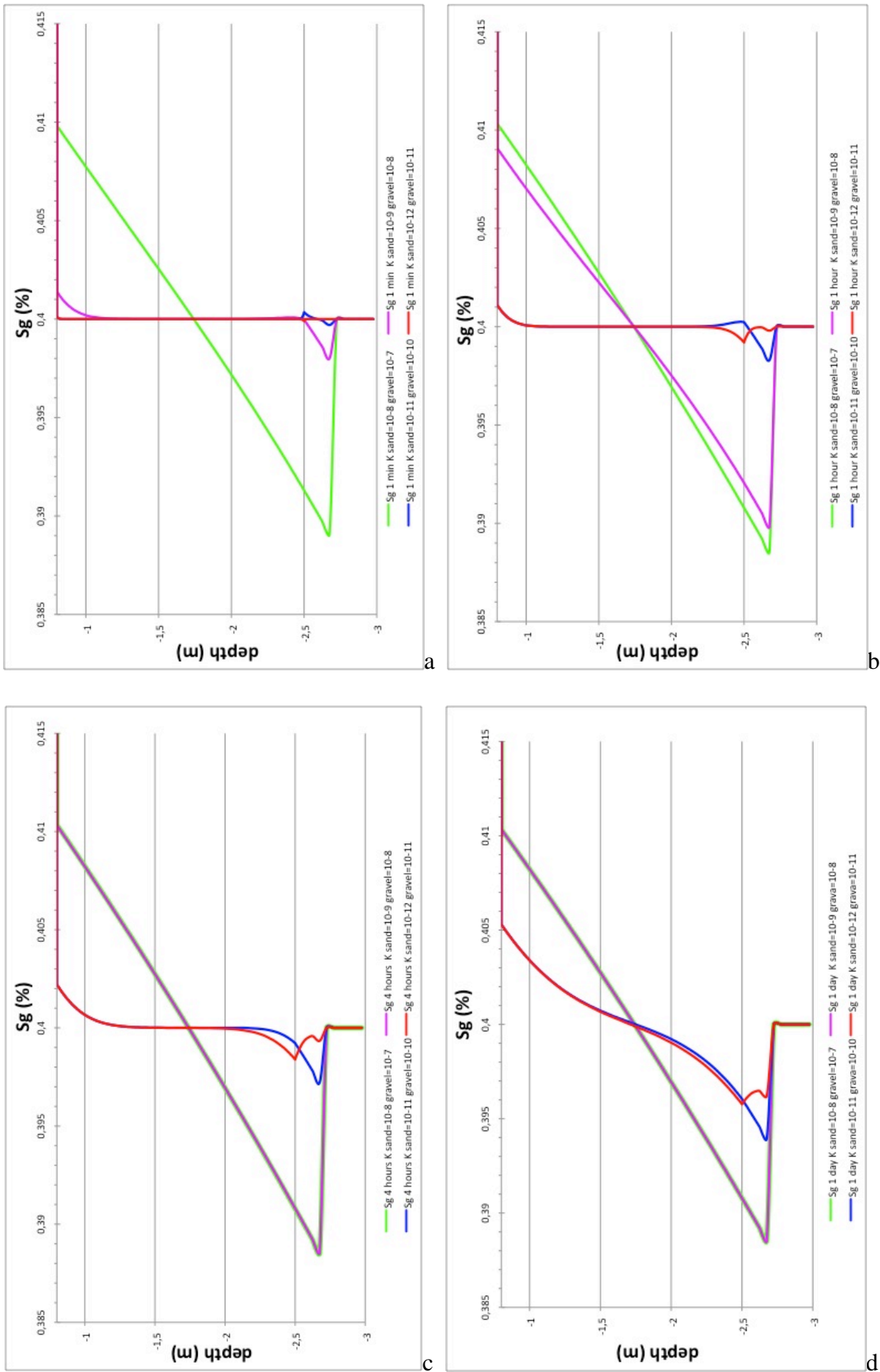


Figure 52. Gas saturation charts at 1 minute (a), 1 hour (b), 4 hours (c) and 1 day (d).

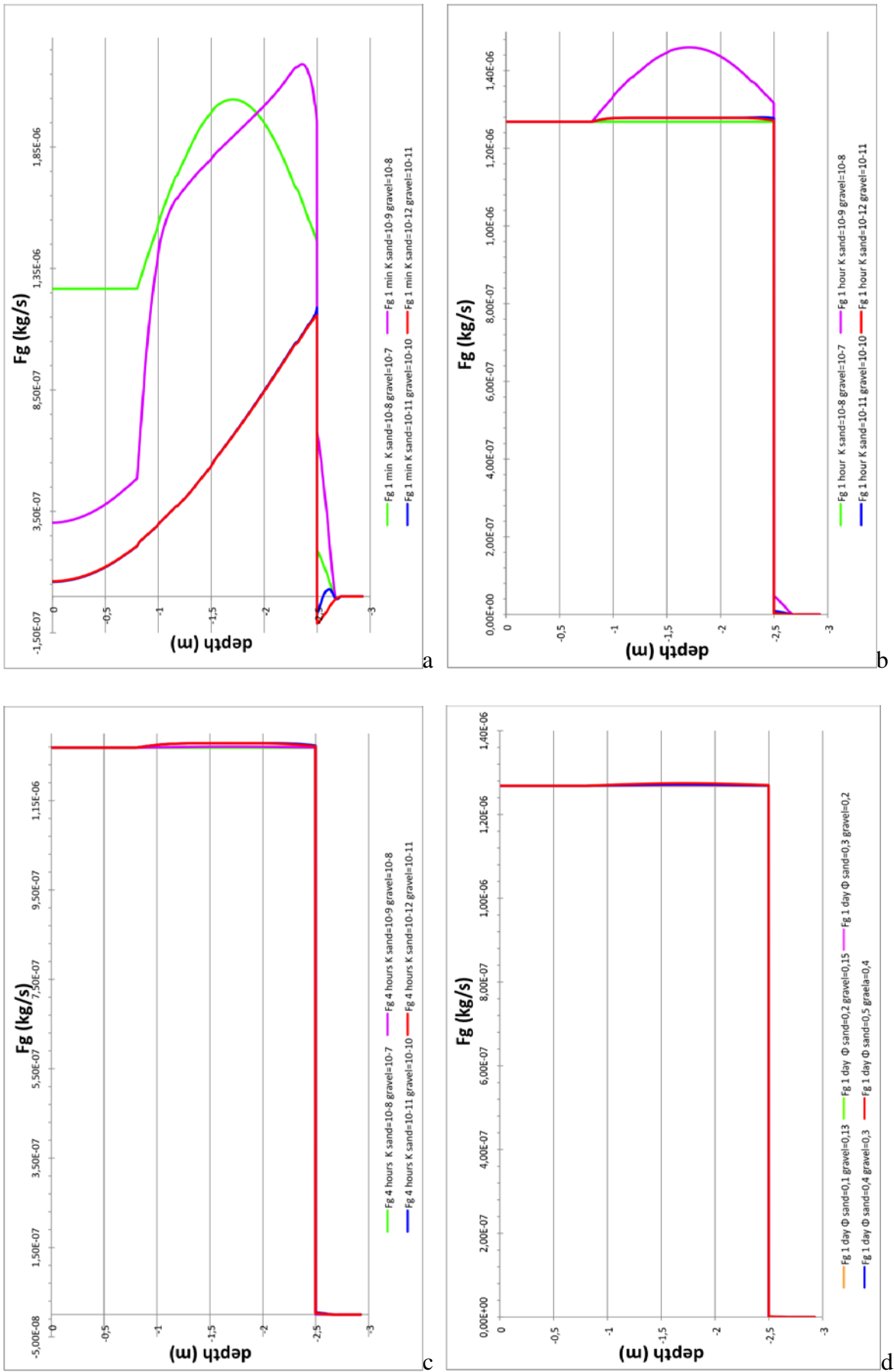


Figure 53. Gas flow plots at 1 minute (a), 1 hour (b), 4 hours (c) and 1 day (d).

### *Sensitivity study for lambda parameter*

The lambda ( $\lambda$ ) parameter refers to Van Genuchten equation properties regarding the hydraulic conductivity of unsaturated soils. It relates the gas and liquid saturation (respectively  $S_g$ ,  $S_{ls}$  and  $S_{lr}$ ), to gas and liquid flow (respectively  $F_g$ ,  $F_l$ ), to maximum system pressure ( $P_{max}$ ), and to bubbling pressure ( $P_0$ ). Hence, first was decided to check  $\lambda$  ranges for rock reservoir or soil reservoir from literature. Because of PISCO2 filling is like a soil reservoir,  $\lambda$  value must be under 0.3 (Table 23).

Four simulations have been performed using values from 0.15 to 0.30 (Table 24) with intervals of 0.05. As reference case for other Van Genuchten parameters were used the data from Oldenburg and Unger (2004).

**Table 23.** Van Genuchten parameters selected from literature.

Lambda ( $\lambda$ ) (Van Genuchten parameter)	
Gherardi et al., (2007)	0.457
André et al., (2007)	0.6
Audigane et al., (2007)	0.75
Gaus et al., (2008)	0.4
Xu et al., (2005)	0.457
Kano and Ishido, (2011)	0.4

**Table 24.** Lambda values for sensibility study.

Test	Sand	Gravel
15a	0.15	0.15
15b	0.2	0.2
15c	0.25	0.25
15d	0.3	0.3

The numerical results (Fig. 54 and 55) show that lower  $\lambda$  values have a straight trend with poor variations at interfaces (air/sand; sand/gravel; gravel/cement). Higher  $\lambda$  values show a sensitive

variation increasing from bottom to top. Gas flow starts with higher flow values, with higher  $\lambda$  and so keeps on until stationary stage at one hour after injection in the sand layer but not in the gravel layer.

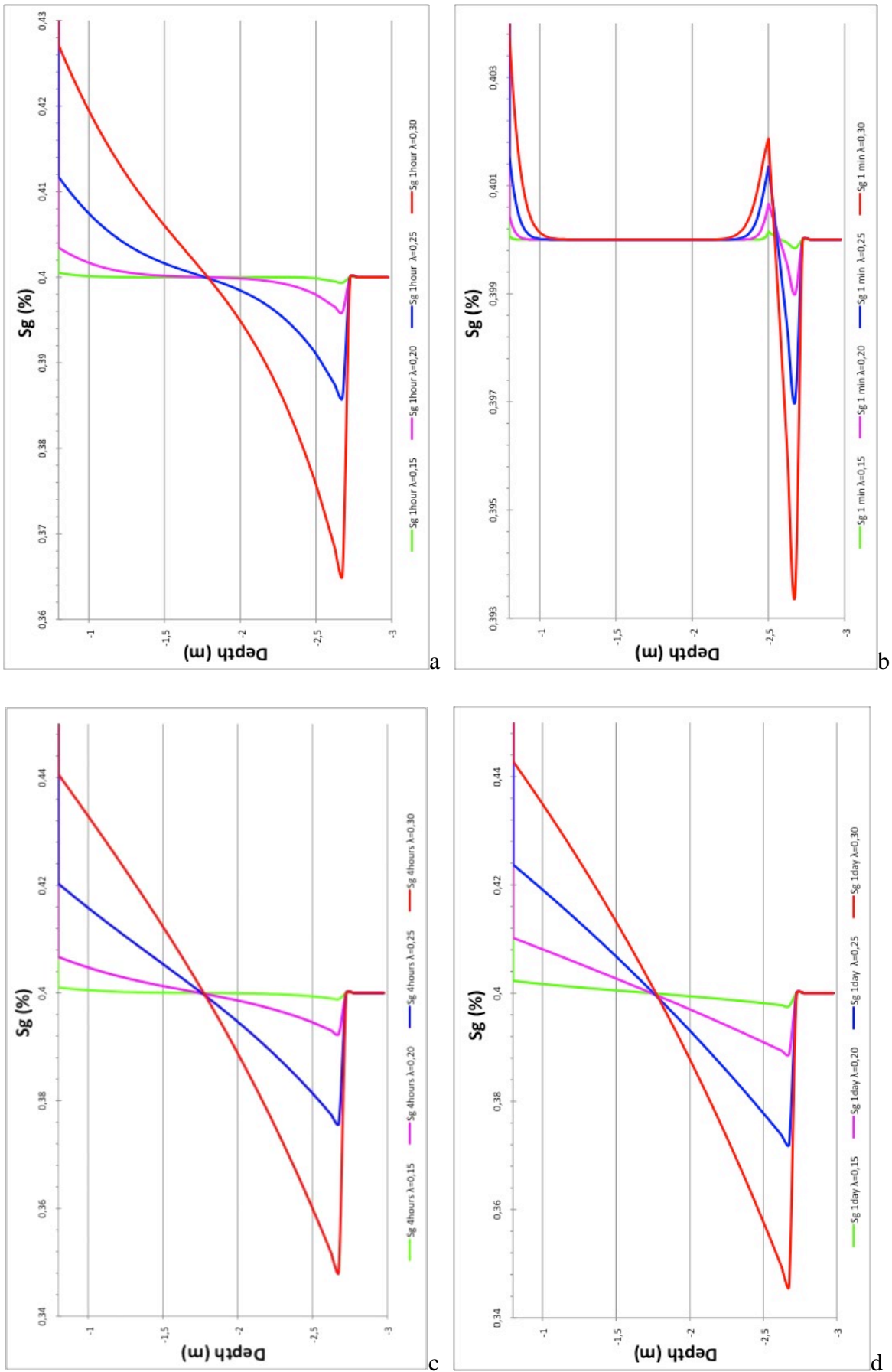


Figure 54. Gas saturation charts at 1 minute (a), 1 hour (b), 4 hours (c) and 1 day (d).

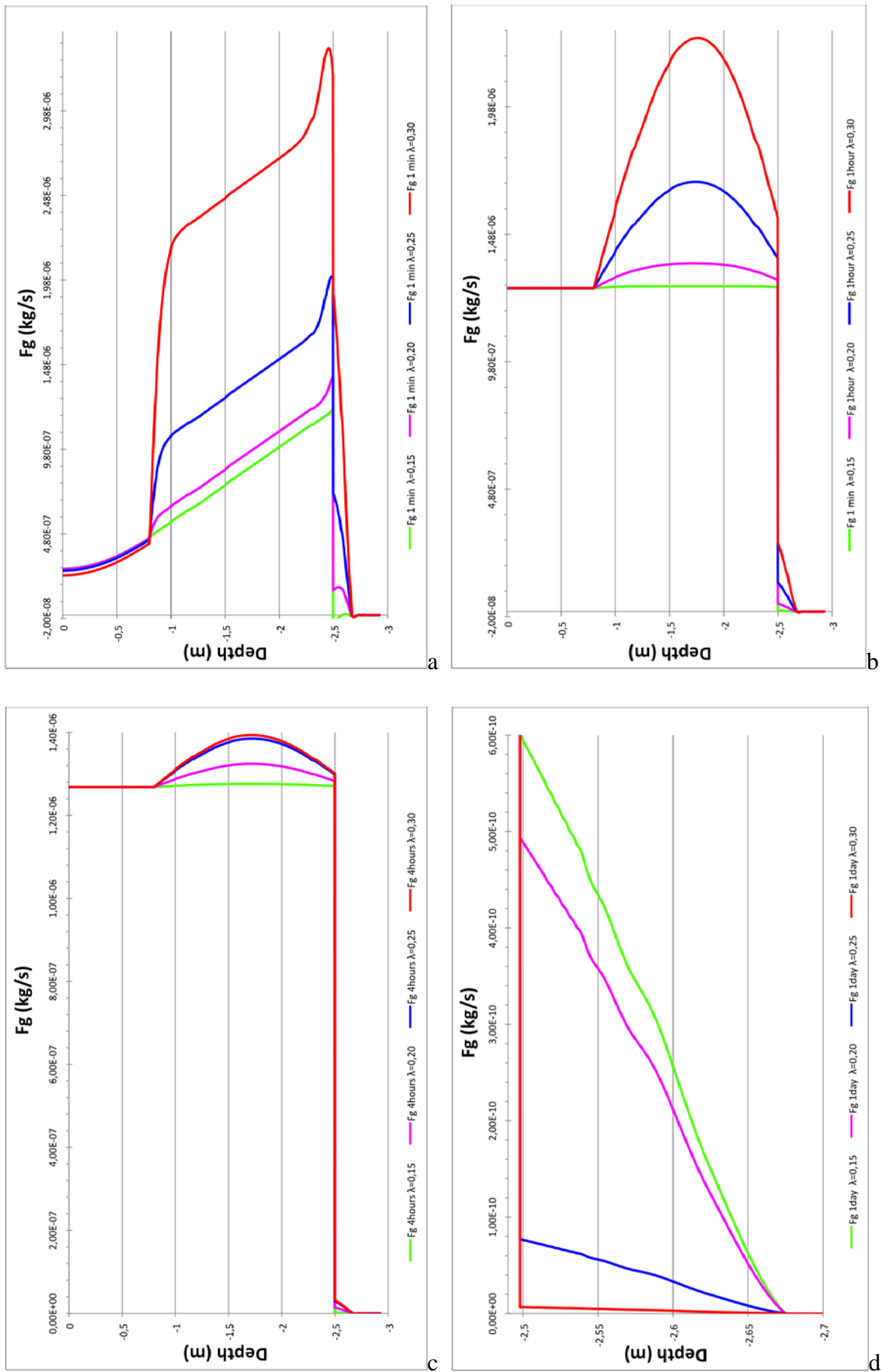


Figure 55. Gas flow charts at 1 minute (a), 1 hour (b), 4 hours (c) and 1 day (d).

***Sensitivity study for gas bubbling pressure (p<sub>0</sub>)***

P<sub>0</sub> is the pressure needed to generate a gas bubble in a saturated water environment (S<sub>w</sub>=1.0) (Stakman, 1969). Such parameter is used to define the capillary pressure in the Van Genuchten function (Van Genuchten, 1980), as showed in equation (eq. 10):

$$P_{cap} = -P_0 ([S]^{-1/\lambda} - 1)^{1-\lambda} \quad (\text{eq.10})$$

This sensibility case study was intended to look at the effects on the flow and saturation of liquid and gas at different pressures. In the following table (Table 25) test values are shown.

**Table 25.** P<sub>0</sub> values for sensibility test.

Test	P <sub>0</sub> (Pa)
16a	500
16b	1000
16c	10000
16d	50000

The results from calculations show that changes in gas saturation (Fig. 56) are observed in the gravel layer, being larger at lower pressure values.

Gas flow (Fig. 57) is higher after 1 minute of simulation close to injector and gradually decreases toward surface. In the gravel, gas flow shows minor changes compared to sand. A stationary stage is reached after 16 hours and higher values of P<sub>0</sub> lead to an earlier stationary stage than with lower values.



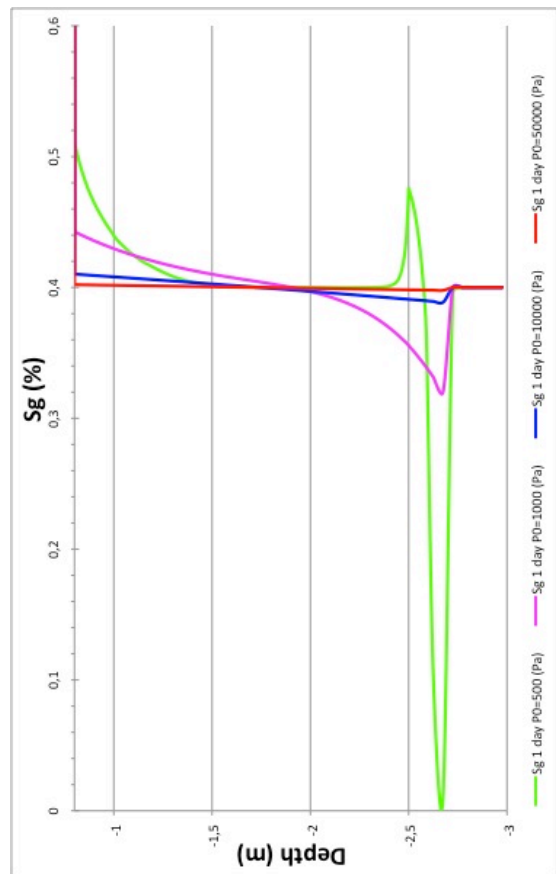
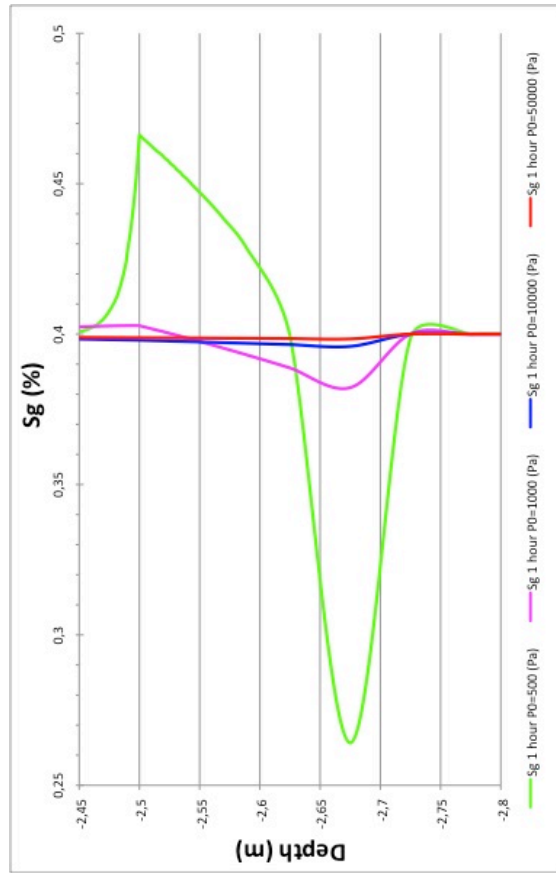
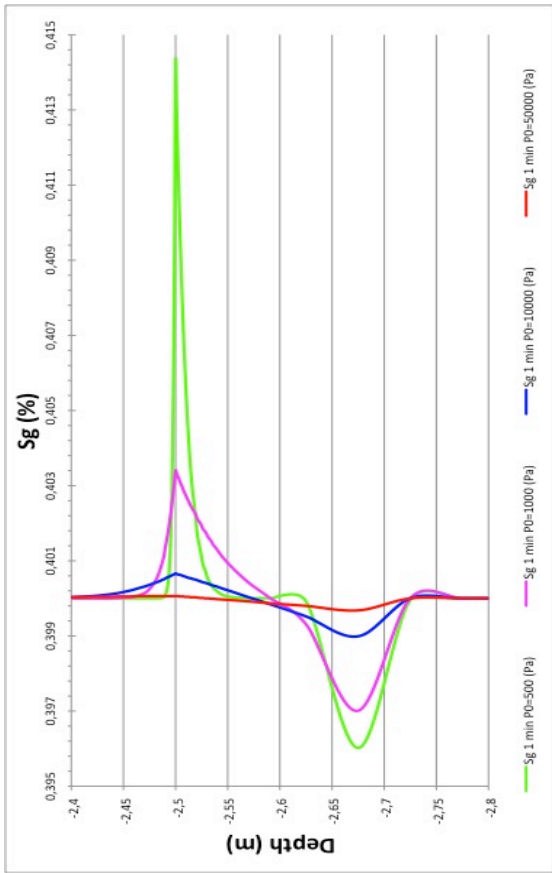


**Figure 56.** Gas saturation charts at 1 minute (a), 1 hour (b), 4 hours (c) and 1 day (d).

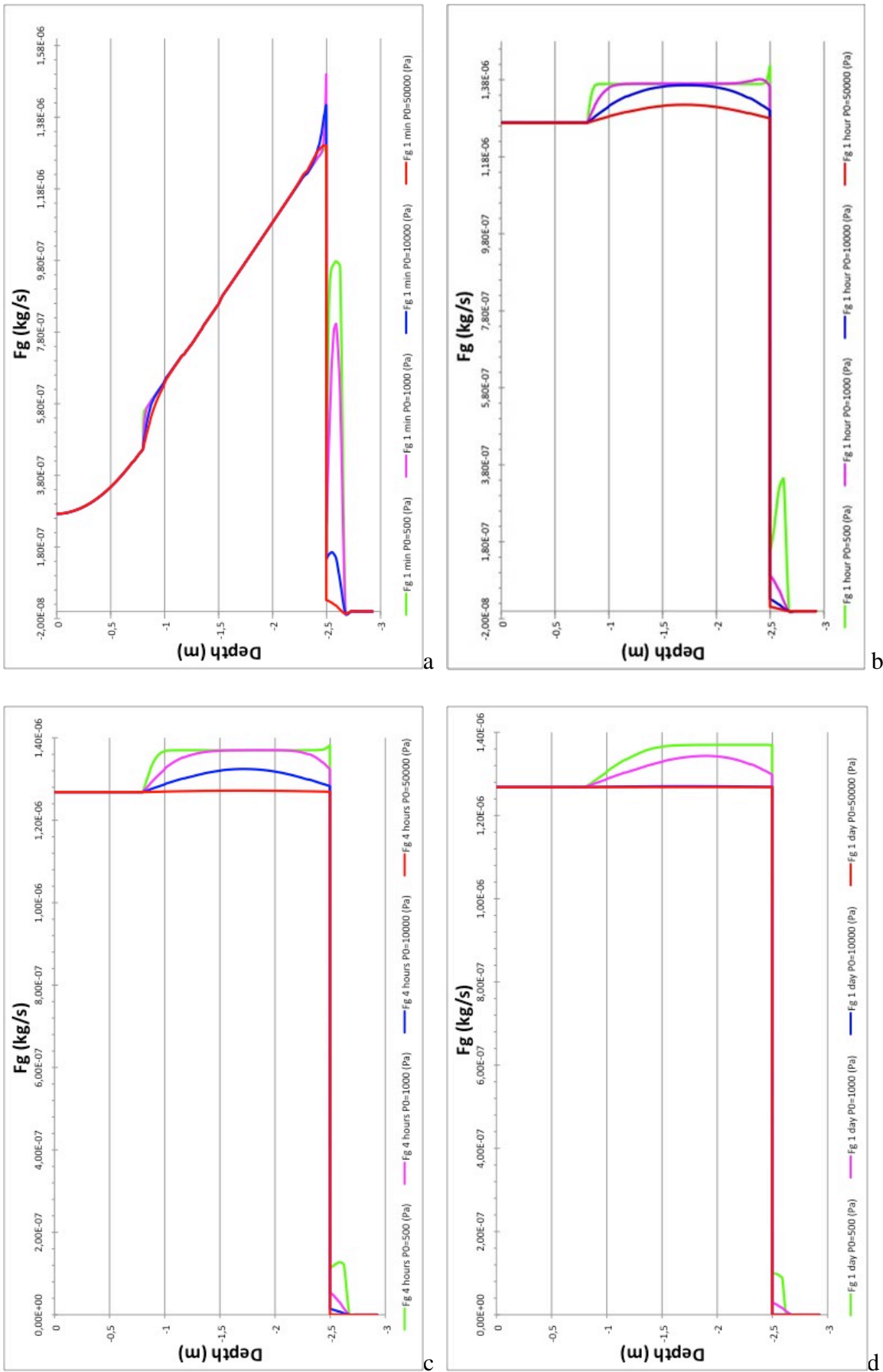


Figure 57. Gas flow charts at 1 minute (a), 1 hour (b), 4 hours (c) and 1 day (d).

### ***Sensitivity study for gas saturation (S<sub>g</sub>)***

This case study was intended to check the limitation of the numerical code in playing with very large or very small values for S<sub>g</sub>. That test was done in order to develop simulations in a real unsaturated zone. Some calculations were preliminarily performed by trying different values. Although real saturation can range from 0 to 1, the code works well using 0.0001 and 0.99999999 kg/s as lower and upper limits.

In the table below (Table 26) test values for S<sub>g</sub> are shown both for injection active or not. In tests 18c and 18d no injection is done in order to compare the results with tests 18a and 18b for a better understanding of the numerical code.

The two tests were developed with gas saturation of the media (Fig. 58) (both sand and gravel) of 0.99999999 kg/s, to keep full saturation for the entire tests. About gas flow (Fig. 59), test 18d has an initial negative flow that sets at zero during the first hour. Test 18b starts with a positive flow in the sand layer and negative in the gravel. During the first hour of simulated time, such flow becomes stationary with a bit larger value around injector element. About the two tests with very low gas saturation, the lowest possible accepted by the numerical code, test 18c does not change its starting setting, both for saturation and flow. On the other hand, test 18a gradually fills the cell with gas.

**Table 26.** Saturation values for sensibility test.

<b>Test</b>	<b>Gas saturation (kg·s<sup>-1</sup>)</b>	<b>Injection</b>
18a	0.0001	Yes
18b	0.99999999	Yes
18c	0.0001	No
18d	0.99999999	No

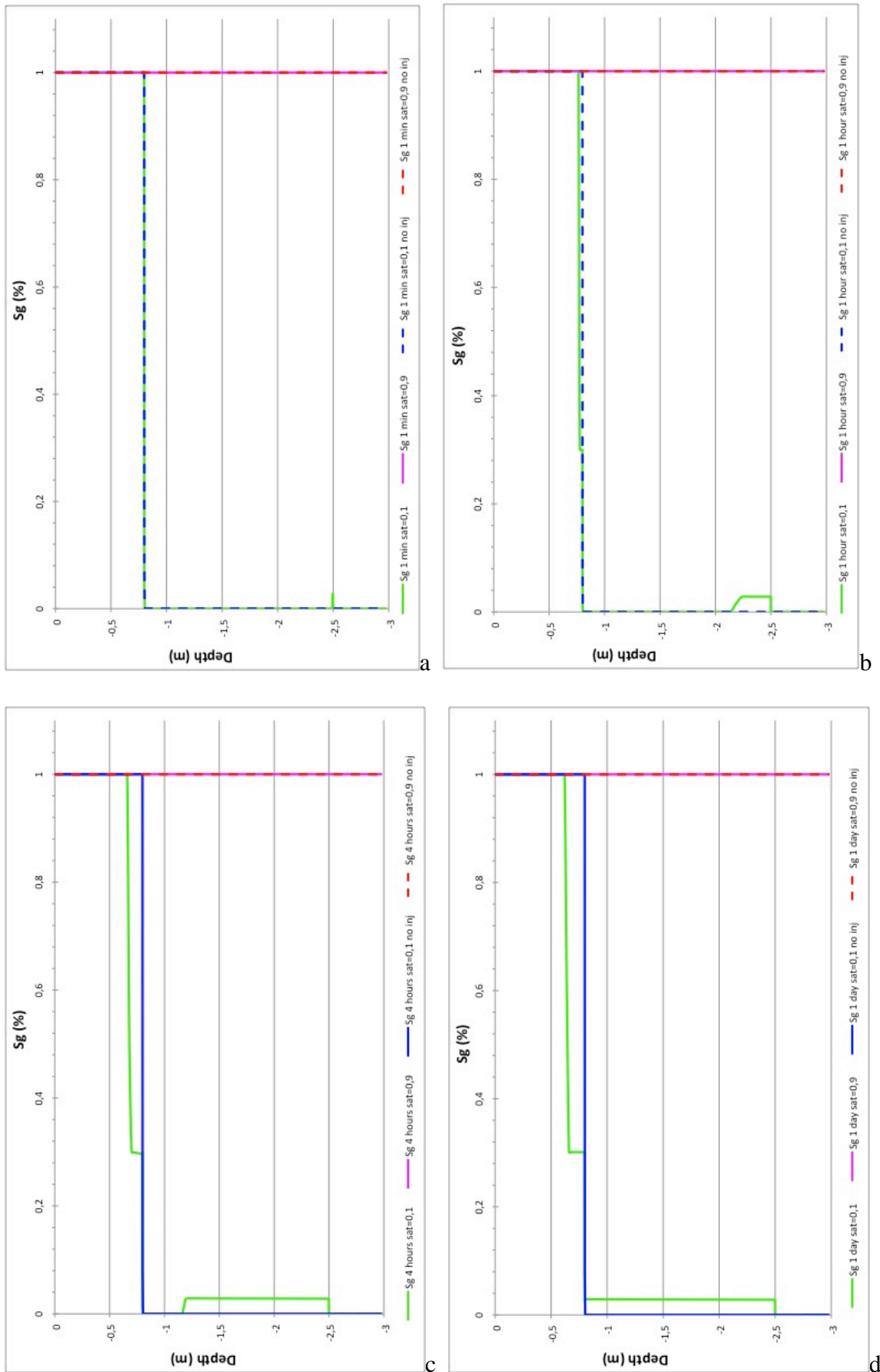


Figure 58. Gas saturation charts at 1 minute (a), 1 hour (b), 4 hours (c) and 1 day (d).

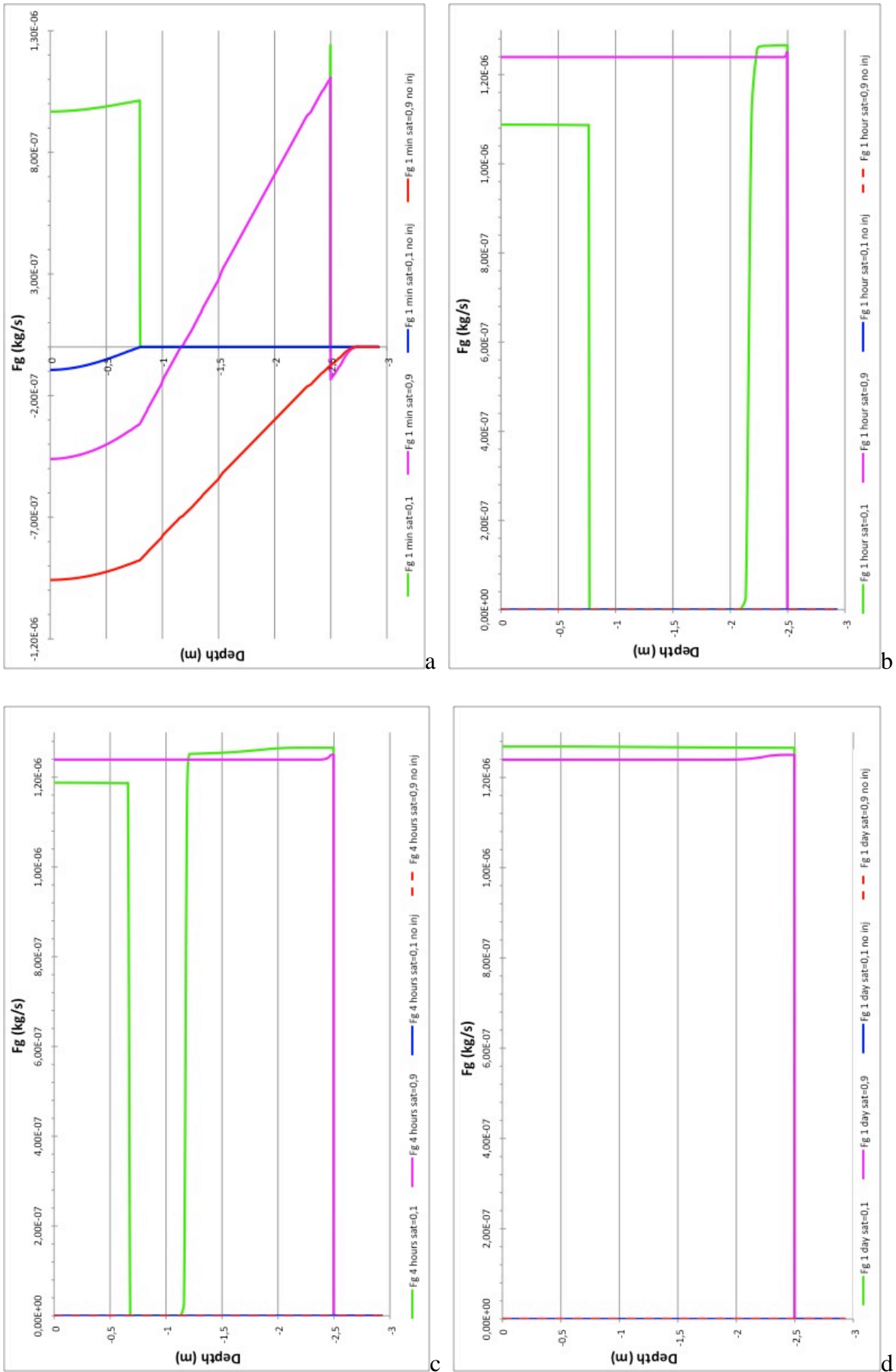


Figure 59. Gas flow charts at 1 minute (a), 1 hour (b), 4 hours (c) and 1 day (d).

### Test 18a

Gas flow during injection starts to fill the bottom of the cell and a positive flux from the gravel to the atmosphere is predicted in the initial times. This means that injected gas goes down until cement and then come back in the upper layers. After 4 hours of simulated injection, two thirds of the cell are filled by gas and after 1 day the flux has a stationary state.

Gas saturation starts from 0.0001 kg/s and at one minute after injection a saturation increase around the injecting element is predicted. Gas saturation increases in time as gas flows.

### Test 18b

This injection case considers full gas saturation, and a stationary flow state is numerically reached after an hour of injection. In the first minute of simulation, there is an outflow of gas observable from sand but not negative in the gravel, no flow in the concrete layer. After four hours of injection, a stationary gas flow is already set. Maybe because of the starting gas saturation value and the injection rate (that is very low) a value bigger than the injection rate is observed only next to the injection element. About gas saturation, it keeps on being fully saturated even with the described outflow.

### Test 18c

In this case, water saturation is the highest possible and no injection is considered. It can be observed at the beginning an air migration from the atmosphere layer to the cell, predicted by negative value of gas flow. A stationary state is early reached. Without injection, gas saturation stands on starting value and increases at the maximum value (1.0) only in the atmosphere.

### Test 18d

In this simulation, the cell is fully saturated by gas and in the first minute there is an escape of gas in the atmosphere. A stationary state is reached with a flux equal to zero after an hour. Gas saturation keeps on at 1.0 during the entire simulation.





## Appendix 2

Governing equation solved in TOUGH2/EOS7CA for isothermal problems (from Oldenburg and Unger, 2004).

Description	Equation
Conservation of mass	$\frac{d}{dt} \int_{V_n} M^\kappa dV = \int_{\Gamma_n} F^\kappa \cdot n d\Gamma + \int_{V_n} q_v^\kappa dV$
Mass accumulation	$M^\kappa = \phi \sum_{\beta=1}^{NPH} S_\beta \rho_\beta X_{\beta^\kappa}$
Phase flux	$F_\beta = -k \frac{k_{r\beta} \rho_\beta}{\mu_\beta} (\nabla P_\beta - \rho_\beta g)$
Component flux	$F^\kappa = \sum_{\beta=1}^{NPH} (X_{\beta^\kappa} F_\beta - \phi \tau_0 \tau_\beta \rho_\beta d_\beta^* \nabla X_{\beta^\kappa})$
Pressure and capillary pressure	$P_\beta = P + P_{c\beta}$
Henry's law	$P_g^\kappa = K_H \chi_{aq}^\kappa$
Relative permeability (after Van Genuchten 1980)	<p>if <math>S_l &lt; S_{ls}</math></p> $k_{rl} = \sqrt{S^*} \{1 - (1 - [S^*]^{1/\lambda})^\lambda\}^2$ <p>if <math>S_l \geq S_{ls}</math> <math>k_{rl} = 1</math></p> <p>if <math>S_{gr} = 0</math> <math>k_{rg} = 1 - k_{rl}</math></p> <p>if <math>S_{gr} &gt; 0</math> <math>k_{rg} = (1 - \hat{S})^2 (1 - \hat{S}^2)</math></p> <p>where <math>S^* = (S_l - S_{lr}) / (S_{ls} - S_{lr})</math>,</p> $\hat{S} = (S_l - S_{lr}) / (1 - S_{lr} - S_{gr})$

Description	Equation
Capillary pressure (after Van Genuchten 1980)	$P_c = P_0([S^*]^{-1/\lambda} - 1)^{1-\lambda}$ <p style="text-align: center;"><i>subject to</i> <math>-P_{\max} \leq P_c \leq 0</math></p>
Molecular diffusion	$f_\beta^k = -\phi \tau_0 \tau_\beta \rho_\beta d_\beta^k \nabla X_{\beta^k}$ <p style="text-align: center;"><i>where</i> <math>\tau_0 \tau_\beta = \tau_0 k_{r\beta}(S_\beta)</math></p> <p style="text-align: center;"><i>and</i></p> $d_\beta^k(P, T) = d_\beta^k(P_0, T_0) \frac{P_0}{T_0} \left[ \frac{T + 27315}{27315} \right]^\theta$

Symbol	Description	Units
d	molecular diffusivity	$m^2 \cdot s^{-1}$
g	acceleration of gravity vector	$m \cdot s^{-2}$
F	Darcy flux vector	$kg \cdot m^{-2} \cdot s^{-1}$
k	permeability	$m^2$
$k_r$	relative permeability	
M	mass accumulation term	$kg \cdot m^{-3}$
n	outward unit normal vector	
NK	number of components	
NPH	number of phases	
P	total pressure	Pa
$P_c$	capillary pressure	Pa

Symbol	Description	Units
q	mass flux	$kg\ m^{-2}\cdot\ s^{-1}$
$q_v$	volumetric source term	$kg\ m^{-3}\cdot\ s^{-1}$
S	Saturation (l liquid; g gas; r residual; s saturated)	
t	time	s
T	temperature	°C
V	volume	$m^3$
X	mass fraction	
Y	Y-coordinate	
Z	Z-coordinate (positive upward)	
$\alpha$	$\rho_w g / P_0$ in Van Genuchten's capillary pressure function	
$\beta$	phase index (subscript)	
$\Gamma$	surface area	$m^2$
$\theta$	exponent for temperature dependence of diffusivity	
$\kappa$	mass components (superscripts)	
$\lambda$	Van Genuchten's m	

Symbol	Description	Units
$\mu$	dynamic viscosity	$kg\ m^{-1}\cdot\ s^{-1}$
$\rho$	Density	$kg\ m^{-3}$
$\tau$	Tortuosity	
$\phi$	Porosity	

---

## Appendix 3

### I. Contribution on other papers during the PhD project:

**Agnelli, M., Grandia, F., Credoz, A., Gasparini, A. (2013).** Use of diffusive gradients in thin films (DGT) as an early detection tool of low-intensity leakage from CO<sub>2</sub> storage. *Greenhouse Gas Sci. Technol.* 1, 1-13.

### II. Contribution on conference papers:

**Grandia, F., Agnelli, M., Credoz, A., Gasparini, A., Bruno, J. (2013).** Enhanced Transport of Trace Metals in Low-Intensity CO<sub>2</sub> Leakage of Campo de Calatrava Natural Laboratory (Central Spain). *Geochemical reactivity in CO<sub>2</sub> geological storage sites* Orleans, CNRS Campus, February 25-26, 1023.

**De Elio, J., Ortega, M., Grandia, F., Gasparini, A., Caballero, J., Sainz Garcia, A., Mazadiago, L.F. (2014).** Enhanced radon emission in natural CO<sub>2</sub> flows in Campo de Calatrava region (central Spain). *ICRER 2014- 3<sup>rd</sup> Intl Conference on Radioecology and Environmental Radioactivity*.

### III. Congress oral presentation

**Gasparini, A. Credoz, A., Grandia, F., Bruno, J (2014).** Experimental and numerical modelling of CO<sub>2</sub> leakage in the vadose zone. *EGU Meeting 2014*, Wien (Austria).

### IV. Congress poster presentations

**Gasparini, A., Credoz, A. Grandia, F., Bruno, J., Quattrocchi, F. (2012).** Experimental and modelling study of CO<sub>2</sub> leakage in the vadose zone. *39th Course of the International School of Geophysics: Understanding geological systems for geothermal energy*, Erice (Italy).

**Credoz, A., Becares, E. Fernández-Montiel, I., Grandia, F., Gasparini, A., Garcia, D.A., Calabuig, L., Terron, A., Saenz de Miera, L., Bruno, J. (2013).** Results on bacterial communities and vadose zone and atmospheric modelling at the PISCO2 facilities. *4th meeting of the Monitoring Network and Environmental Research Network, IEAGHG*. 26-30 Aug 2013, Canberra (Australia).

**Gasparini A., Grandia F., Agnelli, M., Sainz-Garcia, A. (2014).** Risk evaluation of CO<sub>2</sub> "lake" formation at surface: Insights from natural systems emissions and modelling. *The International Carbon Conference*, August 25-29 2014, (Iceland).


**Agnelli, M., Grandia, F., Sainz-Garcia, A., Gasparini, A. (2014).** Enhanced metal transport in CO<sub>2</sub>-bearing waters. *The International Carbon Conference*, August 25-29 2014, (Iceland).


**Gasparini, A., Sainz-Garcia, A., Grandia, F., Bruno, J. (2016).** Experimental and numerical modelling of CO<sub>2</sub> atmospheric dispersion in hazardous gas emission sites. *AGU Fall meeting 2016*, San Francisco (U.S.A.).


## **V. Participation at schools**

39<sup>th</sup> Course of the International School of Geophysics, Understanding geological systems for geothermal energy, Erice (Italy): Erice, Italy "Ettore Majorana" Foundation and Centre for Scientific Culture, 25<sup>th</sup> September – 1<sup>st</sup> October 2012.

## Appendix 4. Posters







A21

### Experimental and modeling study of CO<sub>2</sub> leakage in the vadose zone


Andrea Gasparini<sup>2,3</sup>, Anthony Credoz<sup>1</sup>, Fidel Grandia<sup>1</sup>, Jordi Bruno<sup>1,2</sup>, Fedora Quattrocchi<sup>3</sup>

<sup>1</sup>AMPHOS 21 Consulting S.L., Barcelona, Spain. <sup>2</sup>Càtedra Enresa-Amphos21, UPC, Barcelona, Spain. <sup>3</sup>Istituto Nazionale di Geofisica e Vulcanologia, Rome, Italy.

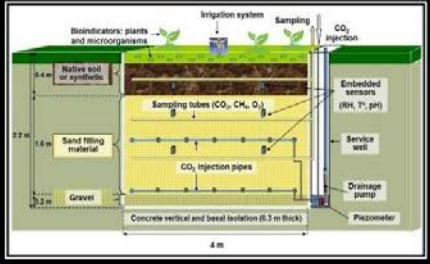
---

**• BACKGROUND:**

- The PISCO2 project deals with the design and building of experimental plots of controlled fluxes of CO<sub>2</sub> to monitor surface flows, water saturation and the effect of CO<sub>2</sub> on terrestrial ecosystems.
- CO<sub>2</sub> leakage through the unsaturated zone and the water and gas mobility and dissolution are investigated.



PISCO, location (Ponferrada, Spain)



**• OBJECTIVES:**

- Understanding dense gas mobility through the unsaturated zone.
- Calibration of the conceptual and numerical models with analytical results from experimental assays performed in the plots.
- Detection of potential leakage during/after the injection operations.
- Set-up of a conceptual model to identify the main parameters influencing the underground gas injection, the stationary conditions and the soil/atmosphere phenomena.


**• CONCEPT:**

- area: 16 m<sup>2</sup> / depth: 2,2 m.
- Filling with sand: homogeneous distribution of CO<sub>2</sub>.
- Calibration of the conceptual and numerical models using TOUGH2/EOS7CA numerical code.

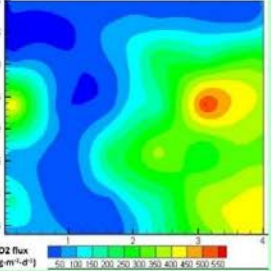
**• EQUIPMENT:**

- Optimized CO<sub>2</sub> injection system (up to 65 L·h<sup>-1</sup>).
- Monitoring of pH, water and gas saturation (CO<sub>2</sub>, CH<sub>4</sub>).
- Control of irrigation and drainage in the unsaturated soil.
- West System accumulation chamber for soil gas flux.

**Experimental test:**  
CO<sub>2</sub> injection and soil gas monitoring.



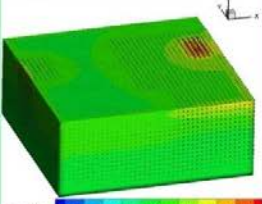
Experimental plot of calibration in PISCO2 platform.



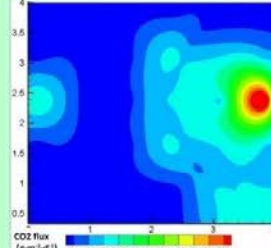
Mapping of surface CO<sub>2</sub> flux performed on 36 points of measurement with accumulation chamber.

**Numerical simulations:** CO<sub>2</sub> migration in the vadose zone using TOUGH2/EOS7CA (Oldenburg & Unger, 2003)

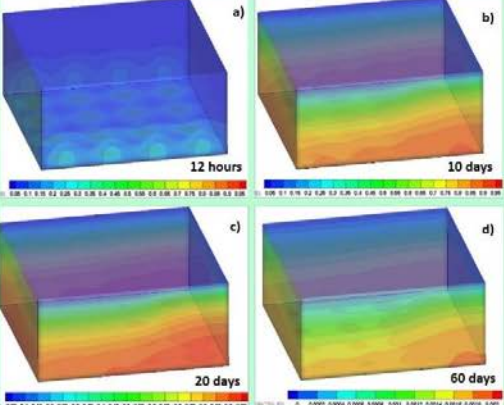
3-D numerical modeling of multiphase CO<sub>2</sub> injection in 16 injectors (1.60 m depth) during 2 months. Mesh of 32000 elements. 3 main porous domains (sand, gravel, atmosphere) with compacted zones (variation of permeability 10<sup>-11</sup> to 5·10<sup>-12</sup> m<sup>2</sup>) in the first 30 cm from the surface.



Gas flow vectors after 60 days of injection, vertical component (z) kg·s<sup>-1</sup>.



Mapping of surface CO<sub>2</sub> flux performed on 36 points of predicted by numerical modeling.



CO<sub>2</sub> mass fraction of in gas phase (a,b,c) and mass fraction of CO<sub>2</sub> in liquid phase (d) for 60-day injection.

**Conclusions:**

- Good agreement between modeling and experiments
- Modeling of a 3 components system in the unsaturated zone
- Sensitivity study on soil features
- Heterogeneous CO<sub>2</sub> flux due mainly to surface compaction



AMPHOS<sup>21</sup>



Co-financed by the European Union  
European Energy Programme for Recovery

## Results on bacterial communities and vadose zone and atmospheric modelling at the PISCO2 facilities

Anthony Creodz<sup>1</sup>, Eloy Bécares<sup>2</sup>, Irena F. Montiel<sup>2</sup>, Fidel Grandia<sup>1</sup>, Andrea Gasparini<sup>4,5</sup>, David A. García<sup>3</sup>, Estanislao de Luis Calabuig<sup>2</sup>, Arsenio Terrón<sup>2</sup>, Luis Sáenz de Miera<sup>2</sup> & Jordi Bruno<sup>3</sup>

<sup>1</sup> Amphos 21 Consulting S.L., Barcelona, Spain (anthony.creodz@amphos21.com)  
<sup>2</sup> University of León, León, Spain  
<sup>3</sup> Fundación Ciudad de la Energía (CIUDEN), Ponferrada, Spain  
<sup>4</sup> Universitat Politècnica de Catalunya  
<sup>5</sup> Istituto Nazionale di Geofisica e Vulcanologia - Roma



Fig. 1. Location of CIUDEN's Facilities in Cubillos del Sil (León, Spain). The CO<sub>2</sub> Capture Plant on the left & PISCO2 experimental platform on the top right.



Fig. 2. Spring vegetation in PISCO2 cells.

### Background

The Fundación Ciudad de la Energía (CIUDEN) is a Spanish state foundation created in 2006 dedicated to different projects related to energy and environment. It's activities include the construction and operation of various facilities for Research and Development in CCS.

### Goals

- Development of economical and ecological biomonitoring tools for safety control of CO<sub>2</sub> geological storages.
- Testing and (if possible) development of these safety control tools.
- Check the effects of CO<sub>2</sub> in agricultural production.

### Research Plan

2011

- 1) Calibration of Experiments  
Ensure the homogeneous CO<sub>2</sub> flow in the surface
- 2) Calibration of Numerical Model  
Simulation of CO<sub>2</sub> injection in vadose zone

2012

- 3) Biological Experiments  
Growing of plants, lichens, microorganisms
- 4) Reactive Transport Modelling  
Simulation of biogeochemical processes during CO<sub>2</sub> multiphase migration
- 5) Ecological Monitoring  
Identification of native and non-native bioindicators of CO<sub>2</sub> leakage

2013

- 6) Atmospheric Dispersion  
Simulation/monitoring of CO<sub>2</sub> migration in soil/atmosphere interface

### Next steps

- Identification of new bio-geo-indicators
- Optimization of agricultural practices
- Calibration of numerical codes in vadose zone

### Current Works

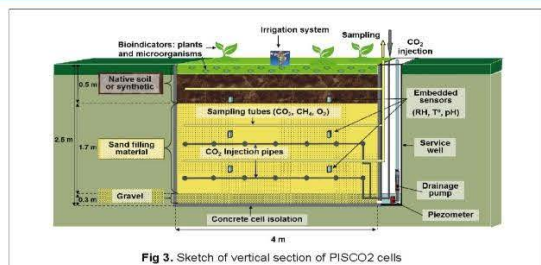
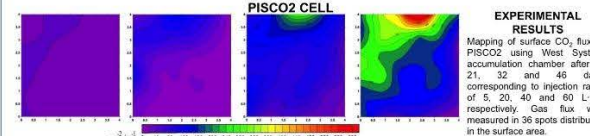


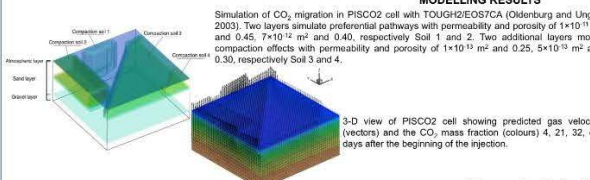
Fig. 3. Sketch of vertical section of PISCO2 cells

### Vadose zone and atmospheric leakage modelling

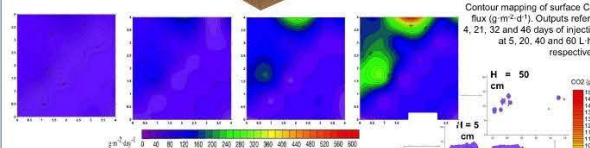
#### EXPERIMENTAL AND MODELLING STUDY OF CO<sub>2</sub> TRANSPORT IN THE VADOSE ZONE OF PISCO2 CELL



**EXPERIMENTAL RESULTS**  
Mapping of surface CO<sub>2</sub> flux in PISCO2 using West System accumulation chamber after 4, 21, 32 and 46 days corresponding to injection rates of 5, 20, 40 and 60 L h<sup>-1</sup>, respectively. Gas flux was measured in 36 spots distributed in the surface area.



**MODELLING RESULTS**  
Simulation of CO<sub>2</sub> migration in PISCO2 cell with TOUGH2/EGS2CA (Oldenburg and Unger, 2003). Two layers simulate preferential pathways with permeability and porosity of 1x10<sup>-11</sup> m<sup>2</sup> and 0.45, 7x10<sup>-12</sup> m<sup>2</sup> and 0.40, respectively Soil 1 and 2. Two additional layers model compaction effects with permeability and porosity of 1x10<sup>-13</sup> m<sup>2</sup> and 0.25, 5x10<sup>-13</sup> m<sup>2</sup> and 0.30, respectively Soil 3 and 4.



**ATMOSPHERIC DISPERSION MODELLING OF CO<sub>2</sub> LEAKAGE**  
Simulation of CO<sub>2</sub> dispersion in the ground/atmosphere interface (from 1 mm to 50 cm) performed with TWODEE-2 (Folch et al., 2008) during summer campaign (35°C). CO<sub>2</sub> emission from 8 PISCO2 cells with a uniform flux of 3500 g m<sup>-2</sup> d<sup>-1</sup> (5 times higher than maximum experimental flux). Concentration of CO<sub>2</sub> (ppmv) is presented after 6 hours of constant emissions and constant wind velocity (1 m s<sup>-1</sup>) and direction. First results show significant CO<sub>2</sub> atmospheric concentrations only in the first centimetres of the soil. Above 10 cm layer, CO<sub>2</sub> concentration approximates atmospheric background (400 ppmv).

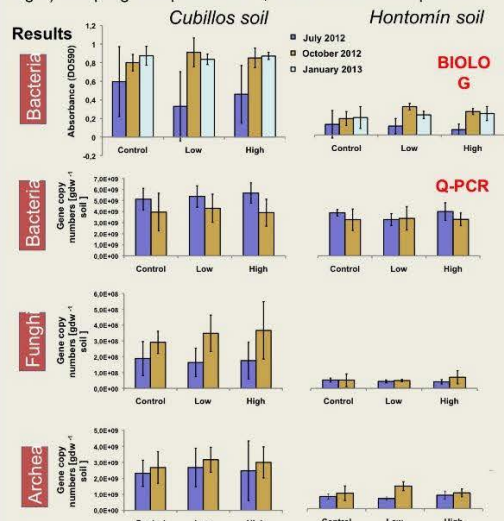
### Effect of CO<sub>2</sub> leakage on edaphic microbial communities

#### Material and methods

- Bacterial metabolic activities were analysed through Biolog Ecoplates<sup>TM</sup> (carbon substrates utilisation profile).
- Archaeal, fungal and bacterial communities were quantified by qPCR.

#### Experimental set-up

- 24 experimental plots (8 m<sup>2</sup>/plot)
- 4 replicates
- Soils from 2 different sites (Cubillos and Hontomin)
- 3 different CO<sub>2</sub> fluxes (0 l h<sup>-1</sup> -control-, 20 l h<sup>-1</sup> -low- and 40 l h<sup>-1</sup> -high-) Sampling took place after 5, 8 and 11 months exposure



#### Discussion and first conclusions

- The results suggest that CO<sub>2</sub> leakage does not affect to soil microbial communities. This is probably due to the unconsolidated state of the soils or to the low CO<sub>2</sub> concentration assayed.





## Risk evaluation of CO<sub>2</sub> “lake” formation at surface: Insights from natural systems emissions and modelling

Andrea Gasparini<sup>1,2</sup> (andrea.gasparini@amphos21.com), Fidel Grandia<sup>1</sup>, Marco Agnelli<sup>1</sup> & Alvaro Sainz<sup>1</sup>

<sup>1</sup> Amphos 21 Consulting S.L, Barcelona – Spain

<sup>2</sup> INGV – Istituto Nazionale di Geofisica e Vulcanologia- Rome – Italy

### Introduction

CO<sub>2</sub> leakage from geological storage is thought to be unlikely due to the very low permeability of the seal formations and the reactivity of CO<sub>2</sub> with both groundwater and rocks. Only the fault re-opening or the loss of well seal integrity may help CO<sub>2</sub> to reach surface environments. In these cases, the impact on the ecosystems would be related to the gas flow intensity and the topography around the gas point source, but the evidence from natural analogue systems tells that this impact is generally low and very rarely affecting human beings. Only in exceptional cases with very high CO<sub>2</sub> (>10,000 g·m<sup>-2</sup>·d<sup>-1</sup>) major impacts on fauna and people can occur under particular ground and weather conditions due to the accumulation of dense CO<sub>2</sub> gas in the atmosphere around the emission source. Such accumulation is sometimes known as CO<sub>2</sub> lakes and they are the main concern of potential human loss due to CO<sub>2</sub> leakage.

### Accumulation of dense CO<sub>2</sub> in atmosphere: The Cañada Real natural emission (Central Spain)

The formation and persistence of CO<sub>2</sub> accumulation in the open atmosphere has been studied in a natural CO<sub>2</sub> emission in the Campo de Calatrava region in Central Spain, called Cañada Real (Fig. 1). There, between 5 to 20 tons of CO<sub>2</sub> are emitted daily from underground.

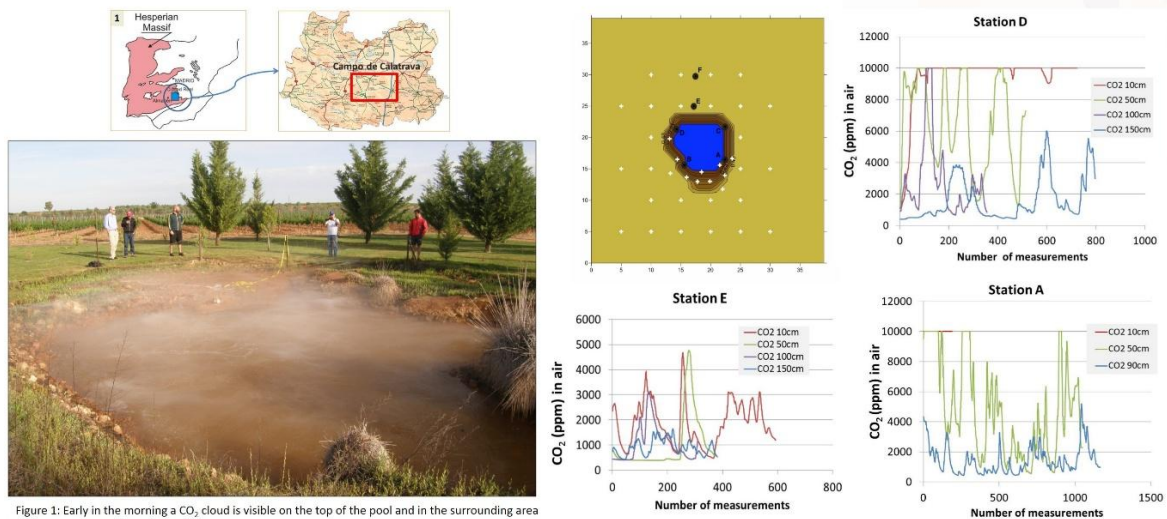
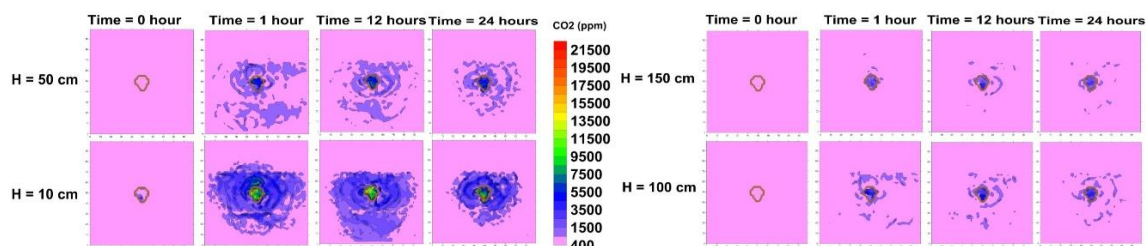


Figure 1: Early in the morning a CO<sub>2</sub> cloud is visible on the top of the pool and in the surrounding area till few centimetres from the surface.

### Numerical modelling

Numerical simulation of atmospheric dispersion from the Cañada Real site has been modelled with the code TWOODEE-2. Results obtained from simulations agree with data recorded at the investigation site.



In the pictures above are shown the results of a simulation with an emission rate of 1 ton/day from the pool in absence of wind.

### Discussion and conclusions

The gas concentration collected at four distinct heights (10, 50, 100 and 150 cm) from ground level ranged from 2000 to >10,000 ppm (the highest concentration measurable by the portable sensor) in the first 50 cm, and from 400 to 6000 ppm at 150 cm above the ground level. The extent of the gas accumulation is small and almost restricted to the area affected by the gas emission. These high gas levels are episodic and only occur under very stable weather conditions, with no wind blowing. The model calculations match the field measurements and predict that the gas concentration in open air can be as high as 25,000 ppm between 0 and 10 cm from ground. This concentration is lethal for human beings and, consequently, some actions should be carried out to minimize the risk in the site.



## Enhanced metal transport in CO<sub>2</sub>-bearing waters

Marco Agnelli<sup>1</sup> (marco.agnelli@amphos21.com), Fidel Grandia<sup>1</sup>, Alvaro Sainz<sup>1</sup> & Andrea Gasparini<sup>1,2</sup>

<sup>1</sup> Amphos 21 Consulting S.L, Barcelona – Spain

<sup>2</sup> INGV – Istituto Nazionale di Geofisica e Vulcanologia- Rome – Italy

### Introduction

The impact of CO<sub>2</sub> gas fluxes on the chemistry of shallow aquifers has been investigated in the Campo de Calatrava region in central Spain to help predicting potential leakage effects in commercial storage of CO<sub>2</sub>. There, mantle-derived gas degassing occurs through faults, leading to CO<sub>2</sub>-bearing groundwaters. It is expected that the CO<sub>2</sub> dissolution enhances leaching and transport of metals, mainly iron, even at relatively high redox and circumneutral pH conditions due to the formation of aqueous Fe(III) carbonate complexes (Grivé et al., 2014). Also, the influence of minor gases such as H<sub>2</sub>S and light hydrocarbons on metal transport needs to be assessed since gas impurities are planned to be co-injected with CO<sub>2</sub> in commercial storage.



Fig. 1. Cold geyser

### Groundwater geochemistry

Water and gas samples have been collected and analysed from 12 springs, pools and cold geysers from unsealed wells (Fig. 1). They show a small range of pH (5.9 to 6.4), an electrical conductivity ranging from 1265 to 3910 μS·cm<sup>-1</sup> and Eh from 167 mV to 360 mV (only one spring showing a reducing Eh value of -52.7 mV). From the solute point of view, these samples are quite fresh with cation molarity below 6.0×10<sup>-2</sup> molar. In general, Na and Mg are the main cations and HCO<sub>3</sub><sup>-</sup> and sulphate are the major anions (Fig. 2).

Despite the circumneutral pH and oxidising condition, Fe is very abundant, between 4.5×10<sup>-4</sup> mmol·L<sup>-1</sup> and 6.1×10<sup>-1</sup> mmol·L<sup>-1</sup>. The highest values are up to three orders of magnitude higher than waters with similar chemistry but CO<sub>2</sub>-free. The studied samples also show anomalous concentrations of Mn (up to 8.0×10<sup>-2</sup> mmol·L<sup>-1</sup>), Zn (up to 1.5 μmol·L<sup>-1</sup>), Ni (up to 1.2 μmol·L<sup>-1</sup>), Co (up to 7.1×10<sup>-1</sup> μmol·L<sup>-1</sup>) and Cu (up to 3.3×10<sup>-1</sup> μmol·L<sup>-1</sup>) (Fig. 3). After degassing, part of the metal content precipitates as hydroxides or are sorbed onto them (Fig. 4). The main dissolved gas dominating all the pools is CO<sub>2</sub>, with a range from 88.3% (0.92 mmol·L<sup>-1</sup>) to 99.9% (28.8 mmol·L<sup>-1</sup>) (Table 1). The remaining gas portion is mainly characterized by the presence of N<sub>2</sub>, CH<sub>4</sub> and Ar. H<sub>2</sub>S is found always under the detection limit.

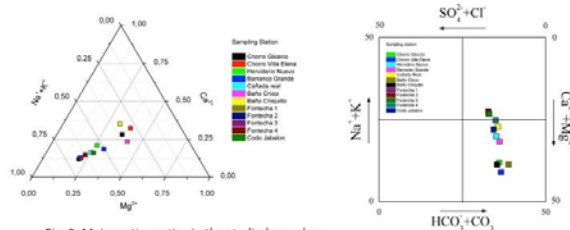


Fig. 2. Major cation ratios in the studied samples



Fig. 4. Fe(III)-hydroxide colloids in degassing pools

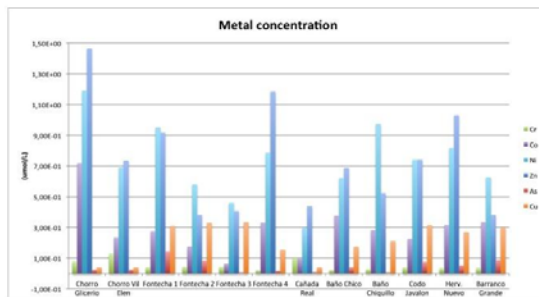


Fig. 3. Metal concentration in the sampled CO<sub>2</sub>-bearing waters

Sample	CO <sub>2</sub> (mmol/L)	N <sub>2</sub> (mmol/L)	Ar (mmol/L)	CH <sub>4</sub> (mmol/L)	O <sub>2</sub> (mmol/L)	Ne (mmol/L)	He (mmol/L)	Tot (mmol/L)
Chorro Glicero	0.994019	0.156082	0.003644	0.000024	0.004834	0.000002	0.000004	1.139608
Chorro Villa Elena	0.923365	0.159410	0.003733	0.000047	0.003537	0.000002	0.000011	1.090104
Cañada Real	28.818	0.123	0.003	0.0025	0.006	0.00001	0.00029	28.9528
Hervidero Nuevo	1.086	0.137	0.0029	0.000015	0.0018	0.000001	0.000000	1.227421
Fuentecha 1	1.318	0.110	0.0025	0.000016	0.0024	0.000001	0.000000	1.433132
Baño Chico	0.865	0.166	0.0042	0.000031	0.0035	0.000005	0.000000	0.000006
Barranco Grande	0.985	0.154	0.0037	0.000018	0.0056	0.000002	0.000000	0.000003

Table 1. Composition of the gas phase.

### Discussion and conclusions

The chemistry of these shallow aquifers is consistent with an interaction between shallow, fresh aquifers and strong CO<sub>2</sub> fluxes ascending from deep faults. The low contents of ions such as Cl<sup>-</sup>, SiO<sub>2</sub>, K<sup>+</sup> or Na<sup>+</sup> and the elevated iron and other metals concentration suggest a short time of interaction between gas and groundwater, with Fe(III) oxyhydroxide dissolution being the key reaction. Such dissolution is thermodynamically feasible due to the formation of aqueous Fe(III) carbonate complexes that allows the solubilisation of elevated amounts of Fe(III). As a side effect, trace metals sorbed onto the surface of Fe(III) oxyhydroxide (e.g., Co, Ni, Zn, As, ...) are also released into the aquifer. The results of this study are relevant for the environmental impact assessment of CO<sub>2</sub> leakage in geological storage since they show that even at oxidizing Eh and circumneutral pH conditions, undesired metal plumes can form and be persistent, jeopardising the quality of water resources.

In the studied samples in Campo de Calatrava, the very low amounts of gases such as light hydrocarbons and H<sub>2</sub>S do not have influence on the redox state of the system and, in turn, on the metal transport.

## Experimental and numerical modelling of CO<sub>2</sub> atmospheric dispersion in hazardous gas emission sites.

ID: 77157  
H51D-1928

Gasparini A.<sup>1,2</sup> (andrea.gasparini@ingv.it), Sainz-Garcia A.<sup>3</sup>, Grandia F.<sup>3</sup>, Bruno J.<sup>2</sup>  
<sup>1</sup>INGV – Istituto Nazionale di Geofisica e Vulcanologia- Rome, Italy - <sup>2</sup>Universitat Politècnica de Catalunya, Barcelona – Spain - <sup>3</sup>Amphos 21 Consulting S.L. Barcelona – Spain

### Introduction

Under stable atmospheric conditions and/or in presence of topographic depressions, CO<sub>2</sub> concentrations can reach high values resulting in lethal effect to living organisms. The distribution of denser than air gases released from the underground is governed by gravity, turbulence and dispersion. Once emitted, the gas distribution is initially driven by buoyancy and a gas cloud accumulates on the ground (gravitational phase), with time the density gradient becomes less important due to dispersion or mixing and gas distribution is mainly governed by wind and atmospheric turbulence (passive dispersion phase). Natural analogues provide evidences of the impact of CO<sub>2</sub> leakage. Dangerous CO<sub>2</sub> concentration in atmosphere related to underground emission have been occasionally reported although the conditions favouring the persistence of such a concentration are barely studied.

### Accumulation of dense CO<sub>2</sub> in atmosphere: The Cañada Real (Central Spain), The Solfiorata di Pomezia (Central Italy) natural emission sites:

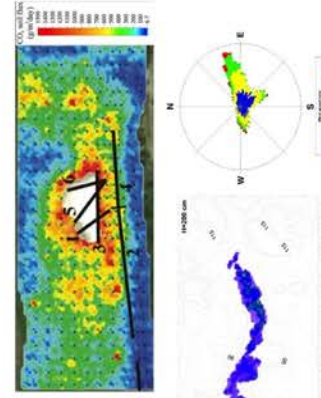
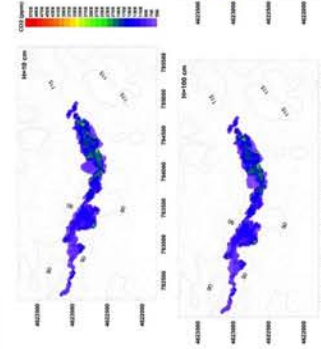
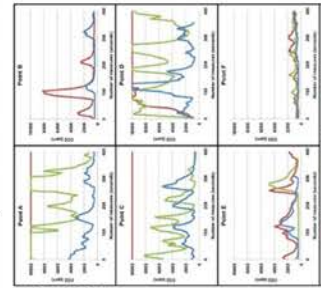
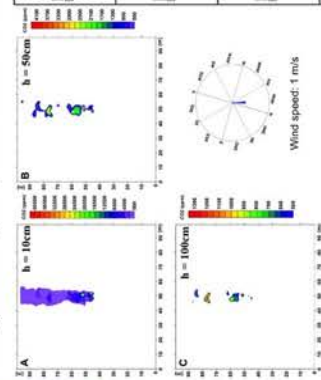


Two sites with different morphology were studied:

- (A) the Cañada Real site, a flat terrain in the Volcanic Field of Campo de Calatrava (Madrid, Spain);
- (B) The Solfiorata di Pomezia site, a rough terrain in the Alban Hills Volcanic Region (Rome, Italy).



A  
h = 10cm



The dynamics of CO<sub>2</sub> in the atmosphere after ground emission is assessed to quantify their potential risk. Two approaches have been followed: (1) direct measurement of air concentration in a natural emission site, where formation of a "CO<sub>2</sub> lake" is common and (2) numerical atmospheric modelling. CO<sub>2</sub> soil flux has been measured at Cañada Real using the SAP system, at Solfiorata di Pomezia using the accumulation chamber method.

### Discussion and Conclusion

The comparison between field data and model calculations reveal that numerical dispersion models are capable of predicting the formation of CO<sub>2</sub> accumulation over the ground as a consequence of underground gas emission. Therefore, atmospheric modelling could be included as a valuable methodology in the risk assessment of leakage in natural degassing systems and in CCS projects. Conclusions from this work provide clues on whether leakage may be a real risk for humans and under which conditions this risk needs to be included in the risk assessment.